THE LIFECYCLE OF ADVANCED FIBERS: (I) A NEW METHOD FOR THE FABRICATION OF FIEBRS, (II) THE FUNCTIONALIZATION OF ELECTROSPUN PLA/PLA-B-PEG FIBERS, AND (III) THE DEGRADATION OF CELLULOSE FIBERS BY OXYGEN PLASMA

A Dissertation

Presented to the Faculty of the Graduate School

of Cornell University

In Partial Fulfillment of the Requirements for the Degree of

Doctor of Philosophy

by

Larissa Marie Shepherd

May 2017

THE LIFECYCLE OF ADVANCED FIBERS: (I) A NEW METHOD FOR THE FABRICATION OF FIEBRS, (II) THE FUNCTIONALIZATION OF ELECTROSPUN PLA/PLA-B-PEG FIBERS, AND (III) THE DEGRADATION OF CELLULOSE FIBERS BY OXYGEN PLASMA

Larissa Marie Shepherd, Ph. D.

Cornell University 2017

This dissertation covers a broad spectra of fiber research that includes (i) fabrication, (ii) functionalization, and (ii) physical/chemical degradation.

In the first stage of this dissertation, a new method for fiber fabrication that combines electro- and wet- spinning, Immersion Electrospinning, was developed to direct fiber deposition by the selective application of voltage.

Next, electrospun PLA/PLA-*b*-PEG (Poly(lactic acid)/Poly(lactic acid)-*b*-Poly(ethylene glycol) fibers were studied for stability over time (i.e. aged). Fiber properties were studied under humid conditions and water wicking properties of PLA/PLA-*b*-PEG fibers came to an equilibrium fairly quickly. While the ability to wick water was lessened with aging, PLA/PLA-*b*-PEG fibers could still wick more than PLA fibers. In the next study, biotin was then added to PLA/PLA-*b*-PEG fibers (where Dimethylformamide, DMF, was the solvent). PLA/PLA-*b*-PEG/biotin fibers resulted in a greater amount of biotin reaching the surface of fibers compared to PLA/biotin fibers. Water stability tests, however, showed a weight loss of the samples over 1 and 7 days,

correlating with biotin and copolymer loss. To reduce this loss, two solvents were investigated, 1,1,1,3,3,3-Hexafluoro-2-propanol (HFIP) and DMF. In addition, the PLA-*b*-PEG block lengths were tailored. Biotin was attached directly to PLA-*b*-PEG. HFIP spun samples resulted in less copolymer loss than DMF spun samples, but there was no biotin present at the surface of fibers. By changing the block lengths of PLA-*b*-PEG, the amount of copolymer and biotin leaching was reduced using DMF as the solvent, and there was still theoretically, enough biotin present at the surface of fibers for use in detection.

Lastly, plasma was used to decrease the stability of (i.e. degrade) cellulosic yarns. With the application of oxygen plasma, severe degradation of of high molecular weight cotton yarns was achieved.

BIOGRAPHICAL SKETCH

Larissa was born and raised in Rochester, New York. Not moving far from home she began perusing her Bachelor's degree at Alfred University. In 2011, she completed her Bachelor's degree in Materials Science and Engineering with a minor in Chemistry.

Larissa then continued on to her Master's degree at Cornell University. In 2013, she completed her Master's degree in Fiber Science & Apparel Design and continued on to her Ph.D.

For her Ph.D., Larissa had several research goals under the advisement of Dr. Margaret Frey; (i) develop a new method of fiber formation by combining two well understood methods, electro- and wet- spinning. (ii) improve and understand electrospun fiber functionality for its potential use in biological applications, and (iii) impart severe degradation on cotton fibers. To aid in her advisement, she had two other committee members, Dr. Christopher Ober who specializes in Materials Science, and Dr. Matthew De Lisa whose expertise is in Biochemical Engineering.

To Ellie and Robbie,

my little girl and loving husband

and to the rest of my family

for their love, belief, and support.

ACKNOWLEDGMENTS

This dissertation was made possible with the help, support, and belief of numerous people. First I would like to acknowledge my family and friends who encouraged me when I need it.

Also I would like to acknowledge my advisor, Dr. Margaret Frey, for all of her support, guidance, and freedom. Many thanks to the Frey research group. A big special thanks to Dr. Edurne González for teaching me polymer synthesis and other lab techniques. A thanks to the wonderful and enthusiastic undergraduates, Laura Saunders and Esther Chen, who I had the opportunity to work with.

I am grateful for all of the equipment across campus that Cornell had to offer and the amazing help and training from facility managers and staff.

TABLE OF CONTENTS

LIST OF FIGURES

LIST OF TABLES

CHAPTER 1

DISSERTATION SCOPE AND ORGANIZATION

This dissertation covers the lifecycle of fibers from fabrication to functionalization, and finally to physical/chemical degradation. In essence this dissertation's main focus is on stability; decreasing the bending instabilities inherent to electrospinning (Chapter 2), increasing the functionality stability of Poly(lactic acid)/Poly(lactic acid)-*b*-Poly(ethylene glycol), (PLA/PLA-b-PEG) fibers (Chapters 3-5), and decreasing the stability of cellulose (Chapter 6).

Over the course of this dissertation, traditional and modified versions of electrospinning nanofibers were utilized. All had a significant drawback, however, in the ability to create 3 dimensionally (3D) patterned structures. The need to maintain voltage drop between the spinneret and collector and the extreme whipping motion of the fibers limit both the thickness and the precision of patterning nanofiber mats. Efforts to produce this kind of structure have been ongoing.

3D Printing is a more than 30 year old technology, starting in 1984 when Chuck Hull of 3D Systems popularized Stereolithography as a printing method for photopolymerizing resins using a rastered laser beam. Since that time, other methods (e.g., Fused Deposition Modeling(FDM), Selective Laser Melting, Direct Ink Writing (DIW), Continuous Liquid Interface Printing (CLIP)) have arisen to fulfill various needs in manufacturing. All of these methods, however, require the movement of either a nozzle, build stage, or light source. In the case of FDM and DIW printing, a nozzle is

moved in (at least) 3-axis motion in a layer by layer fashion to build up a part: every stage of this motion is subject to alignment issues. Though magnetic levitation and pneumatic methods are being used to improve the resolution of these printers (usually by adapting gantries from pick and place machines used in the semiconductor industry), these types of methods will always be fundamentally limited in build resolution and fault tolerance.[1]

By removing mechanical degrees of freedom (DOF) from the build process, there are less opportunities for error—the print resolution will be limited only by the material delivery system (e.g., nozzle). A step in this direction is Digital Mask Projection StereoLithography (DMP-SL)[2] which polymerizes an entire layer at one time using a shaped sheet of light. The substrate on which DMP-SL prints, however, still needs to move, and this 1 DOF motion increases the print time and decreases the variety of shapes that can be printed (e.g., a thin walled balloon is problematic). A potential solution to this limitation is to direct the deposition of material using shaped electric fields. The concept of the controlled deposition of material using electric fields has been shown previously; however, it has not been done in 3D without movement of build platforms or nozzles.

There are several methods for depositing fibers; however, the two that are most relevant here are electro- and wet-spinning. This thesis presents an innovative approach and proof of concept for a novel approach for the potential to create 3D patterned fiber structures by combining aspects of electrospinning and wet spinning. Traditional

electrospinning is a well understood technique that has been used to create fibers with a wide range of chemistries[3], however, due to bending instabilities[4] fibers land in random orientations. While random fiber collection is suitable for some uses, it is not desirable in other applications. Some researchers have managed to increase the thickness of the deposited mat by electrospinning onto a liquid interface, a method called wet electrospinning[5, 6], however, this still results in random and uncontrollable fiber arrangements. Melt electrospinning and hot electrohydrodynamic jet plotting have been used to create more precise architectures but are limited due to mechanical motion and polymers able to be melt spun.[7, 8] Therefore, in Chapter 2, I describe the development of a new method for fabricating fibers, Immersion Electrospinning. By combining electro- and wet- spinning, the ultimate purpose of this modified spinning is to slow the process of electrospinning so that directed deposition can be achieved through the selective application of voltage to an array of electrodes with no mechanical motion. With the needle submerged directly into a coagulation bath, I investigate changing the electric field strength (*E)* on the fiber formation of Poly(acrylonitrile). At $E \sim 50\ \mathrm{kV \cdot m^{-1}}$ using an array of electrodes and selectively applying voltages I am able to direct the fiber into a square.

Electrospinning has been used to create responsive cores[9] and enriched fiber surfaces.[10, 11] By adding a more hydrophilic polymeric material to poly(lactic acid) (PLA) spinning dopes, the fiber chemistry can be altered to be more hydrophilic.[11, 12] Previously, we modified high molecular weight PLA fibers with the addition of poly(lactic acid)-*b*-poly(ethylene glycol) (PLA-*b*-PEG). The addition of 12 wt% PEG

from PLA(1000)-b-PEG(5000) in the final fiber, resulted in a nanofiber mat able to take up 1,300% its weight in water[12] and as a result, 12 wt% PEG in the final fiber has been used in the studies here.

In the following chapters of this dissertation, nanofiber mats made from poly PLA/PLA-*b*-PEG, PLA/PLA-*b*-PEG/biotin and PLA/PLA-*b*-PEG-biotin are studied. The PLA/PLA-b-PEG system consists of insoluble yet hydrophilic fibers[12] that are stable and may serve as an efficient bio-interface. Detection and filtration using nanofibers is not a novel concept.[13-16] Being hydrophilic and water stable is important for biologically active nanofibers as most biological systems are aqueous, yet fiber-forming polymers are usually either (i) hydrophobic and non-water soluble or (ii) hydrophilic and dissolve in water. In the early phases of this research, it became apparent that the PLA/PLA-b-PEG and PLA/PLA-b-PEG/biotin were not as stable over time or in water as initially hypothesized and work shifted to exploring and understanding factors influencing stability. With the addition of biotin, we create nanofiber mats that can capture protein (avidin). Capture is confirmed via a colorimetric assay.

When considering electrospun fibers for in-field use, it is crucial to understand how the fiber properties change with time and storage conditions, however, there have been few studies on the aging of electrospun fibers. The studies that have been performed are over relatively short time scales, for example, Li et al. investigated the aging conditions in relation to the water stability of a green tea polyphenol within an electrospun corn protein fiber, however this study was limited to only three days of aging.[17] A seven-

week study by Kim et al. was interested in tailoring the degradation rate of electrospun fibers by adjusting individual components.[18] While these studies look at specific properties over a short time span, longer duration studies on a variety of electrospun fibers are needed to allow a better understanding of fiber properties with time and ultimately the fiber shelf life. Therefore, in Chapter 3, a long term aging study (i.e. 48-49 weeks) under humid conditions was performed on PLA/PLA-*b*-PEG electrospun fibers that were spun from Dimethylformamide (DMF). While initially, PEG from copolymer PLA(1000)-b-PEG(5000) is at the surface of fibers, with time PEG comes to an equilibrium condition as indicated by fiber mat water wicking ability. Under the spinning and storage conditions of the study, PLA(1000)-*b*-PEG(5000) has a greater impact on the initial water wicking ability of fibers than does PLA(1000)-*b*-PEG(10000). After 8-16 weeks, water wicking properties for fibers containing copolymers equilibrated and maintained a higher water wicking ability than PLA fibers alone. Therefore, while initial fiber properties are not stable, the equilibrated fiber mats maintain a fairly stable shelf life.

Electrospun fibers are ideal for use in biological sensing applications due to their high surface area to volume ratio.[19, 20] By incorporating Biotin into electrospun fibers followed by avidin binding, fibers are able to immobilize proteins[21] and perform as viable biosensors.[10] Therefore, in Chapter 4, Biotin was added freely to PLA/DMF and PLA/PLA-*b*-PEG/DMF dopes. With the addition of PLA-*b*-PEG, surface available biotin is significantly increased over just biotin containing PLA electrospun fibers. The copolymers and biotin incorporated into fibers was found to not be stable for long

durations of water exposure. The purpose of Chapter 5 was to lessen the amount of PLA-*b*-PEG copolymers and biotin migrating from electrospun fibers to the aqueous phase (i.e. increase copolymer and biotin stability). In Chapter 5, first two solvent systems, DMF and 1,1,1,3,3,3,-Hexafluoro-2-propanol (HFIP) are investigated for varying block lengths of PLA-*b*-PEG copolymer loss from PLA/PLA-*b*-PEG electrospun fibers. Biotin is then attached directly to copolymers PLA-*b*-PEG with varying lengths. While HFIP showed little loss of PLA-*b*-PEG-Biotin, there was virtually no surface available Biotin. Attaching biotin directly to PLA-*b*-PEG did result in a reduction of biotin loss over one and seven days of water exposure using DMF compared to Chapter 4, where Biotin was added freely.

Cellulosic material is often degraded by acid hydrolysis,[22] but in Chapter 6, I attempt to use plasma as a way to significantly degrade cotton cellulose. In Chapter 6 the physical and chemical modification of greige and scoured cellulosic yarns is achieved by Oxygen (O_2) plasma. The modification occurs at high power density (0.46 W/cm^2). The exposure times studied were 15, 30, 60, and 90 minutes, which are generally longer than many studies. Through this modification, the load at break and weight average molecular weight were decreased significantly compared to the controls. This type of plasma modification therefore has the potential to serve as a "greener" pretreatment for the degradation of high molecular weight cellulose.

Lastly, in Chapter 7, I provide ideas on how Immersion Electrospinning and surface functionalization of electrospun fibers could be further developed/researched.

REFERENCES

1. Rao, P. K.; Liu, J.; Roberson, D.; Kong, Z.; Williams, C., Online Real-Time Quality Monitoring in Additive Manufacturing Processes Using Heterogeneous Sensors. *Journal of Manufacturing Science and Engineering-Transactions of the Asme* **2015,** *137* (6).
2. Peele, B. N.; Wallin, T. J.; Zhao, H. C.; Shepherd, R. F., 3D printing antagonistic systems of artificial muscle using projection stereolithography. *Bioinspiration & Biomimetics* **2015,** *10* (5).
3. Ramakrishna, S.; Fujihara, K.; Teo, W. E.; Yong, T.; Ma, Z. W.; Ramaseshan, R., Electrospun nanofibers: solving global issues. *Materials Today* **2006,** *9* (3), 40-50.
4. Reneker, D. H.; Yarin, A. L.; Fong, H.; Koombhongse, S., Bending instability of electrically charged liquid jets of polymer solutions in electrospinning. *J. Appl. Phys.* **2000,** *87* (9), 4531-4547.
5. Yang, W. X.; Yang, F.; Wang, Y. N.; Both, S. K.; Jansen, J. A., In vivo bone generation via the endochondral pathway on three-dimensional electrospun fibers. *Acta Biomater.* **2013,** *9* (1), 4505-4512.
6. Yokoyama, Y.; Hattori, S.; Yoshikawa, C.; Yasuda, Y.; Koyama, H.; Takato, T.; Kobayashi, H., Novel wet electrospinning system for fabrication of spongiform nanofiber 3-dimensional fabric. *Mater. Lett.* **2009,** *63* (9-10), 754-756.
7. Brown, T. D.; Dalton, P. D.; Hutmacher, D. W., Direct Writing By Way of Melt Electrospinning. *Adv. Mater.* **2011,** *23* (47), 5651-5657.
8. Wei, C.; Dong, J., Direct fabrication of high-resolution three-dimensional polymeric scaffolds using electrohydrodynamic hot jet plotting. *J. Micromech. Microeng.* **2013,** *23* (2).
9. Buyuktanir, E. A.; Frey, M. W.; West, J. L., Self-assembled, optically responsive nematic liquid crystal/polymer core-shell fibers: Formation and characterization. *Polymer* **2010,** *51* (21), 4823-4830.
10. Li, D.; Frey, M. W.; Vynias, D.; Baeumner, A. J., Availability of Biotin Incorporated in Electrospun PLA Fibers for Streptavidin Binding. *Polymer* **2007,** *48* (21), 6340-6347.
11. Hendrick, E.; Frey, M., Increasing Surface Hydrophilicity in Poly(Lactic Acid) Electrospun Fibers by Addition of Pla-b-Peg Co-Polymers. *J. Eng. Fibers Fabr.* **2014,** *9* (2), 153-164.
12. Buttaro, L. M.; Drufva, E.; Frey, M. W., Phase Separation to Create Hydrophilic Yet Non-Water Soluble PLA/PLA-b-PEG Fibers via Electrospinning. *J. Appl. Polym. Sci.* **2014,** *131* (19), 41030 (7 pp).
13. Li, D. P.; Frey, M. W.; Baeumner, A. J., Electrospun Polylactic Acid Nanofiber Membranes as Substrates for Biosensor Assemblies. *J. Membr. Sci.* **2006,** *279* (1-2), 354-363.
14. Rebovich, M. E.; Vynlas, D.; Frey, M. W., Formation and functions of high-surface-area fabrics *Adv. Sci. Tech.* **2010,** *3* (3), 129-134.
15. Matlock-Colangelo, L.; Cho, D.; Pitner, C. L.; Frey, M. W.; Baeumner, A. J., Functionalized electrospun nanofibers as bioseparators in microfluidic systems. *Lab Chip* **2012,** *12*, 1696-1701.

16. Cho, D. W.; Matlock-Colangelo, L.; Xiang, C. H.; Asiello, P. J.; Baeumner, A. J.; Frey, M. W., Electrospun nanofibers for microfluidic analytical systems. *Polymer* **2011,** *52* (15), 3413-3421.
17. Li, Y.; Lim, L. T.; Kakuda, Y., Electrospun Zein Fibers as Carriers to Stabilize (-)-Epigallocatechin Gallate. *Journal of Food Science* **2009,** *74* (3), C233-C240.
18. Kim, K.; Yu, M.; Zong, X. H.; Chiu, J.; Fang, D. F.; Seo, Y. S.; Hsiao, B. S.; Chu, B.; Hadjiargyrou, M., Control of degradation rate and hydrophilicity in electrospun non-woven poly(D,L-lactide) nanofiber scaffolds for biomedical applications. *Biomaterials* **2003,** *24* (27), 4977-4985.
19. Senecal, A.; Magnone, J.; Marek, P.; Senecal, K., Development of functional nanofibrous membrane assemblies towards biological sensing. *Reactive & Functional Polymers* **2008,** *68* (10), 1429-1434.
20. Tsou, P. H.; Chou, C. K.; Saldana, S. M.; Hung, M. C.; Kameoka, J., The Fabrication and Testing of Electrospun Silica Nanofiber Membranes for the Detection of Proteins. *Nanotechnology* **2008,** *19* (44), 445714 (6 pp).
21. Lu, T. C.; Chen, X. S.; Shi, Q.; Wang, Y.; Zhang, P. B.; Jing, X. B., The immobilization of proteins on biodegradable fibers via biotin-streptavidin bridges. *Acta Biomaterialia* **2008,** *4* (6), 1770-1777.
22. Lin, J.-H.; Chang, Y.-H.; Hsu, Y.-H., Degredation of cotton cellulose treated with hydrochloric acid either in water or in ethanol. *Food Hydrocolloids* **2009,** *23* (6), 1548-1553.

CHAPTER 2

IMMERSION ELECTROSPINNING AS A NEW METHOD TO DIRECT FIBER DEPOSITION[1]

2.1 Introduction

Electrospinning finds applications in many fields, one of which is tissue engineering. For many years the patterning and alignment of fibers in these scaffolds has been of particular interest due to the need for large pore sizes that are required to promote cell infiltration and migration.[1] The design of electrospun fibers is also of importance for electrical applications, for example, sensors and optoelectronics, which often require aligned and ordered structures.[2, 3] In traditional electrospinning, however, the electrically driven fiber follows first a short, straight path followed by bending instabilities[4] that create a chaotic whipping motion. Therefore, while the patterning [5-7] and aligning[2, 8, 9] of fibers can be achieved by electrode design, the precise placement of the fiber jet into a pattern is nearly impossible as the fibers land in an uncontrolled manner. In addition, making scaffolds with truly 3-dimensional (3-D) structures, similar to the natural extracellular matrix, for example, is limited when electrospinning due to the repulsions between fibers, as the result of charge accumulation. This charge accumulation restricts the maximum thickness of the mat [10] and, also, with increasing thickness, the mean pore radius decreases.[1]

Melt electrospinning has been used as a method for patterning 2-D and 3-D structure

[1] Shepherd, L.M.; Frey, M.W.; Yong, L.J. : submitted.

through the use of mechanical motion of the collector and control over various parameters.[10] This method of depositing fibers, however, still has several shortcomings that include: (i) material limitation to melt-spinnable polymers, (ii) mechanical motion of the collector results in long print times, noise, and poor resolution, and (iii) the electrostatic forces between collected fibers restrict the controlled deposition of the 3D constructs to 1 mm.[10] Wet electrospinning, however, has shown promise in significantly increasing the collection depth profile and controlling the porosity of the nonwoven fiber.[11, 12] Differing from traditional electrospinning, fiber formation in wet electrospinning is achieved by spinning first through air followed by deposition within a liquid interface. The resulting fibers, however, are still deposited randomly with no ability to control where an individual fiber is placed.

Two other methods previously explored to gain control over electrically driven fibers are electrohydrodynamic (EHD) jet printing and hot EHD-jet plotting. EHD-jet printing, while capable of forming precise 2D structures, is limited in its ability to pattern in 3D due to material deformation during solvent evaporation.[13] While the method of hot EHD-jet plotting is capable of forming precise 2D and 3D structures, it shares many of the same drawbacks as melt electrospinning—it is confined to polymers that will not degrade upon heating, relies on mechanical motion, and the ultimate thickness of 3D structures is limited.[13]

To reduce the bending instability of electrospinning and time associated with the

mechanical motion of directed deposition gantries, we combine electro- and wet-spinning. Through their combination, this research develops a new method, Immersion Electrospinning, where the ejected jet is directly submerged in the coagulation bath. This allows for the controlled steering of fibers through a coagulation bath by the selective application of an array of collector electrodes that shape the electric field. This new method also allows for the use of polymers not able to be melt spun (e.g., PAN or cellulose) as well as reducing the electrostatic repulsions between fibers for the potential for thick 3-D fiber structures.

2.2 Experimental Section

2.2.1 Experimental Fluids

The spinning dope consisted of 10.5 weight percent (wt%) of Poly(acrylonitrile) (PAN) (Molecular Weight = 150,000 Daltons) in 99.8% anhydrous N,N-Dimethylformamide (DMF) and both were purchased from Sigma-Aldrich. Dopes were exposed to low heat and stirring for at least 16 hours, or until dopes were homogenous. The system under consideration used liquid as a spinning media, as opposed to the conventional electrospinning system where the spinning occurs in air or in vacuum. We used a spinning medium consisting of a 2:1 mixture of chloroform and mineral oil. Light mineral oil was purchased from Fischer Scientific and we used Macron Fine Chemicals chloroform.

VISCOSITY: The viscosity (η) of the 10.5 wt% PAN spinning dope was obtained using a TA instruments AR2000 Rheometer with a 60 mm parallel steel plate. The temperature

was set to 21.1˚C and a linear ramp mode was used to collect 30 sample points over a shear rate from 0 to 90 s^{-1} followed by another linear ramp collection of 30 points over a shear rate from 90 to 0 s^{-1}.

SURFACE TENSION: Surface tension (γ) of the 10.5 wt% PAN dope with respect to mineral oil was measured using a KSV Sigma 701 and a Wilhelmy plate at a speed of 20mm·min^{-1}. We took the average of two 10 minute runs as the value for surface tension. The surface tension measurements could not be performed with the chloroform/mineral oil mixture due to rapid solidification of the PAN fiber.

2.2.2 Immersion Electrospinning Components

We spun the PAN/DMF spinning dope through a stainless steel needle (blunt 25 g x 1”; Small Parts, Inc.) that also acted as the ground electrode. To contain and supply the dope, we used 5 ml syringes (Beckton Dickson & Company). The coagulation bath was made with made from Pyrex® 2” square tubing with an inner diameter of 51 mm and wall thickness of 2.2 mm (Friedrich & Dimmock, Inc.). We attached the needle in the bath using epoxy before each use. The fluid in the syringe was pumped at a flowrate of 0.5 mL hr^{-1} using a programmable PHS Ultra syringe pump (Harvard Apparatus). We applied the voltage at the collector using a high voltage DC amplifier (Gamma High Voltage Research, Inc.). The initial Immersion electrospinning apparatus, with a copper triangular collector is shown in **Figure 1**. We later modified the collector in Figure 1 to provide an electrode array with four collection sites and independent voltages.

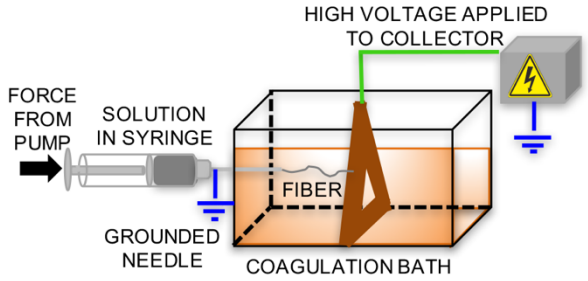

Figure 2.1 Immersion Electrospinning apparatus.

2.2.3 Field Emission Scanning Electron Microscopy (FESEM)

Prior to FESEM imaging we removed residual mineral oil by washing the sample three times in chloroform and allowing it to dry in the fume hood. A Baltec 030 critical point drying chamber was then used to rinse the sample ten times with liquid Carbon Dioxide (CO_2), never letting it dry. The chamber was then filled to ¾ and the submersed sample was heated to 42˚C. While the temperature was maintained the chamber was vented to atmosphere over one hour. The sample was removed, mounted, and finally coated in Carbon using a Denton Bench Top Turbo. Imaging was performed at 5 kV using a LEO 1550 FESEM. We used ImageJ™ to determine the fiber diameter.

2.3 Results and Discussion

In Immersion Electrospinning, we combine the methods of traditional electro- and wet-spinning; we use an electric field to draw fibers while the needle is fully submerged in a dielectric liquid that coagulates the dope into fibers and significantly reduces the speed of the jet due to the drag force of the fluid. This reduction in speed and fiber surface charges mitigates the chaotic whipping motion associated with electrospinning, which is a critical to allow for the steering of fibers by shaping of the electric field.

In order to first test our system, we chose to use 10.5wt% PAN in DMF as our fiber forming dope being drawn electrically through a coagulation bath of chloroform/mineral oil. The PAN/DMF viscosity was measured to be $\eta \sim 1.11$ Pa·s. We specifically chose to produce PAN fibers as they are the precursor to carbon fiber, which may have electrical applications, and the PAN/DMF dopes when exposed to chloroform readily form fibers; precipitating PAN from the solution. We measured the surface tension between the PAN/DMF spinning dope and mineral oil ($\gamma \sim 5.38$ mN·m^{-1}), as measurements with chloroform are not possible due to rapid solidification of PAN. Our choice in coagulation bath media is a fundamental parameter for not only precipitating the PAN fiber but also providing a low conducting media. Like traditional electrospinning, the conductivity of the media the fiber is being spun through (typically air) must be low so that the current is not conducted between the ground and the electrode, which is necessary for the large electric potential needed to create fibers. We investigated the formation of fibers using five different electric field strengths (approximate values =12.5, 25, 125, 250, and 375 kV·m^{-1}).

We considered the dimensionless electric field parameter, $\varphi = (\varepsilon E^2)/(\rho v^2)$, where ε is the absolute permittivity of the chloroform/mineral oil bath (calculated from the dielectric values[14], 4.8 and 2.1, and using rule of mixtures), E is the electric field strength, ρ is the density of the PAN/DMF dope (calculated using rule of mixtures), and v is the velocity at the needle tip as calculated from the infuse rate and known needle inner diameter. In this study the φ (Table 1) is only dependent on the electric field strengths as ε, ρ, and v are not changing. Therefore, we also determined the average

velocity of the fiber jet (Table 1) using time stamps taken from the video footage. The normalized value of velocity was gathered by dividing the average velocity of the jet by the velocity at the needle tip (Table 1).

Table 2.1 List of measured and calculated values for Immersion Electrospinning.

Electric Field Strength ($kV \cdot m^{-1}$)	Electric Field Parameter (φ)	Average Velocity (m/s)	Average Velocity/ Needle Tip Velocity
12.5	*0.7*	*8×10^{-3}*	*3*
25	*3*	*1×10^{-2}*	*4*
125	*70*	*2×10^{-2}*	*7*
250	*300*	*2×10^{-2}*	*7*
375	*700*	[a]	[a]

[a] A continuous fiber does not reach the collector; therefore, an average velocity is not measured from E=375 $kV \cdot m^{-1}$.

We found a critical electric field strength (E_{crit}=125 $kV \cdot m^{-1}$). At and below E_{crit}, the average velocity momentum is low enough to produce continuous fibers, however, with increasing electric field strength, E =250 $kV \cdot m^{-1}$, we found the fibers began to break intermittently during spinning (i.e., "fiber disruption"). With continued increase of the electric field (E = 375 $kV \cdot m^{-1}$), we find that the fibers fragment during spinning and it is not possible to form a continuous filament. The average fiber velocity and normalized velocity values, therefore, could not be calculated since a continuous fiber jet never reaches the collector. Interestingly, with increasing φ and average fiber velocity we begin to observe visually increasing bending instabilities, which partially explains the fiber disruption and fragmentation. We found at a E_{crit}=*125* $kV \cdot m^{-1}$, and above there is an increase in whipping motion, but fiber disruption and fragmentation does not occur until the electric field strength is greater than E_{crit}. In addition, when E= 250 $kV \cdot m^{-1}$ we

observe the same average velocity as seen at E_{crit}=*125* kV·m^{-1}, which we attribute to the increasing bending instabilities interaction with the coagulation bath. Here we do not consider the relationship between fiber velocity and the rate of diffusion in the formation of the PAN fibers, which is also likely to contribute to the breakages of these fibers.

Based on φ, average fiber velocity, and the visual observation of fibers from videos taken, we chose to produce fibers at ~50 kV·m^{-1}. The fibers formed at this electric field are continuous but with some variation in fiber morphology and diameter (Figure 2; fiber diameter = 92.9 ± 21.1 μm). These variations are likely the result of the coagulation bath medium not yet being perfectly tailored to account for the diffusion rate in the solidification of the PAN fibers.

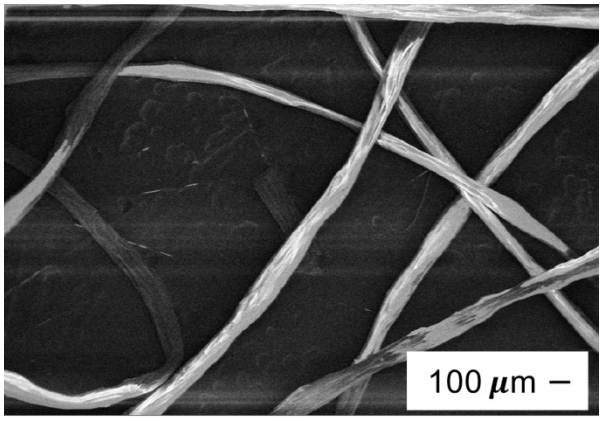

Figure 2.2 FESEM image of fibers formed at ~ 50 kV·m^{-1}.

Using an electric field of ~ 50 kV·m^{-1}, we are able to further modify our immersion apparatus (Figure 3A) to allow fibers to be directed by activating and deactivating an array of electrodes (Figure 3B). Using four independently operated electrodes we were

able to direct the fiber into a square shape (Figure 3C). To do this: (i) we first place our electrodes into the coagulation bath with no voltage applied; (ii) then began directing the fiber to the bottom right electrode by applying a 1 kV voltage (Figure 3C); (iii) as soon as the fiber contacts the electrode 1, the voltage is removed from electrode 1 while the electrode 2 voltage is applied, forming the right line; (iv) after contact to electrode 2, the voltage is removed and placed at electrode 3, forming the top line; (v) we formed the left line after contact to electrode 3 by removing the voltage and applying it to electrode 4; (vi) we finally completed the square shape by removing the voltage from electrode 4 and applying it back to electrode 1 (Figure 3C). In this study, the electric fields were applied manually using four high voltage sources; however, in the video taken it is clear when each electrode is activated by a change in fiber direction.

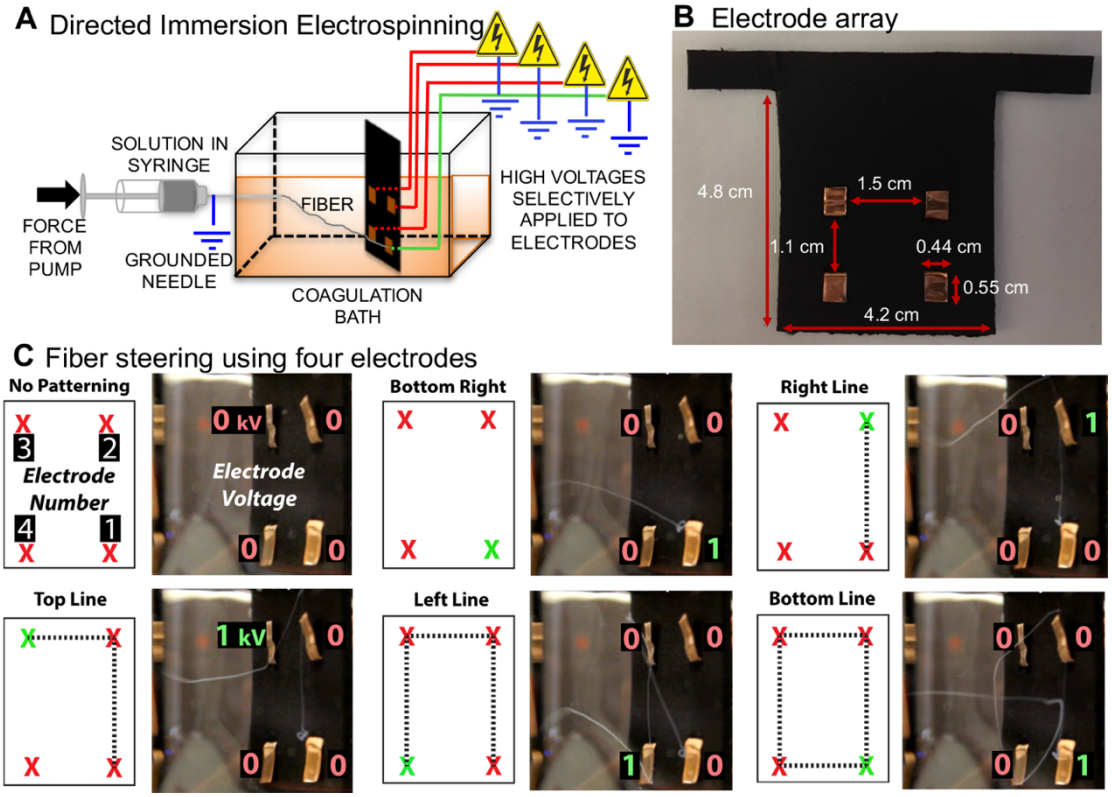

Figure 2.3 (A) Modified Immersion Electrospinng apparatus for controlled deposition of fiber, (B) collector array and its approximate dimensions for directed Immersion Electrospinning, (C) sequential images displaying the directed positioning of fibers in response to applied voltage.

2.4 Conclusions

We have developed a new method, Immersion Electrospinning, to decrease the instabilities presently encountered in electrospinning to allow for greater control of the polymer fiber by spinning directly through a viscous medium. Low electric field parameters produce Immersion Spun fibers with low enough momentum that we can steer them to spatially distributed and actively controlled electrodes. Using the coagulation bath, without the movement of the nozzle head, and the selective application of voltage to an array of electrodes at the collector, we demonstrated that the deposition

of a continuous PAN fiber can be directed into a square path. Directing fiber deposition via immersion electrospinning with electrically guided collection offers a premise to devise an innovative 3D printing scheme where the deposition of the jet can be achieved.

Modeling of the fibers with increasing electric field and their relationship to the rate of diffusion was not performed here; however, it will become important for higher resolution control of fiber deposition. Under the current conditions of this study, fiber diameters are relatively large, however, we expect the tailoring of the system parameters and apparatus will allow for further reduction in fiber diameter. While we have been able to prove the concept of steering fibers, we need to further design the system to ensure the fibers adhere to the collector. While the electrodes were activated manually in this study, ideally this system would be automated using computer control of an array of high voltage relays to provide more precise transitions.

2.5 Acknowledgements

This work was funded by the Department of Fiber Science & Apparel Design at Cornell University. This research made use of the Cornell Center for Materials Research Shared Facilities which are supported through the NSF MRSEC program (DMR-1120296). We would like to acknowledge David Wise at the Cornell Chemistry Glass Shop for fabrication of the coagulation bath vessel, John Grazul for the CO_2 treatment and carbon coating of fibers, and Dr. Anil Netravali for equipment loan.

REFERENCES

1. Sill, T. J.; von Recum, H. A., Electro spinning: Applications in drug delivery and tissue engineering. *Biomaterials* **2008,** *29* (13), 1989-2006.
2. Li, D.; Wang, Y. L.; Xia, Y. N., Electrospinning of polymeric and ceramic nanofibers as uniaxially aligned arrays. *Nano Lett.* **2003,** *3* (8), 1167-1171.
3. Kuo, C. C.; Wang, C. T.; Chen, W. C., Highly-Aligned Electrospun Luminescent Nanofibers Prepared from Polyfluorene/PMMA Blends: Fabrication, Morphology, Photophysical Properties and Sensory Applications. *Macromol. Mater. Eng.* **2008,** *293* (12), 999-1008.
4. Reneker, D. H.; Yarin, A. L.; Fong, H.; Koombhongse, S., Bending instability of electrically charged liquid jets of polymer solutions in electrospinning. *J. Appl. Phys.* **2000,** *87* (9), 4531-4547.
5. Cho, S. J.; Kim, B.; An, T.; Lim, G., Replicable Multilayered Nanofibrous Patterns on a Flexible Film. *Langmuir* **2010,** *26* (18), 14395-14399.
6. Zhao, S. F.; Zhou, Q. H.; Long, Y. Z.; Sun, G. H.; Zhang, Y. Z., Nanofibrous patterns by direct electrospinning of nanofibers onto topographically structured non-conductive substrates. *Nanoscale* **2013,** *5* (11), 4993-5000.
7. Zhang, D. M.; Chang, J., Patterning of electrospun fibers using electroconductive templates. *Adv. Mater.* **2007,** *19* (21), 3664-+.
8. Theron, A.; Zussman, E.; Yarin, A. L., Electrostatic field-assisted alignment of electrospun nanofibres. *Nanotechnology* **2001,** *12* (3), 384-390.
9. Katta, P.; Alessandro, M.; Ramsier, R. D.; Chase, G. G., Continuous electrospinning of aligned polymer nanofibers onto a wire drum collector. *Nano Lett.* **2004,** *4* (11), 2215-2218.
10. Brown, T. D.; Dalton, P. D.; Hutmacher, D. W., Direct Writing By Way of Melt Electrospinning. *Adv. Mater.* **2011,** *23* (47), 5651-5657.
11. Yang, W. X.; Yang, F.; Wang, Y. N.; Both, S. K.; Jansen, J. A., In vivo bone generation via the endochondral pathway on three-dimensional electrospun fibers. *Acta Biomater.* **2013,** *9* (1), 4505-4512.
12. Yokoyama, Y.; Hattori, S.; Yoshikawa, C.; Yasuda, Y.; Koyama, H.; Takato, T.; Kobayashi, H., Novel wet electrospinning system for fabrication of spongiform nanofiber 3-dimensional fabric. *Mater. Lett.* **2009,** *63* (9-10), 754-756.
13. Wei, C.; Dong, J., Direct fabrication of high-resolution three-dimensional polymeric scaffolds using electrohydrodynamic hot jet plotting. *J. Micromech. Microeng.* **2013,** *23* (2).
14. http://www.engineeringtoolbox.com/relative-permittivity-d_1660.html (accessed March 2017).

CHAPTER 3

AGING OF PLA/PLA-*B*-PEG ELECTROSPUN FIBERS UNDER HUMID STORAGE CONDITIONS[2]

3.1 Introduction

Nanofibers, due to their high surface areas and aspect ratios, have been an ideal candidate for both biomedical and biological applications[1-4]; however, little work has been performed to investigate the long-term stability of these fibers. In this work we consider PLA/PLA-*b*-PEG nanofibers and their properties over 48 to 49 weeks to determine their initial and equilibrated fiber properties (i.e. shelf life).

The surface chemistry of PLA nanofibers can be altered to impart hydrophilicity by incorporating more hydrophilic compounds to the electrospinng dope[5-7], and with the addition of PLA-*b*-PEG copolymers short term water stability can be achieved,[6, 8] however, aging of these electrospun fibers has not investigated. Mechanical properties of PLA with plasticizer PEG at ambient conditions have been studied in regard to films over short time durations[9, 10]; however, the wetting properties have not been extensively explored, and in particularly for electrospun fibers.

Some short term aging studies for specific properties have been performed on electrospun fibers, for example, Li et al. investigated the aging conditions in relation to the water stability of a green tea polyphenol within an electrospun corn protein fiber,

[2] Shepherd, L.M.; Frey, M.W.: to be submitted.

however, this study was limited to only three days of aging.[11] Kim et al. investigated the degradation and hydrophilic nature of PLA/lactide/PLA-*b*-PEG-PLA nanofibers over the slightly longer duration of seven weeks for a potential use in biodegradable biomedical membranes.[7] In this study we demonstrate the stability of fiber mats, and give an indication of the shelf life, where our main concern is that the wetting properties remain relatively unchanged over time under humid storage conditions.

It has been demonstrated that modified electrospinning system, PLA/PLA-*b*-PEG creates a continuous nanofiber that enhances phase separation of the hydrophilic component, PEG, to the fiber's surface (for a final fiber concentration of 12 wt% PEG).[6] The phase behavior and location of hydrophilic PEG in the spun nanofibers has not been investigated with time (i.e., aging) in PLA/PLA-*b*-PEG nanofibers. This paper describes whether a quasi-equilibrium condition, particularly in water wicking ability is reached during aging of PLA/PLA-*b*-PEG nanofibers and its viability in long term storage.

3.2 Experimental Section

3.2.1 Materials

Needle Deflect point 20 gauge x 2 inches is purchased from Fisher Scientific Company LLC. Copolymers (mPEG-*b*-PLA): PLA(1000)-*b*-PEG(5000) and PLA(1000)-*b*-PEG(10000) are purchased from Advanced Polymer Materials Inc. N,N-Dimethylformamide (DMF), Anhydrous, 99.8% is purchased from Sigma-Aldrich. PLA 4043D pellets (For spun PLA fibers, MW= 150,000 g/mol, PDI=1.81)

manufactured by NatureWorks LLC were purchased through Jamplast. Inc.

3.2.2 Electrospinning

Electrospinning solutions in this study are made of high molecular weight PLA with 12wt% PEG from PLA(1000)-*b*-PEG(5000) and PLA(1000)-*b*-PEG(10000) copolymers in the final fibers. All solutions containing PLA-*b*-PEG are made to contain a total of 22wt% PLA in solution. Before electrospinning, we dissolved the polymeric dopes containing DMF homogeneously with heat. A modified electrospinning apparatus, previously described[6] is used to keep the syringe at 70˚C ± 5˚C during electrospinning while a heat gun (Master Appliances Corp.) is used to keep approximately 2/3 the way up the needle at 75˚C ± 6˚C. We measure the needle's temperature using a digital thermometer (Fisher Scientific Company LLC). A voltage of 15 kV (Gamma High Voltage Research Inc.) is applied to the needle and placed ~10 cm away from the grounded collector. We maintain a solution feed rate of 10 μL/min using a programmable PHS Ultra syringe pump (Harvard Apparatus). A metal plate is used for collection of water wicking samples, while all other samples are electrospun onto aluminum foil.

3.2.3 Aging of Fibers

To hasten the aging effects of the electrospun fibers, all samples are stored in at 21°C and 65% relative humidity (RH) for the duration of the study (48 to 49 weeks), except when being removed for sample testing.

3.2.4 Field Emission Scanning Electron Microscopy (FESEM)

This research uses FESEM imaging to investigate the morphology of the electrospun fibers that have been stored for varying times. We sputter coat samples in gold-palladium prior to imaging them with a LEO 1550 FESEM using a 1kV accelerating voltage. Utilizing ImageJ™ software on the recorded SEM images, we determined the average diameters of the fibers. Three separate images of samples were used to collect a total of 50 measurements.

3.2.5 Differential Scanning Calorimetry (DSC)

Using a DSC Q2000 we determine the effects of PEG on the overall fiber properties. Cycling thermographs of our samples are heated from -80°C to 180°C at a rate of 5°C/min, cooled to -80°C at a rate of 2°C/min, and re-heated at a rate of 5°C/min to investigate the thermal properties of PLA and PLA/PLA-*b*-PEG fibers as a function of time under humid storage conditions.

3.2.6 Wettability in Water

Each electrospun sample was cut into 3 cm x ½ cm fabrics. We weighed the samples and then put a fishhook through the nanofiber mat to ensure the fabric penetrated the meniscus; this method was previously described.[6] Water wicking tests were done using a KSV Sigma 701.

3.3 Results and Discussion

3.3.1 SEM & Fiber Diameter

When possible we took SEM images to see if there were any morphological or fiber

diameter changes with aging and being exposed to the humid conditions. Initial images and final images are shown in Figure 3.1.

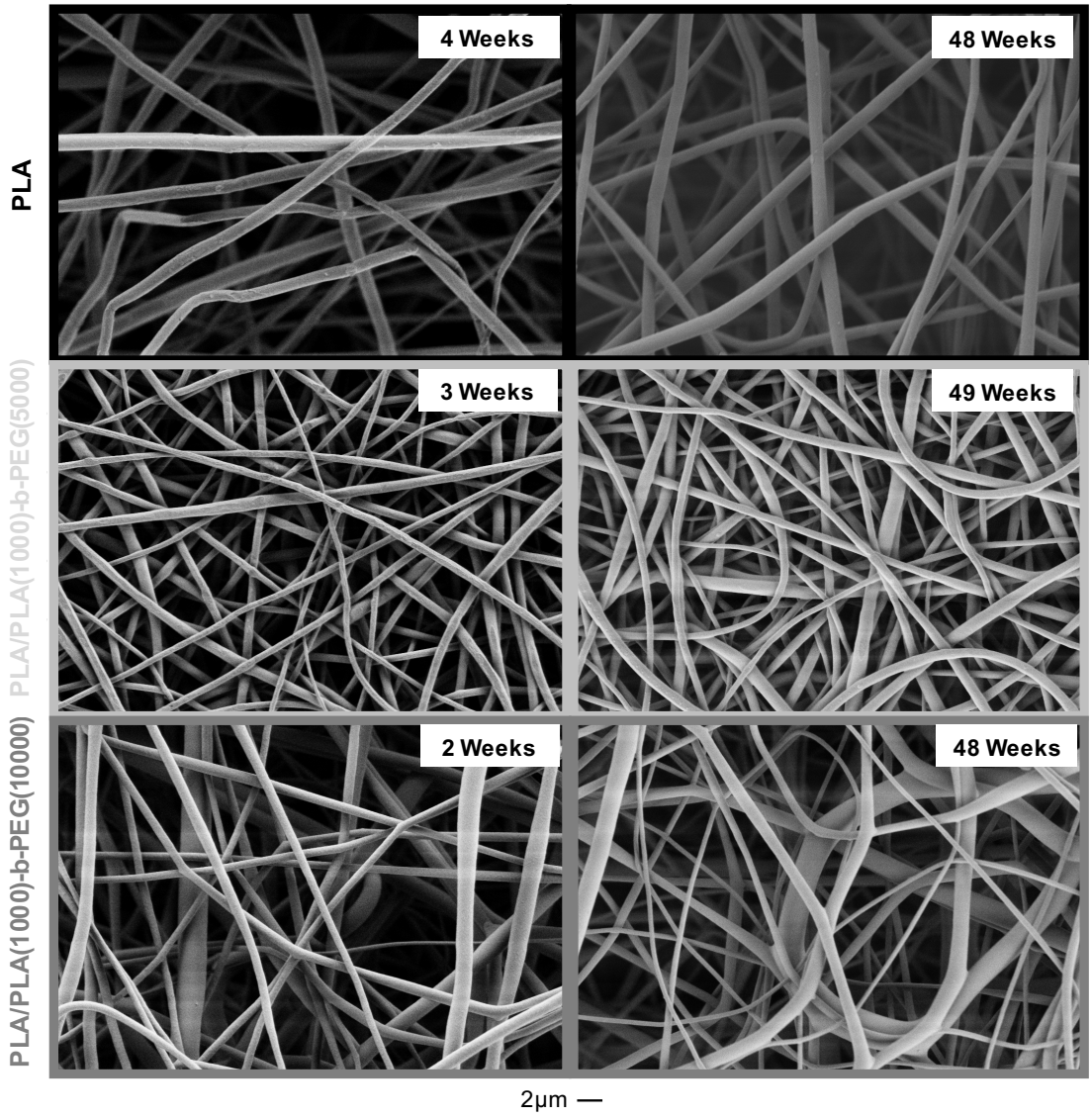

Figure 3.1 Aged SEM images of PLA and PLA/PLA-*b*-PEG fibers.

There did not appear to be any significant changes in fiber morphology for any of the spun fibers. Along with no significant change in morphology, fiber diameters also did not significantly change from the first measurements to the last (Figure 3.2). Therefore, the storing of these fibers for long durations will not much affect the surface area of

fiber mats.

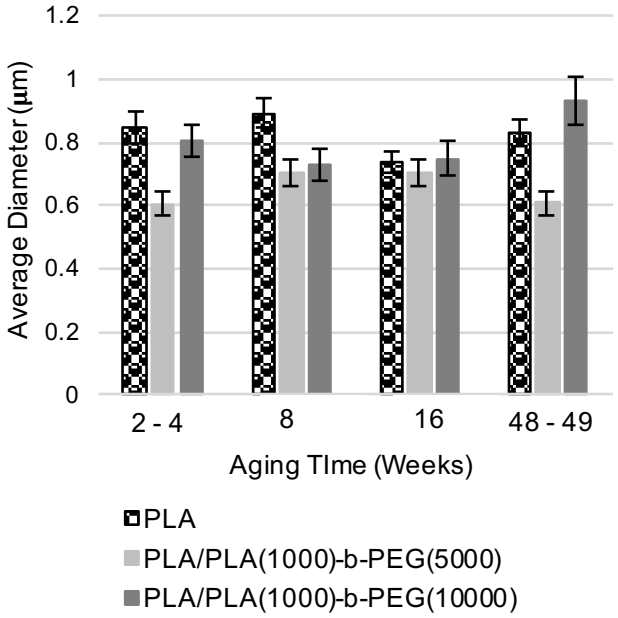

Figure 3.2 Fiber diameters for aged PLA and PLA/PLA-*b*-PEG fibers. Note: error bars represent standard error.

3.3.2 Differential Scanning Calorimetry (DSC) Thermal Analysis

Using the first heat thermographs, we calculate the crystallinity of PLA using equation 3.1, where X_c is the % crystallinity of PLA, ΔH_c is the heat of cold crystallization ($J \cdot g^{-1}$) , ΔH_f is the heat of fusion ($J \cdot g^{-1}$), and ΔH_{m° is the heat of fussion for 100 % crystalline PLA (here we use 93.6 $J \cdot g^{-1}$ [12]). We correct for samples containing PEG by dividing by the weight fraction of PLA (f_{PLA}) in the final fibers (0.88 for fibers containing 12 wt% PEG).

$$X_c = \frac{\Delta H_f - \Delta H_c}{(\Delta H_{m^o})(f_{PLA})} \, x\, 100 \qquad \text{Equation 3.1}$$

Incorporating copolymers increases the crystallinity of PLA, with shorter block length PEG more effectively crystallizing PLA (Figure 3.3a). Over 48 weeks the increase of

PLA's crystallization by PLA(1000)-*b*-PEG(5000) was greater than PLA(1000)-*b*-PEG(10000), confirming lower molecular weight copolymers are better able to plasticize PLA.

With our copolymer addition, the glass transition temperauter of PLA (T_g^{PLA}) is decreased as the result of PEG's plasticizing effect (Figure 3.3 and Figure 3.4). With aging, however, the T_g^{PLA} increases by ~13 and 9 ºC for PLA(1000)-*b*-PEG(5000) and PLA(1000)-*b*-PEG(10000) respectively (Figure 3.3b). These values for T_g^{PLA} , however should not be considered absolute since the melting temperature of PEG (T_m^{PEG}) merges with this value over time.

The observance of the T_m^{PEG} in blends and electrospun fibers has been thought to indicate phase separation.[13, 14] Even with different storage conditions and a higher temperature at the needle tip than previously used by Buttaro et al., we still find two peaks representing the T_g^{PLA} and the T_m^{PEG} ; this indicates the process of electrospinning results in polymer-polymer phase separation of PEG for PLA(1000)-*b*-PEG(5000) (circled in Figure 3.4b). After 16 weeks of aging, however, these two peaks merge into one (Figure 3.4). There may also be some indication that the PEG from PLA(1000)-*b*-PEG(10000) after 24 hours of aging is also phase separated, however instead of two peaks we observe a shallowing of the T_g^{PLA} that deepens after 8 weeks of aging (Figure 3.4c) After 16 weeks for PLA/PLA(1000)-*b*-PEG(5000) and 8 weeks for PLA/PLA(1000)-*b*-PEG(10000) first heat thermographs show no significant changes.

It should be noted that in cooling thermographs we also observed a peak that may be associated with the crystallization temperature of PEG. This occurrence would likely indicate PEG phase separation.[13] There is a distinct peak for PLA/PLA(1000)-*b*-PEG(5000) starting at 24 hours of aging, but we do not clearly see this peak in PLA/PLA(1000)-*b*-PEG(10000) until 16 weeks of aging (possibly 8 weeks).

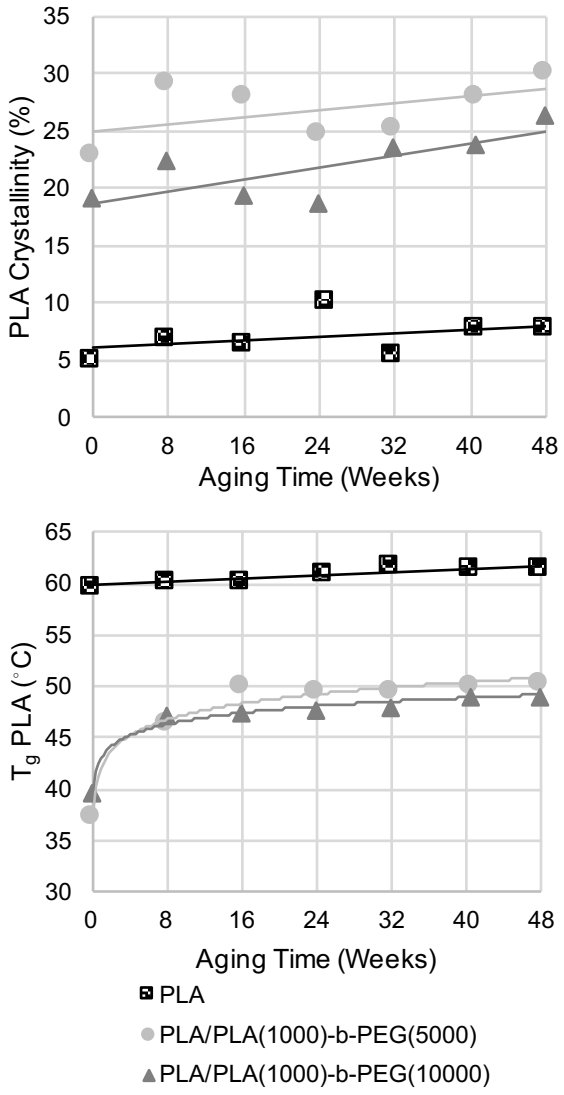

Figure 3.3 (a) the calculated PLA percent crystallinity and (b) T_g^{PLA}. Note: Initial measurements are taken after aging 24 hours.

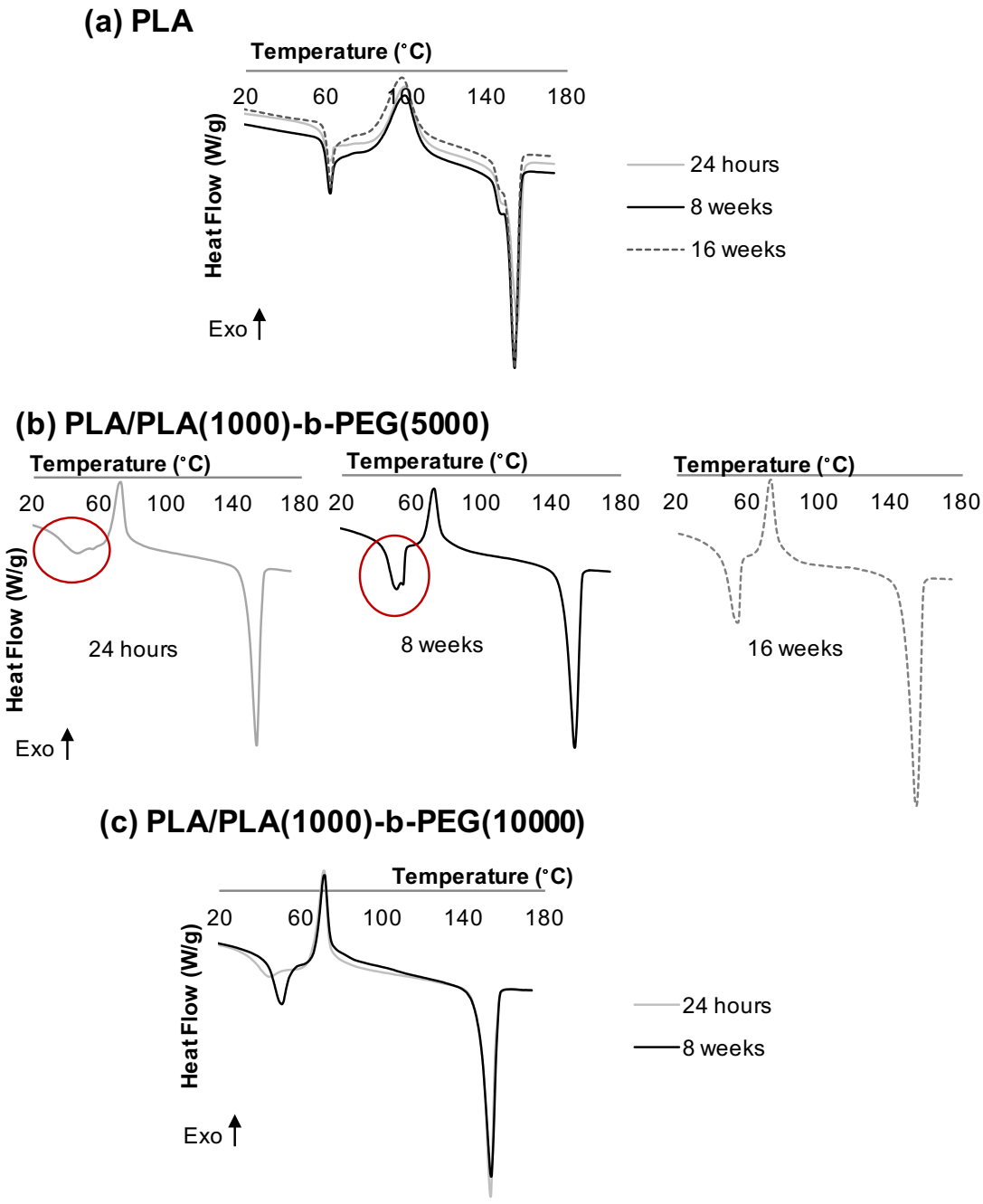

Figure 3.4 DSC first heat thermographs (a) PLA, (b) PLA/PLA(1000)-*b*-PEG(5000), and (c) PLA/PLA(1000)-*b*-PEG(10000).

3.3.3 Water Wicking

With the addition of copolymers to PLA fibers, the water wicking ability of the fiber mats is increased over plain PLA fibers (Figure 3.5). Under the conditions of this study, at the initial wettability measurement of 24 hours of aging, fibers containing PLA(1000)-*b*-PEG(5000) are able to wick more water than those containing PLA(1000)-*b*-PEG(10000). We find fibers containing PLA(1000)-*b*-PEG(5000) also quickly equilibrate to their equilibrium condition compared to PLA(1000)-*b*-PEG(10000), whose wicking ability follows less of a trend. With the shorter block length of PEG, PLA(1000)-*b*-PEG(5000) is better able to migrate within the fiber. An equilibrium condition is met for the fibers containing copolymers after 8 and 16 weeks for PLA(1000)-*b*-PEG(5000) and PLA(1000)-*b*-PEG(10000), respectively. The equilibrium condition for water wicking of PLA/PLA(1000)-*b*-PEG(5000) and PLA/PLA(1000)-*b*-PEG(10000) fibers remains higher than that of PLA fibers alone. These findings suggest that electrospun fiber initial properties are not necessarily the equilibrium properties, therefore for real use applications the properties should be tested after an equilibrium is achieved.

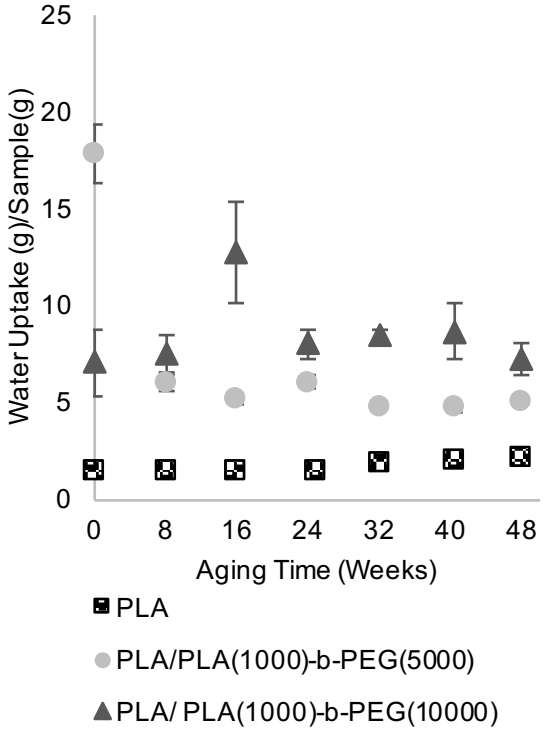

Figure 3.5 Water wicking data for PLA and PLA/PLA-*b*-PEG fibers aged from 24 hours to 48 weeks. Note: error bars represent standard error.

3.4 Conclusions

Electrospun fibers of PLA/PLA(1000)-*b*-PEG(5000) and PLA/PLA(1000)-*b*-PEG(10000) (containing 12 wt% of PEG in the final fibers) were aged for 48-49 weeks in humid conditions. There are no real changes in morphology or fiber diameter over time.

There is an increase in the crystallization of PLA with the addition of copolymers, and the DSC reveals slight changes in the % crystallinity of PLA over time. The T_g^{PLA} was decreased with copolymer addition however after 8 weeks of aging this value increased, and after which remained fairly constant. The T_m^{PEG} was present for fibers containing

PLA(1000)-*b*-PEG(5000) at 24 hours and 8 weeks of aging, however after this point the T_m^{PEG} merged with the T_g^{PLA}. Fibers containing PLA(1000)-*b*-PEG(10000) showed a shallowing of the T_g^{PLA} at 24 hours of aging instead of a distinct PEG melting; after this time, the transition deepened.

Water wicking properties were fairly consistent after 8 weeks of aging for PLA/PLA(1000)-*b*-PEG(5000) and after 16 weeks for PLA/PLA(1000)-*b*-PEG(10000). PLA-*b*-PEG additions to PLA equilibrated to a higher water wicking amount of water in comparison to PLA fibers alone. These findings suggest that electrospun fiber initial properties are not necessarily the equilibrium properties, therefore for real use applications the properties should be tested after an equilibrium is achieved. Based on these results it may be an interesting study to investigate aging on the water wicking properties over the short time scale for PLA/PLA-*b*-PEG fibers to determine if the drastic change in water wicking at 8 weeks for PLA/PLA(1000)-*b*-PEG(5000) happened gradually or not.

3.5 Acknowledgements

This work was also in part funded by a grant from the Department of Fiber Science & Apparel Design Graduate Student Research Awards Fund. Heating element apparatus used in electrospinning was provided by Dr. Daehwan Cho. This research made use of the Cornell Center for Materials Research Shared Facilities which are supported through the NSF MRSEC program (DMR-1120296).

REFERENCES

1. Tsou, P. H.; Chou, C. K.; Saldana, S. M.; Hung, M. C.; Kameoka, J., The fabrication and testing of electrospun silica nanofiber membranes for the detection of proteins. *Nanotechnology* **2008,** *19* (44).
2. Yoo, H. S.; Kim, T. G.; Park, T. G., Surface-functionalized electrospun nanofibers for tissue engineering and drug delivery. *Advanced Drug Delivery Reviews* **2009,** *61* (12), 1033-1042.
3. Senecal, A.; Magnone, J.; Marek, P.; Senecal, K., Development of functional nanofibrous membrane assemblies towards biological sensing. *Reactive & Functional Polymers* **2008,** *68* (10), 1429-1434.
4. Cho, D. W.; Matlock-Colangelo, L.; Xiang, C. H.; Asiello, P. J.; Baeumner, A. J.; Frey, M. W., Electrospun nanofibers for microfluidic analytical systems. *Polymer* **2011,** *52* (15), 3413-3421.
5. Hendrick, E.; Frey, M., Increasing Surface Hydrophilicity in Poly(Lactic Acid) Electrospun Fibers by Addition of Pla-b-Peg Co-Polymers. *Journal of Engineered Fibers and Fabrics* **2014,** *9* (2), 153-164.
6. Buttaro, L. M.; Drufva, E.; Frey, M. W., Phase Separation to Create Hydrophilic Yet Non-Water Soluble PLA/PLA-b-PEG Fibers via Electrospinning. *Journal of Applied Polymer Science* **2014,** *131* (19).
7. Kim, K.; Yu, M.; Zong, X. H.; Chiu, J.; Fang, D. F.; Seo, Y. S.; Hsiao, B. S.; Chu, B.; Hadjiargyrou, M., Control of degradation rate and hydrophilicity in electrospun non-woven poly(D,L-lactide) nanofiber scaffolds for biomedical applications. *Biomaterials* **2003,** *24* (27), 4977-4985.
8. González, E.; Shepherd, L. M.; Saunders, L.; Frey, M. W., Surface Functional Poly (lactic Acid) Electrospun Nanofibers for Biosensor Applications. *Materials* **2016,** *9* (1), 47.
9. Hu, Y.; Rogunova, M.; Topolkaraev, V.; Hiltner, A.; Baer, E., Aging of poly(lactide)/poly(ethylene glycol) blends. Part 1. Poly(lactide) with low stereoregularity. *Polymer* **2003,** *44* (19), 5701-5710.
10. Hu, Y.; Hu, Y. S.; Topolkaraev, V.; Hiltner, A.; Baer, E., Aging of poly(lactide)/poly(ethylene glycol) blends. Part 2. Poly(lactide) with high stereoregularity. *Polymer* **2003,** *44* (19), 5711-5720.
11. Li, Y.; Lim, L. T.; Kakuda, Y., Electrospun Zein Fibers as Carriers to Stabilize (-)-Epigallocatechin Gallate. *Journal of Food Science* **2009,** *74* (3), C233-C240.
12. Ero-Phillips, O.; Jenkins, M.; Stamboulis, A., Tailoring Crystallinity of Electrospun Plla Fibres by Control of Electrospinning Parameters. *Polymers* **2012,** *4* (3), 1331-1348.
13. Li, F. J.; Zhang, S. D.; Liang, J. Z.; Wang, J. Z., Effect of polyethylene glycol on the crystallization and impact properties of polylactide-based blends. *Polymers for Advanced Technologies* **2015,** *26* (5), 465-475.
14. Buttaro, L. M.; Drufva, E.; Frey, M. W., Phase Separation to Create Hydrophilic Yet Non-Water Soluble PLA/PLA-b-PEG Fibers via Electrospinning. *J. Appl. Polym. Sci.* **2014,** *131* (19), 41030 (7 pp).

CHAPTER 4

SURFACE FUNCTIONAL POLY(LACTIC ACID) ELECTROSPUN NANOFIBERS FOR BIOSENSOR APPLICATIONS[3]

4.1 Introduction

Electrospinning is a well-established technique widely used to create continuous fibers with diameters ranging from a few micrometers down to tens of nanometers. This technique has gained extraordinary relevance in the last few decades due to its inexpensive nature and simplicity [1–4]. Electrospun polymeric nanofibers present unique properties, such as high surface area to volume ratio, porous structure and excellent pore interconnectivity, which make them attractive for a wide range of applications [1,4,5] including biosensors [6–9]. A small volume of electrospun fiber mat may provide a large surface area for sensing together with an easy access for the analyte to detection sites.

When nanofibers are used to construct biosensors, different important factors must be considered and combined; (1) surface functionality; (2) hydrophilicity; and (3) water solubility of the fibers. The nanofiber surface must be functional to interact with (or immobilize) biological molecules. Moreover, as most biological systems are aqueous, hydrophilic surfaces have shown to provide an increase in the materials function as biosensor as well as their biocompatibility [10,11]. Lastly, the fiber mat must be water insoluble to avoid its degradation in the aqueous phase.

[3] González, E.; Shepherd, L.M.; Saunders L.; Frey, M.W. Surface Functional Poly(Lactic Acid) Electrospun Nanofibers for Biosensor Applications. *Materials* **2016**, 9(1), 47.

Biotin and avidin (or streptavidin) binding has been broadly used to immobilize biologically active materials on surfaces in tissue engineering and biosensor applications [12–15]. Our research group has successfully synthesized biocompatible functional nanofibers incorporating biotin to poly(lactic acid) (PLA) nanofibers up to 18 weight total percent (wt %). These nanofiber membranes were able to immobilize streptavidin, which at the same time, was able to immobilize biotinylated nucleic acid probes and antibodies [6,16,17]. Li *et al*. [17] quantified the amount of incorporated biotin that was available for streptavidin binding at the PLA fibers surface by competitive colorimetric assays. They observed a non-linear increase of the surface available biotin compared to the overall biotin concentration, obtaining a maximum of 11% of the total incorporated biotin available at the fiber surface.

One of the major drawbacks of using PLA as a biosensor substrate is its high hydrophobicity, which has a negative impact in the wettability of the final nanofibers. A feasible method to increase the hydrophilicity of PLA is by blending it with a hydrophilic polymer [18–22]. Researchers have been able to increase the wettability of PLA nanofibers by the incorporation of poly(lactic acid)-*block*-poly(ethylene glycol) (PLA-*b*-PEG) block copolymers and PEG oligomers into the spinning dope [20,21]. During the electrospinning process, block copolymers and oligomers phase separated to create a fiber with hydrophilic PEG at the surface. Incorporation of PLA-*b*-PEG block copolymers was more efficient than PEG oligomers, resulting in fibers with higher homogeneity and wettability [20,21]. Buttaro *et al*. [21] studied the influence of block copolymer length and concentration, finding that the maximum wettability was obtained

when PLA(1000)-*b*-PEG(5000) block copolymers were used at 12 wt % of PEG in the final fiber.

In this work, biotin surface functionalized hydrophilic PLA nanofibers were developed by the addition of different concentrations of biotin (up to 18 wt %) together with PLA-*b*-PEG block polymers to the spinning dope. For this purpose a modified electrospinning apparatus with a heating component [21] was used and the morphology, surface-available biotin and water stability of the final fibers was studied. The incorporation of the PLA-*b*-PEG block polymers to the fibers not only increased their wettability but also aided the migration of biotin to the surface producing a 506% increase of surface-available biotin.

4.2 Experimental Section

4.2.1 Materials

Needle Deflect point 20 g × 2 in. was purchased from Fisher Scientific Company (Atlanta, GA, USA). PLA-*b*-PEG block copolymer was synthesized by ring opening polymerization of lactide (Sigma-Aldrich, Allentown, PA, USA) in the presence of poly(ethylene glycol) methyl ether (Number average molecular weight (Mn): 5000 g/mol, Sigma-Aldrich), using stannous octoate (Sigma-Aldrich) as catalyst [23-26]. The final block copolymer contained 10 units of lactic acid and a molar mass dispersity value of 1.05 determined by nuclear magnetic resonance (NMR) and gel permeation chromatography (GPC) (see supplementary material for detailed synthesis procedure and characterization). Anhydrous DMF 99.8%, PBS and Tween 20 were all purchased from Sigma-Aldrich. PLA 4043D (M_W: 1.5×10^5 g/mol, molar-mass disperisity (Đ):

1.81) was purchased from NatureWorks (Blair, NE, USA). Pierce™ Biotin HABA/avidin Quantitation Kit was purchased from ThermoFisher Scientific (Rockford, IL, USA).

4.2.2 Preparation of Electrospinning Solutions

Two homogeneous electrospinning solution sets were prepared by dissolving them in DMF for at least 1.5 h at 70 ± 5 °C; (1) high molecular weight PLA and biotin (0, 5, 10, and 18 wt % in the final fiber) and (2) high molecular weight PLA, PLA-*b*-PEG block copolymer and biotin (0, 5, 10 and 18 wt % in the final fiber). All initial solutions contained a total of 22 wt % of PLA. The amount PLA-*b*-PEG block copolymers added was adjusted to obtain a final fiber with a composition of 12 wt % of PEG.

4.2.3 Electrospinning

We utilized the modified electrospinning apparatus and procedure described previously by Buttaro *et al*. [21]. A high voltage supply (Gamma high Voltage Research) provided 15 kV to the needle tip and a grounded copper collector was placed 10 cm away. The solution feed rate was maintained at 10 μL/min using a programmable PHS Ultrasyringe pump (Harvard Apparatus, Holliston, MA, USA). During electrospinning, a shielded heating unit preheated to 70 ± 5 °C controlled the syringe temperature. A heat gun (Master Appliances Corp., Racine, WI, USA) was used to keep the needle temperature at 70 ± 5 °C. The temperature at the needle was verified approximately every 30 min using a digital thermometer (Fisher Scientific Company, Pittsburgh, PA, USA). The polymer solution was spun for 45 min to 1 h obtaining a fiber mat with a thickness of approximately 400

μm.

4.2.4 FESEM Imaging and Energy Dispersive Spectroscopy (EDS)

Images were taken at 1 kV voltage using a Zeiss 1550 FESEM (Zeiss, Oberkochen, Germany to analyze fiber morphology. Samples were left uncoated during imaging. ImageJ™ open source software (National Institutes of Health, Bethesda, MD, USA, http://imagej.nih.gov/ij/) was used on the FESEM images to measure the mean average fiber diameters. Fifty measurements were taken for each sample from three separate images.

EDS was used was used to confirm the presence of biotin in the fibers and to analyze its distribution. Sulfur atom was used as an indicator of biotin molecules in the spun fiber. Polymer and biotin structures as well as EDS spectra are shown in supplementary material. Five spectra were collected at 10 kV for 30 seconds in random areas (11 × 7.5 μm) of each sample and S/C atom ratio was quantified in all of them.

4.2.5 Colorimetric Assay

A competitive colorimetric assay was performed based on the work carried out by Li and co-workers [17] to quantify the amount of available biotin at the fibers surface. A Lambda 35 UV/Vis Spectrophotometer from Perkin Elmer (Beaconsfield, England) was employed to measure the change in absorbance at 500 nm. Experiments were performed using a Pierce™ Biotin Quantitation Kit from ThermoFisher Scientific (Rockford, IL, USA). Reconstitution of the HABA/avidin solution was performed as per the

manufacturer protocol. First, the absorbance of the HABA/avidin solution in PBS Buffer was measured at 500 nm. Then, a pre-weighted small piece of the fiber mat was placed into the cuvette and shaken for three minutes, the fiber was removed and the absorbance of the solution was measured again. The absorbance measurement was repeated until the obtained value was stable. The surface-available biotin was calculated using the following equation [17]:

$$Surface\ available\ biotin\ (mg\ biotin/g\ fiber) = (A_{500}^{0} - A_{500})\left(\frac{Mw_{biotin}V}{\varepsilon bW}\right)\times 10^{3} \quad \text{Equation 4.1}$$

where, A_{500}^{0} is the absorbance of the solution prior to the addition of nanofiber; A_{500} is the absorbance of the solution after reaction with nanofiber; Mw_{biotin} is the molecular 1weight of the biotin (244.3 g/mol);V is the volume of the solution (L); b is the cuvette path length (1 cm); ε is the extinction coefficient of the HABA/avidin complex at 500 nm (3.4×10^4 L/(mol cm)); and W is fiber mat weight (g).

4.2.6 Water Stability

PLA and PLA/PLA-*b*-PEG fibers with 0 and 18 wt % of biotin were cut into 3 × 1 cm rectangles, weighed and immersed in individual vials with 15 mL of DI water for one day and one week. Three replicates of each sample were prepared. Once the samples were removed from the water, they were dried in a vacuum oven at room temperature for 24 h and reweighed to determine their weight loss. Another competitive colorimetric assay was performed on the fibers to assess the amount of biotin retained at the fiber surface.

4.3 Results and Discussion

4.3.1 Fiber Morphology by Field Emission Scanning Electron Microscopy (FESEM)

Two sample sets were prepared and their fiber morphology was analyzed by FESEM. In the first set, varying concentrations of biotin (0, 5, 10, and 18 wt % in the final fiber) were incorporated into PLA fibers by dissolving it in the initial PLA/dimethylformamide (DMF) spinning dope at elevated temperatures. DMF was chosen as solvent since it has shown to improve the dispersion of biotin in the final fiber [16]. In the second set, the same biotin concentrations were incorporated to the PLA/DMF spinning solutions with the addition of PLA-*b*-PEG block copolymers. The amount of PLA-*b*-PEG was adjusted to obtain 12 wt % of PEG in the final fibers in order to achieve maximum wettability [21].

Fibers containing just biotin and PLA (Figure 4.1) show a smooth, bead-free and uniform morphology. No clear trend was observed in the mean average fiber diameters as the amount of biotin added increased (Figure 4.2). Thus, as previously observed by Frey and co-workers [16], addition of biotin to the spinning dope did not affect the final fiber morphology. When PLA-*b*-PEG copolymers were added (Figure 4.3), fibers appeared significantly smaller and again, no clear difference or trend was observed in the fiber diameter with the addition of biotin (Figure 4.2). Other authors also observed a decrease in fiber diameter when PLA-*b*-PEG or PEG oligomers were added to the spinning dopes [20,21,27–29] and was attributed to a decrease in the electrospinning solution viscosity.

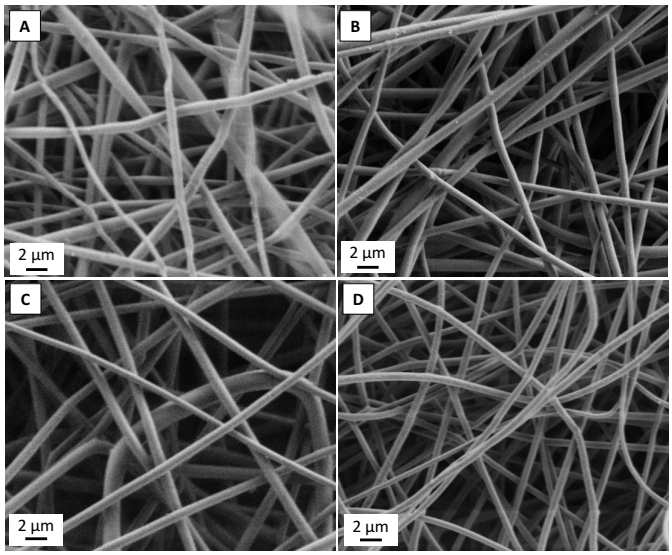

Figure 4.1 SEM images of PLA samples containing different amounts of biotin: (**A**) 0 wt %; (**B**) 5 wt %; (**C**) 10 wt % and (**D**) 18 wt %.

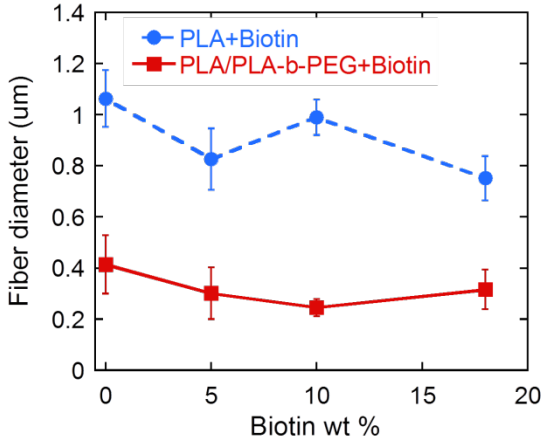

Figure 4.2 Average fiber diameter of PLA and PLA/PLA-*b*-PEG samples containing different amounts of biotin.

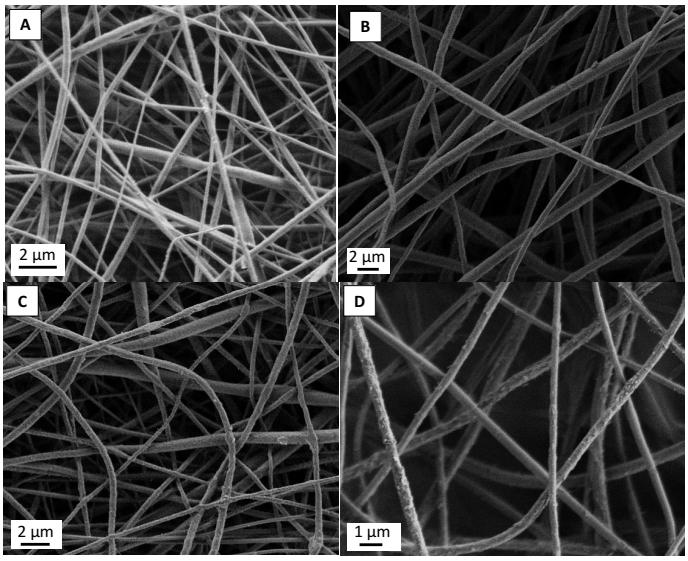

Figure 4.3 SEM images of PLA/PLA-*b*-PEG samples containing different amounts of biotin: (**A**) 0 wt %; (**B**) 5 wt %; (**C**) 10 wt % and (**D**) 18 wt %.

4.3.2 Biotin Distribution and Measurement of Surface-Available Biotin

Energy dispersive spectroscopy (EDS) was used to analyze the distribution of biotin in the nanofiber mats. Five spectra were collected in random areas of each sample and the sulfur/carbon atom (S/C) ratio was quantified. Results are shown in Figure 4.4. As expected, the S/C atom ratio increased as the amount of biotin in the sample was increased. No statistically significant differences were observed between the results of PLA and PLA/PLA-*b*-PEG samples when 5 and 18 wt % of biotin was added and, more importantly, low standard deviation values were obtained in all cases, indicating that the amount of biotin was similar in all analyzed areas. Thus, it can be concluded that in both cases, PLA and PLA/PLA-*b*-PEG samples, biotin was well dispersed and the distribution of biotin in the fiber mats was mainly homogeneous.

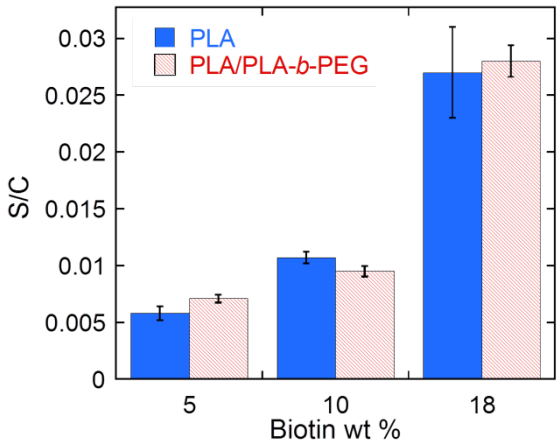

Figure 4.4 Sulfur/carbon (S/C) atom ratio of PLA and PLA/PLA-*b*-PEG samples with different biotin loading quantify by EDS analysis.

The penetration depth of the EDS analysis is on the micron scale (around 1 to 3 μm) and sulfur atoms associated with biotin in this analysis were located throughout the fiber thickness. As only the molecules located at the fiber surface are of interest, competitive colorimetric assays were used to quantify the amount of biotin available at the surface of the nanofibers [17]. The method consisted of adding a small, pre-weighed piece of fiber mat into a 4′-hydroxyazobenzene-2-carboxylic acid (HABA)/avidin solution and measuring the difference in the absorbance of the solution at 500 nm. HABA and avidin bind strongly to produce an orange colored complex that absorbs light at 500 nm. When a fiber mat containing biotin is added to the HABA/avidin complex solution, avidin is removed from the complex and binds with biotin due to its higher affinity, causing a decrease in the absorbance. Figure 4.5 shows the distinct visual color change between the orange HABA/avidin complex solution and the yellow HABA solution after avidin selectively binds to the biotin in the submerged fiber mat. It should be mentioned that no change in the absorbance of the HABA/avidin complex solution was observed when the control PLA and PLA/PLA-*b*-PEG samples (with 0 wt % biotin) were added. This

indicates that the change in the absorbance of the solution can only be attributed to the presence of biotin at the fiber surface.

Results of the colorimetric assays are shown in Figure 4.6. In the case of the PLA fibers, results correlate well with those reported by Li *et al*. [17]. Still in agreement with the previous work, the increment in the surface-available biotin was not linear regarding the total concentration of biotin added to the spinning dope. A small amount of surface-available biotin was measured in fibers containing an overall concentration of 5 and 10 wt % of biotin, 0.75 ± 0.18 and 0.50 ± 0.05 mg biotin/g fiber respectively. In these cases, only about 0.5%–1.5% of the overall amount of biotin added was present at the fiber surface. The amount of surface-available biotin drastically increased to 17.7 ± 5.2 mg biotin/g fiber when 18 wt % of biotin was added to the spinning dope, corresponding to 9.8% of the overall amount of biotin.

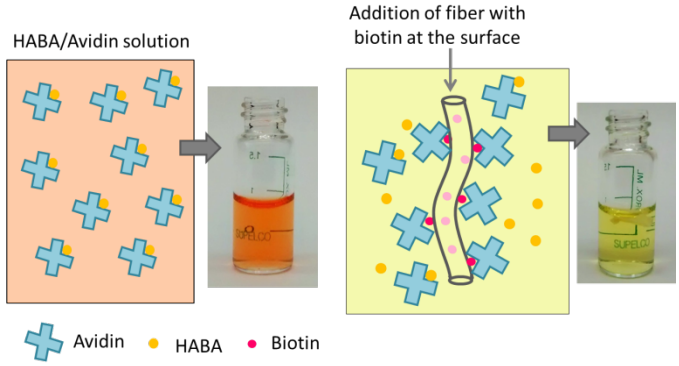

Figure 4.5 Illustrations and real pictures of the HABA/avidin solutions. Initially, HABA and avidin form a complex with a strong orange color (absorbs light at 500 nm). When a fiber containing biotin is added to the solution, avidin binds biotin due its higher affinity breaking the HABA/avidin complex and leading to a color change (decrease in the absorbance at 500 nm).

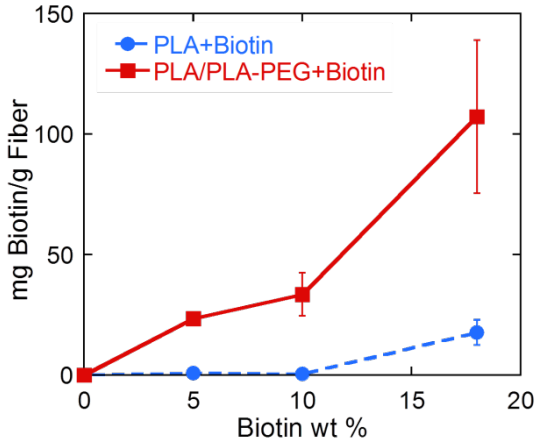

Figure 4.6 Surface available biotin of PLA and PLA/PLA-*b*-PEG samples containing different amounts of overall biotin.

In the case of PLA/PLA-*b*-PEG fibers, the surface-available biotin was significantly higher than in PLA fibers for all biotin concentrations (Figure 4.6). Again, a non-proportional relationship was observed between the overall biotin concentration and the surface-available biotin. 23.4 ± 2.1 and 33.5 ± 8.9 mg Biotin/g fiber were measured in fibers containing 5 and 10 wt % of biotin, respectively, and a drastic increase to 107.2 ± 31.8 mg biotin/g fiber was observed when the overall amount of biotin was 18 wt %. Thus, when PLA-*b*-PEG is present, the addition of just 5 wt % of biotin leads to fibers with slightly higher surface-available biotin than when 18 wt % of biotin is added to PLA fibers. For PLA/PLA-*b*-PEG fibers containing 5, 10 and 18 wt % of biotin, 46.8%, 33.5% and 59.6% of the total biotin added was available at the surface respectively.

According to Li *et al.* [17], phase separation of biotin towards the fiber surface was driven by two main phenomena; the first one was the enhancement of the migration of polarizable species (biotin in this case) to the fiber surface due to electric field applied

during the electrospinning process [30–32]. The second one was the lack of entropy of mixing in the polymer system that favors the phase separation of the components [23].

One of the parameters that could have influenced the colorimetric assay is the wettability of the sample. Penetration of HABA/avidin complex solution into the fiber mat might be easier in hydrophilic samples. Since the wettability of the PLA/PLA-*b*-PEG fibers was higher than the wettability of PLA fibers [21], several of the colorimetric assays for PLA samples were repeated increasing the wetting by the use of Tween 20 surfactant (Sigma-Aldrich, Milwaukee, WI, USA) [17]. Nevertheless, no significant differences were observed in the obtained results, proving that the low surface-available biotin measured in the case of PLA samples was not an artifact of the low wettability of the samples.

Another important parameter to be considered is the surface area of the sample. Therefore, in order to check if the increase in the surface-available biotin of the PLA/PLA-*b*-PEG samples was due to the enhanced migration of the biotin to the fiber surface or simply due to the larger surface area of these samples (as fiber diameter was smaller, the surface area of the samples was larger for the same sample mass), the amount of biotin molecules per square nanometer in the fibers surface was calculated (calculations are explained in the supplementary material). Results are shown in Table 4.1. It can be clearly observed that PLA/PLA-*b*-PEG fibers contained more biotin molecules at their surface compared to PLA fibers for the same area.

Table 4.1 Fiber surface area values and amount of biotin molecules per square nanometer at the fibers surface.

	Surface Area of the Fiber (m^2/g)		Biotin Molecules/nm^2	
Overall Biotin %	**PLA**	**PLA/PLA-*b*-PEG**	**PLA**	**PLA/PLA-*b*-PEG**
0	2.1	5.5	0	0
5	2.7	7.5	0.7	8
10	2.3	9.3	0.5	9
18	3.0	7.2	14	37

Taking all the above mentioned results into consideration, it can be concluded that the presence of PLA-*b*-PEG block copolymers enhances the migration of biotin to the fiber surface, giving rise to final fibers with larger concentrations of surface-available biotin.

4.3.3 Water Stability of Fibers

Although biotin [6,16,17] or block copolymers [20,21,27] have been previously incorporated into PLA fibers, their stability in water for long periods of time has never been thoroughly investigated. To this end, fibers (PLA and PLA/PLA-*b*-PEG) containing 0 and 18 wt % of biotin were immersed in water for 24 h and one week. After removing the samples from the water and drying them, their loss of weight as well as their surface-available biotin (by competitive colorimetric assay) were measured. Results are shown in Figures 4.7 and 4.8.

PLA/PLA-*b*-PEG fiber containing 18 wt % of biotin lost 97% of its surface-available biotin after being immersed in water for 24 h (Figure 4.7). The amount of surface-available biotin dropped from 107.2 ± 31.8 to 3.4 ± 1.0 mg biotin/g fiber. On the contrary, in the case of the PLA sample containing 18 wt % of biotin, an unexpected

increase of surface-available biotin was observed after one day of water immersion. Surface-available biotin increased from 17.7 ± 5.2 to 37.2 ± 8.2 mg biotin/g fiber, indicating that, in this case, the immersion of the fiber into the water enhanced the migration of the biotin buried inside the fiber to the surface due to its high hydrophilicity. Nonetheless, after one week in water, the amount of biotin dropped to 0.8 ± 0.2 mg biotin/g fiber. Thus, even if the migration of biotin to the surface was first enhanced when PLA fibers were immersed in water, after longer periods of time, biotin migrated from the fiber surface to the aqueous phase.

The loss of weight of the fibers after being immersed in water (Figure 8) was attributed to the migration (or dissolution) of the biotin, PLA-*b*-PEG block copolymers or both to the aqueous phase. High molecular weight PLA (the main fiber forming component) was expected to be unaffected by the presence of water due to its high hydrophobicity. Overall, PLA/PLA-*b*-PEG fibers resulted in a greater weight loss than PLA fibers. The small weight differences observed for the PLA sample are attributed to experimental errors. There was no statistical difference between the weight loss after one day and one week of water immersion in PLA samples (containing 0 and 18 wt % of biotin). On the contrary, the difference was statistically significant in the case of PLA/PLA-*b*-PEG samples (containing 0 and 18 wt % of biotin). PLA/PLA-*b*-PEG samples with no biotin lost little to no weight after one day of water immersion, whereas PLA/PEG-*b*-PEG fibers with 18 wt % of biotin lost around 20% of its original weight, which was attributed mainly to the migration of biotin to the water phase (see Figure 4.7). After one week of water immersion, a loss of weight of 10% and 25% were observed for PLA/PLA-*b*-PEG

samples with no biotin and 18 wt % of biotin respectively, indicating that PLA-*b*-PEG block copolymers also migrated to the aqueous phase with time. As smaller molecules diffuse faster than larger ones, migration of biotin to the aqueous phase occurs just after one day, whereas PLA-*b*-PEG block copolymers require lengthier periods of exposure to the aqueous system.

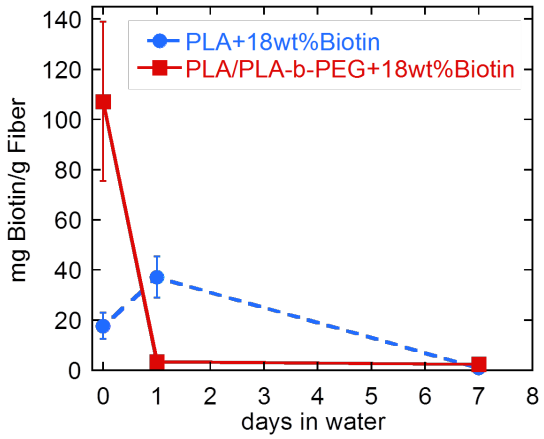

Figure 4.7 Surface available biotin of PLA and PLA/PLA-*b*-PEG fibers containing 18 wt % of biotin after being immersed in water for different periods of time.

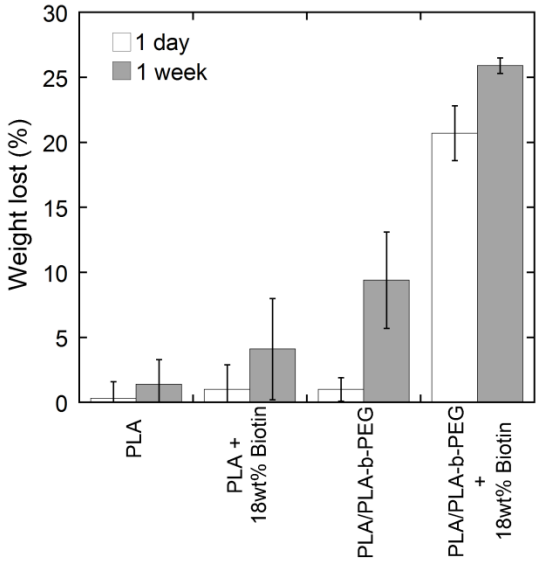

Figure 4.8 Weight loss of PLA and PLA/PLA-*b*-PEG fibers containing 0 and 18 wt % of biotin after being immersed in water for different periods of time.

Li *et al*. [6] incorporated 3 wt % of biotin into PLA fibers and proved that biotin remained on the fiber surface after washing it with phosphate buffered saline (PBS) solution. The reason for the migration of the biotin observed in this work may be due to the fact that samples were immersed in water for long time durations (one day and one week). As a conclusion, the functional hydrophilic non-water-soluble fibers presented in this work show a potential application for their use as biosensors in point-of-care diagnostics, such as paper based diagnostic devices, where short contact periods of times are required between the sensing substrate material and the sample solution [34]. Reinholt *et al.* demonstrate that PLA based electrospun nanofibers could be successfully incorporated as platform in paper-based biological lateral flow assays. By a simple adsorption of the antibodies to the nanofiber, they were able to develop an enzymatic sandwich immunoassay for the detection of *E. coli* [34]. A similar approach could be used in the future to functionalize the nanofibers developed in this work, where biotinylated antibodies could be strongly bound to fiber mat due to the biotin-avidin/streptavidin complex.

4.4 Conclusions

In this work, biotin surface functionalized hydrophilic non-water soluble PLA nanofibers were produced for their potential use as biosensors. Varying concentrations of biotin (up to 18 wt %) were incorporated into PLA/DMF spinning dopes, and PLA/PLA-*b*-PEG/DMF spinning dopes. Fibers containing biotin and PLA-*b*-PEG block copolymers showed smaller fiber diameters and rougher morphologies than PLA fibers containing just biotin. In addition, the amount biotin at the fiber surface

dramatically increased when PLA-*b*-PEG block copolymers were added, obtaining fibers with up to 60% of their total amount of biotin available at the surface. Finally, water stability test show that after immersing the fibers in water for long durations of time, both biotin and PLA-*b*-PEG block copolymers tended to migrate to the aqueous phase. As a conclusion, the functional hydrophilic nanofibers created in this work show potential application for use in point-of-care diagnostics where short contact times are required between the sensing substrate material and the sample solution.

4.5 Supplementary Materials

PLA-*b*-PEG block copolymers were synthesized by ring opening polymerization of lactide in the presence of poly(ethylene glycol) methyl ether (MeOPEG, number average molecular weight (M_n): 5000 g/mol), using stannous octoate ($Sn(Oct)_2$) as catalyst [23-24]. Polymerization reaction was performed at 140 °C in a three neck round bottom flak under continuous N_2 flow. First, MeOPEG and Lactide (previously recrystalized from ethyl acetate and dried under vacuum at 40 °C [3]) were added to the round bottom flask, the temperature was increased to 90 °C and the reaction mixture was stir under N_2 atmosphere until both components were completely melted (1 h). Then, $Sn(Oct)_2$ solution in toluene (50 wt %, being the amount of $Sn(Oct)_2$ 5 wt % respect to the total MeOPEG and lacite) was added to the reaction mixture and the temperature was increased to 140 °C to start the reaction. After 16 h, polymerization reaction was stopped by cooling it to 50 °C. The reaction product was dissolved in dichloromethane and precipitated in cold diethyl ether (by adding the solution dropwise). Finally, the polymer was isolated by vacuum filtration and dried at 40 °C

under vacuum overnight.

Molecular weight and molar mass dispersity of the synthesized copolymers was determined by Gel Permeation Chromatography (GPC) and Nuclear Magnetic Resonance (NMR). A Waters Ambient-Temperature GPC equipped with a Waters 410 differential refractive index detector (Millipore Corporation, Milford, MA, USA was used. Tetrahydrofuran (THF) was used as mobile phase with a flow rate of 1 mL/min. Obtained molecular weight values were referred to polystyrene standards. ^{1}H-NMR experiments were recorded at room temperature with a INOVA 400 spectrometer (Varian Inc., Palo Alto, CA, USA) operating at 400 MHz. $CDCl_3$ was used as solvent and tetramethylsilane (TMS) as an internal reference. The Lactide/Ethylen glycol (LA/EG) ratio of the block copolymer was determined from the integration of ^{1}H-NMR resonances belonging to the PEG blocks at 3.6 ppm (-O-CH_2-CH_2- singlet) and to the PLA blocks at 5.2 ppm (-CH quartet), as previously described in the literature [24-26]. M_n of the block copolymers was calculated according to the following equations:

$$M_n = DP_{PEG} \times 44 + DP_{PLA} \times 72 \qquad \text{Equation 4.S1}$$

$$DP_{PEG} = M_{nPEG}/44 \qquad \text{Equation 4.S2}$$

$$DP_{PLA} = DP_{PEG} \times (LA/EG) \qquad \text{Equation 4.S3}$$

where DP_{PEG} and DP_{PLA} are the polymerization degree of PEG and PLA chains respectively; and 44 and 72 are the molecular weight of EG and LA units respectively. Figure 4.S1 shows the PLA-*b*-PEG block copolymer spectra.

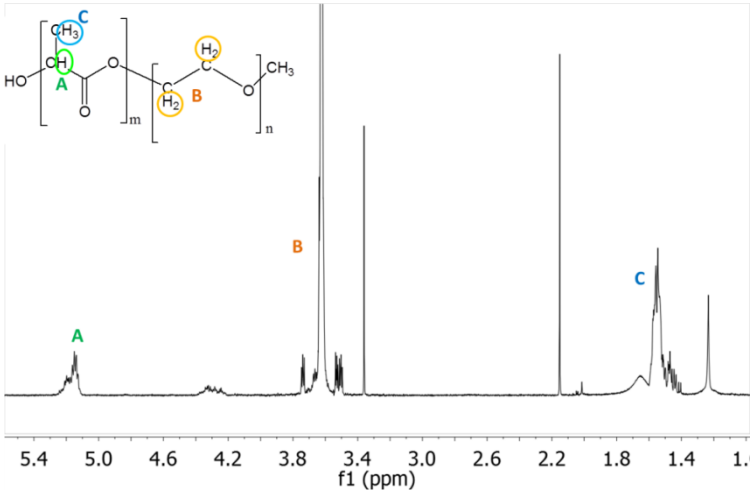

Figure 4.S1 ^{1}H-NMR spectra of a PLA-*b*-PEG block copolymer.

Energy-Dispersive X-ray Spectroscopy (EDS)

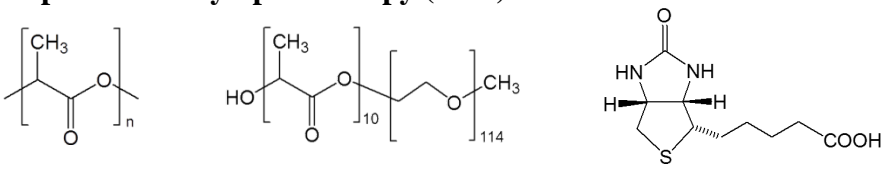

(a) (b) (c)

Figure 4.S2 (a) PLA polymer structure; (b) PLA-*b*-PEG block copolymer structure and (c) biotin molecule.

As sulfur atom is only presented in biotin molecule, it can be used as indicator of the presence of biotin in the sample. Figures 4.S3 and 4.S4 show the EDS spectra of the PLA/PLA-*b*-PEG fiber containing 0 and 18 wt % of biotin. No S signal was observed when no biotin was present in the sample.

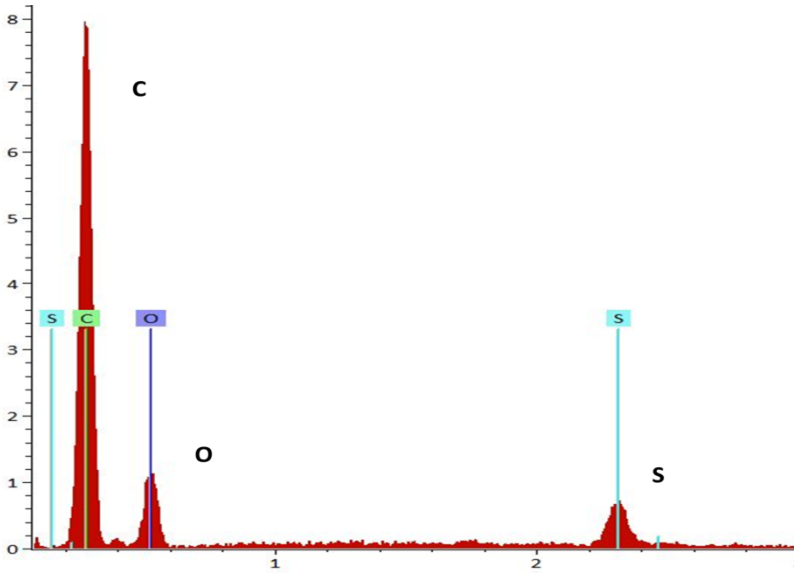

Figure 4.S3 EDS spectra of PLA/PLA-*b*-PEG fiber containing 18 wt % of biotin.

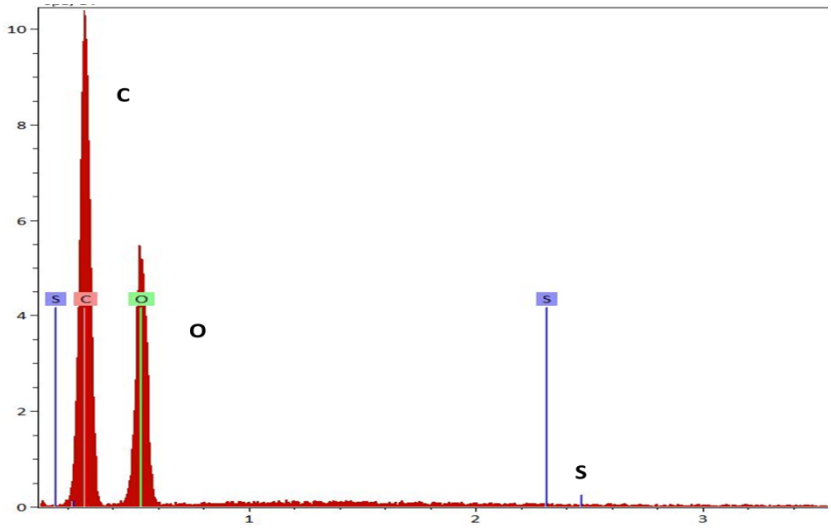

Figure 4.S4 EDS spectra of PLA/PLA-*b*-PEG fiber containing 0 wt % of biotin.

Surface Area and Biotin Molecules per nm^2

Surface area (SA) of fibers was calculated according to the following equation:

$$\mathrm{SA}\ (\mathrm{m^2/g}) = \frac{\mathrm{A_f(cm^2)}}{\mathrm{m_f(g)}} \times 10^{-4} \qquad \text{Equation 4.S4}$$

where A_f is the area of the fiber (cm^2); and m_f is the fiber mass (g).

A_f was calculated according to Equation 4.S5:

$$A_f(cm^2) = 2\pi rh \quad \text{Equation 4.S5}$$

where r is the fiber radius (cm); and h is the fiber length (cm). Fiber diameter (and therefore radius) was measured using the SEM images as explained in Section 4.2.4 of the experimental work. Fiber length (h) was calculated using Equation 4.S8:

$$m_f = \rho \times v \quad \text{Equation 4.S6}$$

$$v = \pi r^2 h \quad \text{Equation 4.S7}$$

$$h = \frac{m_f/\rho}{\pi r^2} \quad \text{Equation 4.S8}$$

where ρ is the fiber density (g/cm^3); and v is the volume of the fiber (cm^3). PLA density value (1.2 g/cm^3) was used for calculations.

Therefore, measuring the fiber mat sample mas (m_f) and fiber radius (r), surface area of the fiber mat (SA, area of the fiber mat per gram of the sample) can be calculated using Equations 4.S4, 4.S5, and 4.S8.

Biotin molecules per nm^2 were calculated using Equation 4.S9:

$$\frac{\text{Biotin molecules}}{nm^2} = \frac{g_{sb}/g_f \times N_A}{M_{Wb} \times SA \times 10^{18}} \quad \text{Equation 4.S9}$$

where g_{sb}/g_f is the grams of surface available biotin per fiber gram calculated by colorimetric assay; M_{Wb} is the molar mass of biotin (244.3 g/mol); SA is the surface area (m^2/g) calculated from section 3.5 of experimental work; and N_A is the Avogadro´s constant (6.022×10^{23} molecule/mol); 10^{18} is the conversion number to change the units of the fiber area from m^2 to nm^2.

4.6 Acknowledgments

This work made use of the Cornell Center for Materials Research Shared Facilities, which are supported through the (NSF MRSEC (National Science Foundation Materials Research Science and Engineering Centers) program (DMR-1120296). This work is/was supported by the USDA (United States Department of Agriculture) National Institute of Food and Agriculture, Hatch NC1194 project No. 3297816. Any opinions, findings, conclusions, or recommendations expressed in this publication are those of the author(s) and do not necessarily reflect the view of the National Institute of Food and Agriculture (NIFA) or the United States Department of Agriculture (USDA).

REFERENCES

1. Supaphol, P.; Suwantong, O.; Sangsanoh, P.; Srinivasan, S.; Jayakumar, R.; Nair, S.V. Electrospinning of biocompatible polymers and their potentials in biomedical applications. *Adv. Polym. Sci.* **2012**, *246*, 213–240.
2. Greiner, A.; Wendorff, J.H. Electrospinning: A fascinating method for the preparation of ultrathin fibers. *Angew. Chem. Int. Ed.* **2007**, *46*, 5670–5703.
3. Rogina, A. Electrospinning process: Versatile preparation method for biodegradable and natural polymers and biocomposite systems applied in tissue engineering and drug delivery. *Appl. Surf. Sci.* **2014**, *296*, 221–230.
4. Persano, L.; Camposeo, A.; Tekmen, C.; Pisignano, D. Industrial upscaling of electrospinning and applications of polymer nanofibers: A review. *Macromol. Mater. Eng.* **2013**, *298*, 504–520.
5. Pham, Q.P.; Sharma, U.; Mikos, A.G. Electrospinning of polymeric nanofibers for tissue engineering applications: A review. *Tissue Eng.* **2006**, *12*, 1197–1211.
6. Li, D.; Frey, M.W.; Baeumner, A.J. Electrospun polylactic acid nanofiber membranes as substrates for biosensor assemblies. *J. Membr. Sci.* **2006**, *279*, 354–363.
7. Senecal, A.; Magnone, J.; Marek, P.; Senecal, K. Development of functional nanofibrous membrane assemblies towards biological sensing. *React. Funct. Polym.* **2008**, *68*, 1429–1434.
8. Luo, Y.; Nartker, S.; Miller, H.; Hochhalter, D.; Wiederoder, M.; Wiederoder, S.; Setterington, E.; Drzal, L.T.; Alocilja, E.C. Surface functionalization of electrospun nanofibers for detecting *E. coli* O157:H7 and BVDV cells in a direct-charge transfer biosensor. *Biosens. Bioelectron.* **2010**, *26*, 1612–1617.

9. Ren, G.; Xu, X.; Liu, Q.; Cheng, J.; Yuan, X.; Wu, L.; Wan, Y. Electrospun poly(vinyl alcohol)/glucose oxidase biocomposite membranes for biosensor applications. *React. Funct. Polym.* **2006**, *66*, 1559–1564.
10. Rossi, A.M.; Wang, L.; Reipa, V.; Murphy, T.E. Porous silicon biosensor for detection of viruses. *Biosens. Bioelectron.* **2007**, *23*, 741–745.
11. Menzies, K.L.; Jones, L. The impact of contact angle on the biocompatibility of biomaterials. *Optom. Vis. Sci.* **2010**, *87*, 387–399.
12. Dupont-Filliard, A.; Billon, M.; Livache, T.; Guillerez, S. Biotin/avidin system for the generation of fully renewable DNA sensor based on biotinylated polypyrrole film. *Anal. Chim. Acta* **2004**, *515*, 271–277.
13. Baeumner, A.; Jones, C.; Wong, C.; Price, A. A generic sandwich-type biosensor with nanomolar detection limits. *Anal. Bioanal. Chem.* **2004**, *378*, 1587–1593.
14. Kwakye, S.; Goral, V.N.; Baeumner, A.J. Electrochemical microfluidic biosensor for nucleic acid detection with integrated minipotentiostat. *Biosens. Bioelectron.* **2006**, *21*, 2217–2223.
15. Edwards, K.; Clancy, H.; Baeumner, A. Bacillus anthracis: Toxicology, epidemiology and current rapid-detection methods. *Anal. Bioanal. Chem.* **2006**, *384*, 73–84.
16. Frey, M.W.; Li, D.; Tsong, T.; Baeumner, A.J.; Joo, Y.L. Incorporation of biotin into PLA nanofibers via suspension and dissolution in the electrospinning dope. *J. Biobased Mater. Bioenergy* **2007**, *1*, 219–227.
17. Li, D.; Frey, M.W.; Vynias, D.; Baeumner, A.J. Availability of biotin incorporated in electrospun PLA fibers for streptavidin binding. *Polymer* **2007**, *48*, 6340–6347.
18. Kiss, É.; Bertóti, I.; Vargha-Butler, E.I. XPS and wettability characterization of modified poly(lactic acid) and poly(lactic/glycolic acid) films. *J. Colloid Interface Sci.* **2002**, *245*, 91–98.
19. Bhattarai, S.R.; Bhattarai, N.; Viswanathamurthi, P.; Yi, H.K.; Hwang, P.H.; Kim, H.Y. Hydrophilic nanofibrous structure of polylactide; fabrication and cell affinity. *J. Biomed. Mater. Res. A* **2006**, *78A*, 247–257.
20. Hendrick, E.; Frey, M. Increasing surface hydrophilicity in poly(lactic acid) electrospun fibers by addition of PLA-*b*-PEG co-polymers. *J. Eng. Fibers Fabr.* **2014**, *9*, 153–164.
21. Buttaro, L.M.; Drufva, E.; Frey, M.W. Phase separation to create hydrophilic yet non-water soluble PLA/PLA-*b*-PEG fibers via electrospinning. *J. Appl. Polym. Sci.* **2014**, doi:10.1002/APP.41030.
22. Li, L.; Ding, S.; Zhou, C. Preparation and degradation of PLA/chitosan composite materials. *J. Appl. Polym. Sci.* **2004**, *91*, 274–277.
23. Riley, T.; Stolnik, S.; Heald, C.R.; Xiong, C.D.; Garnett, M.C.; Illum, L.; Davis, S.S.; Purkiss, S.C.; Barlow, R.J.; Gellert, P.R. Physicochemical evaluation of nanoparticles assembled from poly(lactic acid)-poly(ethylene glycol) (PLA-PEG) block copolymers as drug delivery vehicles. *Langmuir* **2001**, *17*, 3168–3174.
24. Li, S.; Vert, M. Synthesis, characterization, and stereocomplex-induced gelation of block copolymers prepared by ring-opening polymerization of L(D)-lactide in the presence of poly(ethylene glycol), *Macromolecules* **2003**, *36*, 8008–8014.

25. Molina, I.; Li, S.; Martinez, M.B.; Vert, M. Protein release from physically crosslinked hydrogels of the PLA/PEO/PLA triblock copolymer-type. *Biomaterials* **2001**, *22*, 363–369.
26. Venkatraman, S.S.; Jie, P.; Min, F.; Freddy, B.Y.C.; Leong-Huat, G. Micelle-like nanoparticles of PLA-PEG-PLA triblock copolymer as chemotherapeutic carrier. *Int. J. Pharm.* **2005**, *298*, 219–232.
27. Kim, T.G.; Park, T.G. Surface functionalized electrospun biodegradable nanofibers for immobilization of bioactive molecules. *Biotechnol. Prog.* **2006**, *22*, 1108–1113.
28. Luu, Y.K.; Kim, K.; Hsiao, B.S.; Chu, B.; Hadjiargyrou, M. Development of a nanostructured DNA delivery scaffold via electrospinning of PLGA and PLA-PEG block copolymers. *J. Control. Release* **2003**, *89*, 341–353.
29. Spasova, M.; Stoilova, O.; Manolova, N.; Rashkov, I. Preparation of PLLA/PEG nanofibers by electrospinning and potential applications. *J. Bioact. Compat. Polym.* **2007**, *22*, 62–75.
30. Van Royen, P.; Schacht, E.; Ruys, L.; Vaeck, L.V. Static secondary ion mass spectrometry for nanoscale analysis: Surface characterisation of electrospun nanofibres. *Rapid Commun. Mass Spectrom.* **2006**, *20*, 346–352.
31. Sun, X.-Y.; Shankar, R.; Börner, H.G.; Ghosh, T.K.; Spontak, R.J. Field-driven biofunctionalization of polymer fiber surfaces during electrospinning. *Adv. Mater.* **2007**, *19*, 87–91.
32. Yoo, H.S.; Kim, T.G.; Park, T.G. Surface-functionalized electrospun nanofibers for tissue engineering and drug delivery. *Adv. Drug Deliv. Rev.* **2009**, *61*, 1033–1042.
33. Reddy, M.R.; Erion, M.D. *Free Energy Calculations in Rational Drug Design*; Springer: New York, NY, USA, 2001.
34. Reinholt, S.J.; Sonnenfeldt, A.; Naik, A.; Frey, M.W.; Baeumner, A.J. Developing new materials for paper-based diagnostics using electrospun nanofibers. *Anal. Bioanal. Chem*. **2014**, *406*, 3297–3304.

CHAPTER 5

INCREASING STABILITY OF BIOTIN FUNCTIONALIZED ELECTROSPUN FIBERS FOR BIOSENSOR APPLICATIONS[4]

5.1 Introduction

Nanofiber membranes have very high surface area to volume ratios and porous structures, making them excellent candidates for chemical detection and biosensor applications [1-4]. A nanofiber mat's ability to be implemented as a biosensor, however, is limited by the ability to control several polymer characteristics that include: (i) hydrophobicity that limits performance in aqueous biological systems, (ii) increased hydrophilicity that concurrently increases solubility and degradation in aqueous media, and (iii) specific surface functionality relevant to the individual biosensor application.

One method used to tailor fiber and membrane properties is incorporating functional polymeric and oligomeric materials directly to the processing dopes. For example, the blending of a hydrophobic polymer and a hydrophilic additive may yield a less hydrophobic membrane.[5-7] Using a modified electrospinning system with poly(lactic acid) (PLA)/PLA-*b*-poly(ethylene glycol) (PLA-*b*-PEG) Buttaro et al. found phase separation of PEG to the surface of the fibers resulting in a hydrophilic polymer.[8] In this paper, we build on this work in order to increase the surface functionality of fibers.

[4] Reprinted (adapted) with permission from (Shepherd, L.M.; González, E.; Chen E.X.; Frey, M.W. Increasing Stability of Biotin Functionalized Electrospun Fibers for Biosensor Applications. *ACS App. Mater. Interfaces* **2017**, 9(2), 1968-1974.) Copyright (2016) American Chemical Society.

Biotin finds common use in biosensor applications based on rapid protein binding, and a wide variety of biotin functionalized chemistries are available for specific biomolecule capture. [4, 9-11] Li. et al. functionalized PLA nanofibers with biotin by adding biotin directly to the PLA electrospinning solution. Biotin was present and available for protein binding at the surface of the resulting PLA fibers, but the hydrophobic nature of PLA and the long term stability under aqueous conditions of biotin in the fiber were not investigated.[9] Gonzalez et al. significantly increased the amount of available biotin at the surface by adding PLA-*b*-PEG to the PLA/biotin system as the PLA-*b*-PEG aided in the migration of biotin to the surface of the fibers. After 1 to 7 days of immersion in water, however, both the biotin and the PLA-*b*-PEG preferentially diffuse out of the fiber into the surrounding water; the remaining fiber is no longer effective for protein binding.[12]

If biotin functionalized PLA/PLA-*b*-PEG fibers are to be useful as sensors in aqueous environments for long duration, we must address the water stability of PLA/PLA-*b*-PEG fibers by finding appropriate block lengths of PLA-*b*-PEG. In this work we present three approaches to increasing stability of hydrophilic, biotin functionalized nanofibers: (i) alteration of block lengths, (ii) covalent attachment of biotin, and (iii) comparing two solvents, DMF and HFIP. Block lengths of PEG and PLA within the copolymer are optimized to both maximize hydrophilicity of the fiber and minimize diffusion of the block co-polymer into the aqueous phase. Through covalent bonding of biotin directly to PLA-*b*-PEG, diffusion of biotin out of the fiber is significantly reduced. Finally, the

influence of the solvent used for electrospinning on the stability and functionality of the final fibers is investigated. Both DMF and HFIP have been reported as compatible solvents for PLA electrospinning. While biotin functionalization of PLA fibers spun from HFIP has not been reported, HFIP has been useful in spinning other types of biomolecules. Nuansing et al. electrospun pure protein from the fluorinated solvent HFIP and found little to no denaturing of the protein.[13]

5.2 Experimental Section

5.2.1 Materials

PLA-*b*-PEG block copolymers were synthesized by ring opening polymerization[14] of lactide (Sigma-Aldrich) in the presence of poly(ethylene glycol) methyl ether (Number average molecular weights, M_n : 1000, 2000, and 5000 g/mol) using catalyst stannous octate (Sigma- Aldrich). The copolymers produced were PLA(5200)-*b*-PEG(1000), PLA(2800)-*b*-PEG(2000), and PLA(5300)-*b*-PEG(5000). To produced biotin functionalized polymer PLA(3600)-*b*-PEG(2000)-Biotin and PLA(5700)-*b*-PEG(1000)-Biotin, biotin-PEG with M_n of 1000 and 2000 g/mol were purchased from Creative PEGWorks. PLA 4043D (MW= 153,315 g/mol, PDI=1.81) was purchased from NatureWorks LLC. Solvents 1,1,1,3,3,3,-Hexafluoro-2-propanol and 99.8 % anhydrous N,N-Dimethylformamide were purchased from Sigma-Aldrich. 25-gauge x 1 needles were purchased from Small Parts, Inc., and needle deflect point 20-gauge x 2inch were purchased from Fisher Scientific Company LLC. For colorimetric assays we used Pierce™ biotin quantification kits purchased from ThermoFisher Scientific.

5.2.2 Electrospinning

All spinning dopes in this study are made of high molecular weight PLA and PLA-*b*-PEG copolymers. The amount of block copolymer was adjusted to obtain 12 wt% or 26 wt% of PEG in the final fibers. All DMF solutions had 12 wt% PEG, as previous work showed that the greatest water wicking occurred at this concentration. [8] For comparison, we also investigated 12 wt% PEG with HFIP. After characterization of the block lengths of PLA-*b*-PEG (Figure 5.1A) that promote the greatest water wicking and demonstrate excellent water stability, we synthesized PLA-*b*-PEG with biotin at the other terminal end of the PEG blocks (Figure 5.1B). The maximum biotin loading was limited by the PLA-*b*-PEG block length as the PEG loadings were fixed throughout these

studies.

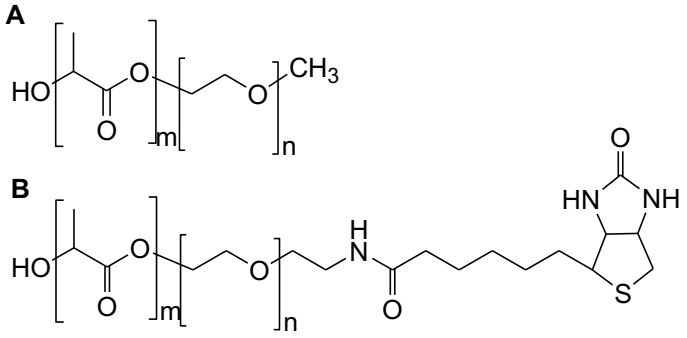

Figure 5.1 Molecular structures of polymers synthesized by solution polymerization (A) PLA-*b*-PEG, and (B) PLA-*b*-PEG-Biotin.

Using HFIP as the solvent for PLA in the electrospinning dope resulted in the formation of a suspension when we added PLA-*b*-PEG or PLA-*b*-PEG-Biotin (note PLA is

completely soluble in HFIP). This suspension does settle over time, so we agitated them prior to use. The spinning dopes contained 3.6 wt% PLA (high molecular weight homopolymer) and were placed on a wrist shaker for at least 16 hours prior to electrospinning to form the spinning dopes. We used a standard electrospinning system at a feed rate of 1.5mL/hr (PHS Ultra syringe pump, Harvard Apparatus) to form fibers from the PLA-*b*-PEG and PLA-*b*-PEG-Biotin suspensions. We drove fiber formation by applying 15 kV (Gamma High Voltage Research Inc., FL) between a 25 g needle tip and grounded collector consisting a copper sheet wrapped in aluminum ~ 22 cm away (68 kV m^{-1} electric field).

For comparison, we also used DMF as a solvent because, with heating, it can dissolve homopolymer PLA and copolymers of PLA (22 wt%)[8, 12] without forming a suspension. We used a modified electrospinning apparatus[8] to keep the syringe and needle at 70˚C ± 5˚C and applied a voltage of 15 kV (Gamma High Voltage Research Inc., FL) between the metal needle and the grounded collector (copper sheet wrapped in aluminum) placed ~10 cm away (150 kV m^{-1} electric field). We maintained a solution feed rate of 10 μL/min using a programmable PHS Ultra syringe pump (Harvard Apparatus).

We stored all samples in a desiccator prior to water wicking, stability, DSC, and SEM studies. PLA fibers spun from DMF were prepared previously and stored at room temperature prior to experiments.

5.2.3 Water Stability

To study the stability of the nanofiber membranes in water, we cut ~ 4 x 1/2 cm rectangles of the deposited mats. Cut samples were placed in 15mL of DI water for either 24 hrs or 7 days. After we removed them from the DI water, we placed them in a vacuum oven set to 25°C (oven temperature ranged from 24 to 29°C) for 24 hrs. Note: fiber mat samples of PLA/PLA(5700)-*b*-PEG(1000)-Biotin shrunk a couple of centimeters prior to experiments.

5.2.4 Nuclear Magnetic Resonance Spectroscopy (NMR)

We analyzed the NMR spectra on the control and dried samples (after water immersion) to accurately measure copolymer dissolution. ^{1}H-NMR experiments were recorded at room temperature with an INOVA 400 spectrometer (Varian Inc., Palo Alto, CA, USA) operating at 400 MHz. Deuterated chloroform (CDCl3) was used to dissolve fibers mats and tetramethylsilane (TMS) was used as an internal reference. The PLA/PEG ratio of the samples was determined from the integration of ^{1}H-NMR resonances belonging to the PEG blocks at 3.6 ppm (-O-CH_2-CH_2- singlet) and to the PLA blocks at 5.2 ppm (-CH quartet).[15-17] The difference in the PLA/PEG ratio between control samples and the samples immersed in water was considered to be caused by the dissolution of the PLA-*b*-PEG block copolymer into the water phase.

5.2.5 Field Emission Scanning Electron Microscopy (FESEM)

By using an FESEM, we observed the microstructure of the fiber mats in high contrast. We sputter coat samples in gold-palladium for 30s prior to imaging them with a LEO 1550 FESEM using a 1kV accelerating voltage and 50:50 mixture of SE2 and InLens

detectors. Using ImageJ™ software on the recorded SEM images, we calculated the average diameters from 50 measurements gathered from two images.

5.2.6 Water Wicking

Each electrospun sample was cut into 3 x ½ cm fabrics. We weighed the samples and then put a fishhook through the nanofiber mat to ensure the membrane penetrated the meniscus.[8] Wettability testing was done using the KSV Sigma 701 and DI water. Note: fiber mat samples of PLA/PLA(5700)-*b*-PEG(1000)-Biotin shrunk a couple of centimeters prior to experiments.

5.2.7 Biotin/Avidin Binding

We are able to compare the effect of solvent on biotin reaching the fiber surface by using a quantifiable competitive colorimetric assay, whose change in absorbance at 500 nm signifies the Avidin removal from a 4'-hydroxyazobenzene-2-carboxylic acid (HABA)/Avidin solution to the fiber surface containing biotin. A Lambda 35 UV/Vis spectrophotometer from Perkin Elmer is used to measure the change in absorbance. We reconstituted HABA/Avidin solutions by the manufacturer's protocol, and took its absorbance in PBS Buffer at 500nm. We weighed the nanofiber fabrics prior to placing them into a cuvette and shaking for three minutes; afterwards, we removed the fiber mat and measured the absorbance. For each sample we perform at least three replicates. Equation 5.1 is used to calculate the available biotin at the surface of fibers.[12]

$$Surface\ Available\ Biotin\ \left(\frac{mg\ Biotin}{g\ fiber}\right) = \left(A_{500}^{0} - A_{500}\right)\left(\frac{Mw_{biotin}V}{\varepsilon bW}\right) x\ 10^{3} \qquad \textit{Equation 5.1}$$

Where A^{o}_{500} is the absorbance of the solution prior to the addition of nanofiber, A_{500} is the absorbance of the solution after reaction with nanofiber, MW_{biotin} is the molecular weight of the biotin (244.3 g/mol), V is the volume of the solution (L), b is the cuvette path length (1 cm) and ε is the extinction coefficient of the HABA/Avidin complex at 500 nm (3.4×10^4 L/(mol·cm)).

5.3 Results and discussion

5.3.1 PLA/PLA-b-PEG Fiber Stability in Water

Changing PLA and PEG block lengths and electrospinning solvent both significantly impacted the stability of the resulting electrospun fiber mats in water (Figure 5.2). While it was possible to form good nanofibers containing 26 wt% PEG from PLA(5300)-*b*-PEG(5000) using HFIP as the solvent, stability of these fibers in water was very poor with a 35 % loss of copolymer as determined by NMR after seven days (Figure 5.2). Fibers containing 26 wt% PEG from PLA/PLA(2800)-*b*-PEG(2000) spun from HFIP produced insufficient nanofibers and lost ~ 50 % of copolymer after seven days of water exposure. Also, due to the drastic mat differences, we do not consider any trends at 26 wt% PEG. Therefore, for the remainder of this article we will focus on fibers containing 12 wt% PEG.

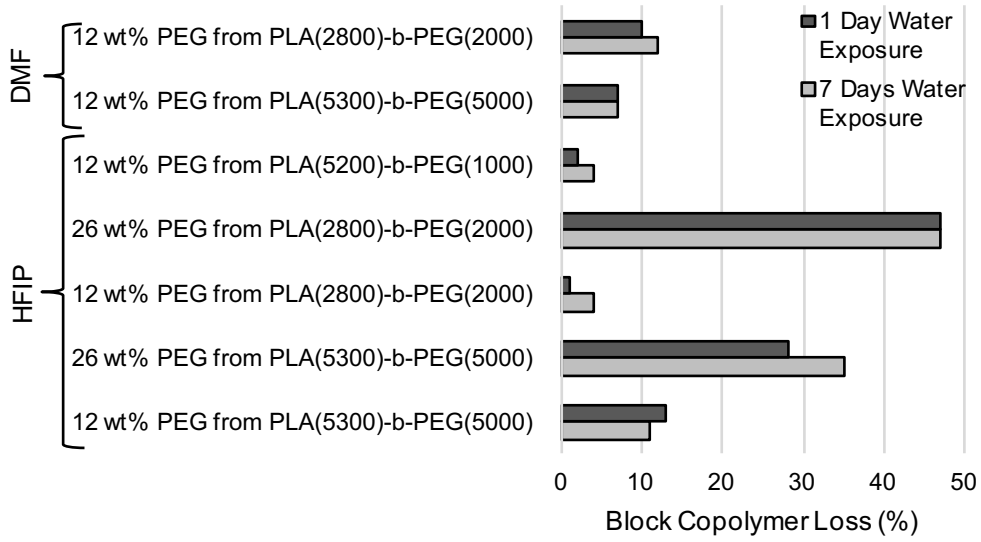

Figure 5.2 Block copolymer lost after one day and seven days of water exposure as determined by NMR.

Electrospun fibers containing 12 wt% PEG from PLA(5300)-*b*-PEG(5000), and PLA(2800)-*b*-PEG(2000) spun from DMF and HFIP were studied for copolymer loss by a change of composition in NMR spectra (Figure 5.2). As reported previously, solutions with 12 wt% PEG from PLA(5200)-*b*-PEG(1000) in DMF were not spinnable,[8] however fibers could be formed and studied for copolymer loss when spun from HFIP. Considering just copolymers spun from DMF, by only altering the block lengths, we are able to significantly decrease the loss of copolymer from 64 % for PLA(730)-*b*-PEG(5000) reported by Gonzalez et al.[12] to less than 10 % after seven days of water exposure. We further increased the stability of the copolymer when we used HFIP as the electrospinning solvent.

Interestingly, block copolymer stability within fibers spun from DMF slightly improves for longer block lengths of PEG, which also have increasing block length of PLA; being

spun from a homogeneous solution, the longer block lengths of PLA are likely to cause greater chain entanglements with the high molecular weight PLA of the fiber. HFIP spun samples, however, are more stable with shorter PEG block lengths (at 12 wt% PEG fiber loadings). Differences in both the spinning dopes and the resulting fiber morphologies contribute to the difference observed in water stability. The HFIP spinning dope is spun from a suspension that is likely to contain micelles and their aggregates and is not homogenous like the DMF dopes. We imaged an HFIP suspension with copolymer that has sediment (Supplementary Figure 5.S1) and therefore assume micelle aggregates have formed as the PLA is soluble in HFIP; however, under the conditions of this study the PEG was not. By changing the solvent of the spinning dopes from DMF to HFIP, over seven days of water exposure we decreased the copolymer loss of PLA(2800)-*b*-PEG(2000) (for 12 wt% PEG in the final fiber) from 12 % to 4 % (Figure 5.2). Further analysis presented below details the differences in the PEG phase formation within the fiber and fiber structure.

5.3.2 PLA/PLA-b-PEG Fiber Morphology

Compared to pure PLA fibers, fibers spun from DMF decrease in fiber diameter when copolymers are added to the dope, however, fibers spun from HFIP increase in fiber diameter when copolymers are added. HFIP and DMF spun fibers both increase in fiber diameter for increasing PEG block length (Figure 5.3). HFIP fibers containing PLA(5200)-*b*-PEG(1000) have the largest diameter; this increase is associated with the melding of fibers as a result of landing wet with residual solvent. Since fibers land wet, they take on a ribbon shape rather than a circular or oval shape. As a result, when we

measure fiber diameters, larger diameters are observed. While the cross section perpendicular to the fiber's axis has a larger diameter, the cross section along the fiber axis would have a much smaller diameter since it is not circular. In addition, the copolymers themselves differed in texture, which may have further contributed to this observance; the higher molecular weight copolymers form powders while the lower molecular weights form a tacky viscous substance (Supplementary Figure 5S2).

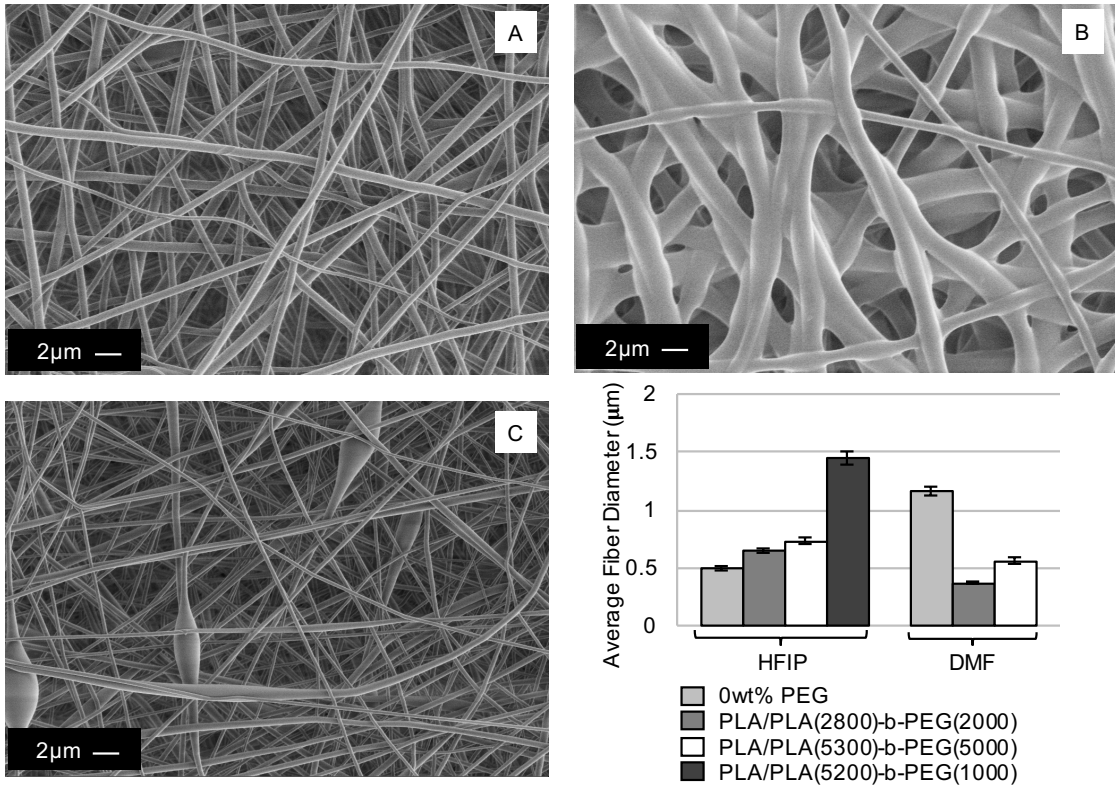

Figure 5.3 SEM images of (A) 12 wt% PEG from PLA(2800)-b-PEG(2000) spun from HFIP, (B) 12 wt% PEG from PLA(5200)-b-PEG(1000) spun from HFIP, and (C) 12 wt% PEG from PLA(2800)-b-PEG(2000) spun from DMF. Average fiber diameters are represented in the graph for control PLA fibers and fibers containing 12 wt% PEG from PLA-b-PEG copolymers. Error bars represent standard error.

5.3.3 PLA/PLA-b-PEG Fiber Water Wicking

Fibers containing copolymers with PEG block lengths of 2,000 and 5,000 do not wick as much water per their weight when spun from HFIP as compared to DMF spun samples (Figure 5.4). This indicates DMF promotes PEG to the fiber surface more effectively than HFIP. DMF samples spun from PLA/PLA(5300)-*b*-PEG(5000) wicked approximately 1,100 % its own fiber weight in water. Fibers of PLA/PLA(2800)-*b*-PEG(2000) spun from DMF were also able to wick a similar amount. Interestingly, fibers of PLA/PLA(5200)-*b*-PEG(1000) spun from HFIP had an increase in water wicking, which is associated with the flat ribbon-like fiber morphology previously mentioned.

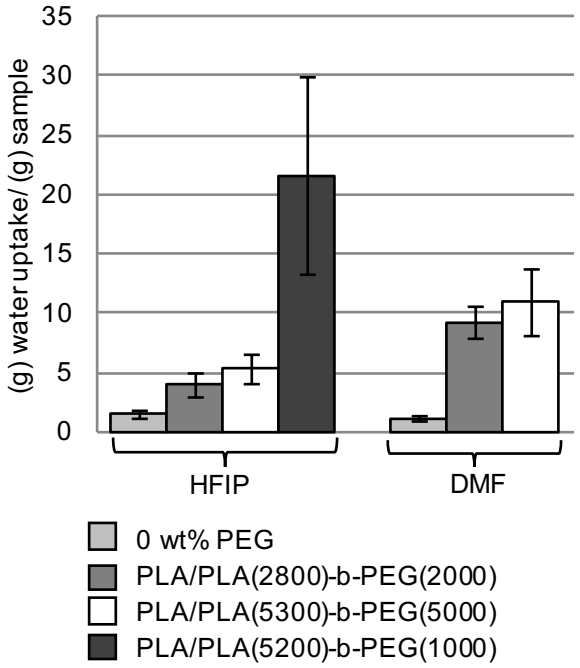

Figure 5.4 Water wicking data for control PLA fibers and fibers containing 12 wt% PEG in the final fiber from PLA-*b*-PEG. Error bars represent standard error.

We considered the amount of copolymer lost and water wicking data of the fiber mats

to be the most important parameters in deciding what copolymers to synthesize with biotin attached. For this reason, we synthesized PLA(5700)-*b*-PEG(1000)-Biotin. As mentioned earlier PLA(5200)-*b*-PEG(1000) was not able to be spun from DMF, for this reason we also synthesized PLA(3600)-*b*-PEG(2000)-Biotin in order to be able to compare it to the fibers spun from HFIP. We extensively study both copolymers in the following sections. Although DMF spun samples had the lowest copolymer loss with PLA(5300)-*b*-PEG(5000), we chose not to investigate it further; if we maintain 12 wt% PEG in the final fiber we are limited to the amount of biotin we can incorporate, as with longer block lengths of PEG, the amount of biotin able to be incorporated decreases. We aimed at creating copolymers with identical molecular weights to the ones studied in the previous sections, but with biotin attached. Due to the nature of solution polymerization, however, we were able to create similar but not identical block lengths of PLA.

5.3.4 PLA-b-PEG-Biotin Fiber Stability in Water

We use NMR to determine copolymer lost after 1 and 7 days of water exposure for fibers spun from HFIP and DMF (Figure 5.5). As with the polymers synthesized without biotin attached, we observe some loss of PLA-*b*-PEG-Biotin copolymers with exposure to water. The fiber spun from DMF lost the most PLA-*b*-PEG-Biotin, up to 16 % of the total copolymer put into the fiber after 7 days. This loss is the result of the phase separated copolymer being present at the surface of fibers and preferentially migrating to the aqueous media. Fibers spun from HFIP lost far less PLA-*b*-PEG-Biotin compared to the DMF spun fibers, which was also previously shown in our study of PLA/PLA-*b*-

PEG spun fibers.

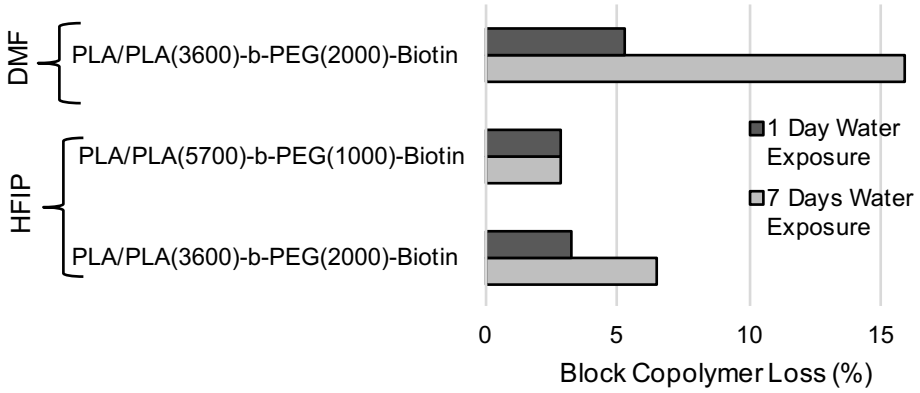

Figure 5.5 PLA-*b*-PEG-Biotin block copolymer lost after one day and seven days of water exposure as determined by NMR.

5.3.5 PLA/PLA-b-PEG-Biotin Fiber Morphology

To be complete, we again look at fiber morphology and diameter size (Figure 5.6). With the exception of PLA/PLA(5700)-*b*-PEG(1000)-Biotin, fiber diameter decreases when biotin is attached. When PLA/PLA(5700)-*b*-PEG(1000)-Biotin is spun from HFIP, the fibers take on a larger diameter and a more spherical shape as compared to when biotin was not attached to the copolymer, PLA(5200)-*b*-PEG(1000). This change in morphology is a function of both biotin being attached and because the PLA block length is slightly longer, we no longer have flattening of the fibers by residual solvent.

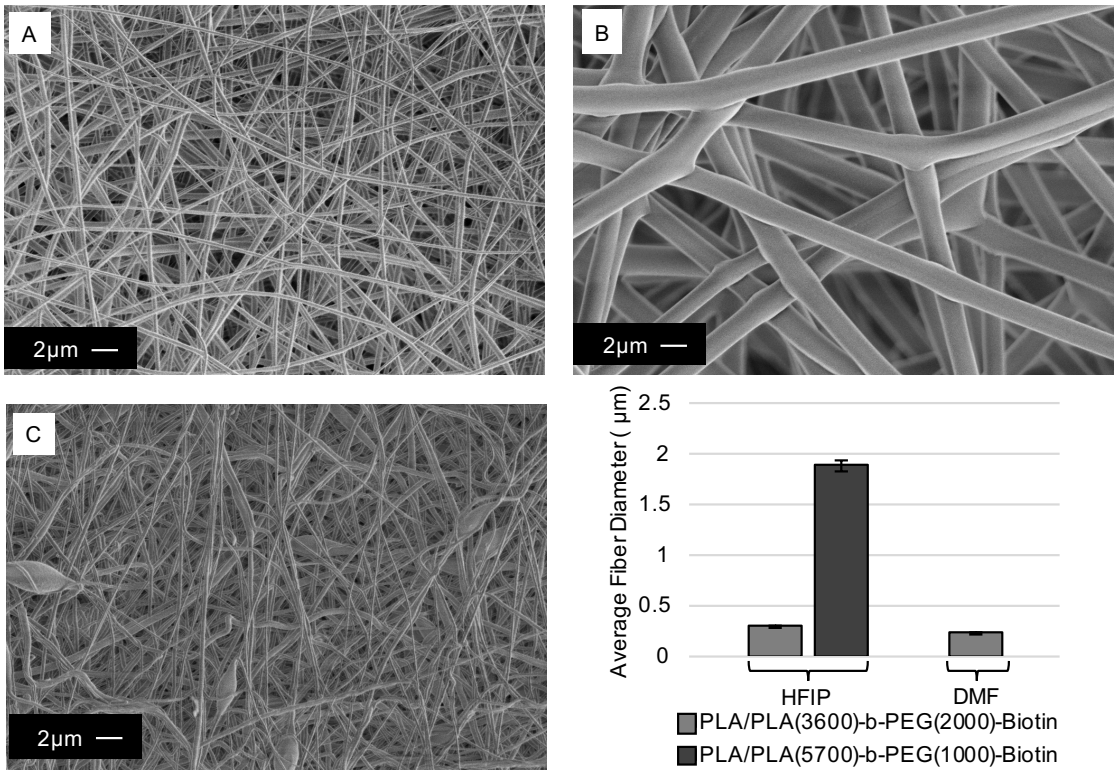

Figure 5.6 SEM images of (A) 12 wt% PEG from PLA(3600)-*b*-PEG(2000)-Biotin spun from HFIP, (B) 12 wt% PEG from PLA(5700)-*b*-PEG(1000)-Biotin spun from HFIP, and (C) 12 wt% PEG from PLA(3600)-*b*-PEG(2000)-Biotin spun from DMF. Average fiber diameters are represented in the graph for fibers containing 12 wt% PEG from PLA-*b*-PEG-Biotin. Error bars represent standard error.

5.3.6 PLA/PLA-b-PEG-Biotin Fiber Water Wicking

While the fibers spun from HFIP lost less copolymer, the low water wicking provides evidence of smaller quantities of PEG and biotin present at a fiber's surface compared to fibers spun from DMF (Figure 5.7). Interestingly, the hydrophilic nature of the fibers spun from DMF increases with the incorporation of biotin, while the fibers spun from HFIP remain relatively unchanged or decrease in hydrophilicity. The fibers spun from HFIP containing PLA(5700)-*b*-PEG(1000)-Biotin show a drastic loss in hydrophilicity compared to when the copolymer PLA(5200)-*b*-PEG(1000) was electrospun. This

change is explained by fiber diameter being larger and the circular morphology, rather than ribbon and oval shaped. As a result of the water wicking data, DMF electrospun samples would be more useful as biosensors in aqueous environments than the less hydrophilic samples spun using HFIP.

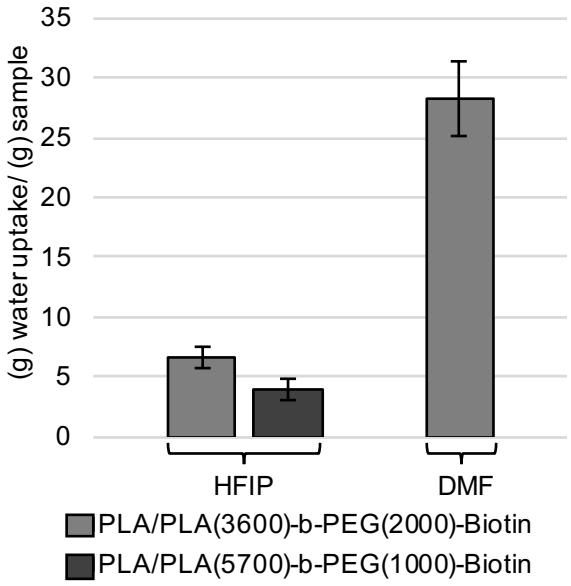

Figure 5.7 Water wicking data for fibers containing 12 wt% PEG from PLA-*b*-PEG-Biotin. Error bars represent standard error.

5.3.7 PLA/PLA-b-PEG-Biotin Surface Available Biotin

The available biotin at the fiber's surface is significantly impacted by the solvent system used. The use of HFIP dopes with either PLA(3600)-*b*-PEG(2000)-Biotin or PLA(5700)-*b*-PEG(1000)- Biotin have little to no biotin at the surface of fibers (Figure 5.8), and with exposure to DI water for one and seven days there is virtually no increase in biotin at the surface. This phenomenon is again explained by the insolubility of PEG in HFIP that is likely producing micelle aggregates in the spinning dopes, preventing the phase separation of PEG-Biotin to the fiber's surface. On the contrary, with dopes

of DMF where phase separation is known to be aided by the modified electrospinning process used in this study[8], we are able to increase the amount of surface available biotin to a far greater degree than when Li et al. added biotin freely to the electrospinning dope. With ~15 mg of biotin per gram of fiber, we detect on average 7.6 % of available biotin at the surface of the fibers (assuming every PEG has one biotin attached), resulting in 1.1 mg of biotin per gram of fiber (Figure 5.8); Li et al. who incorporated 10 wt% biotin (100 mg of biotin per gram of fiber) was only able to detect 1.2 mg of biotin per gram of fiber, resulting in detection of only 1.2 % of the biotin incorporated into the fiber.[9] Consequently, by attaching biotin directly to the copolymers we are able to add 85 % less biotin, but still achieve the same relative amount of biotin at the fiber's surface.

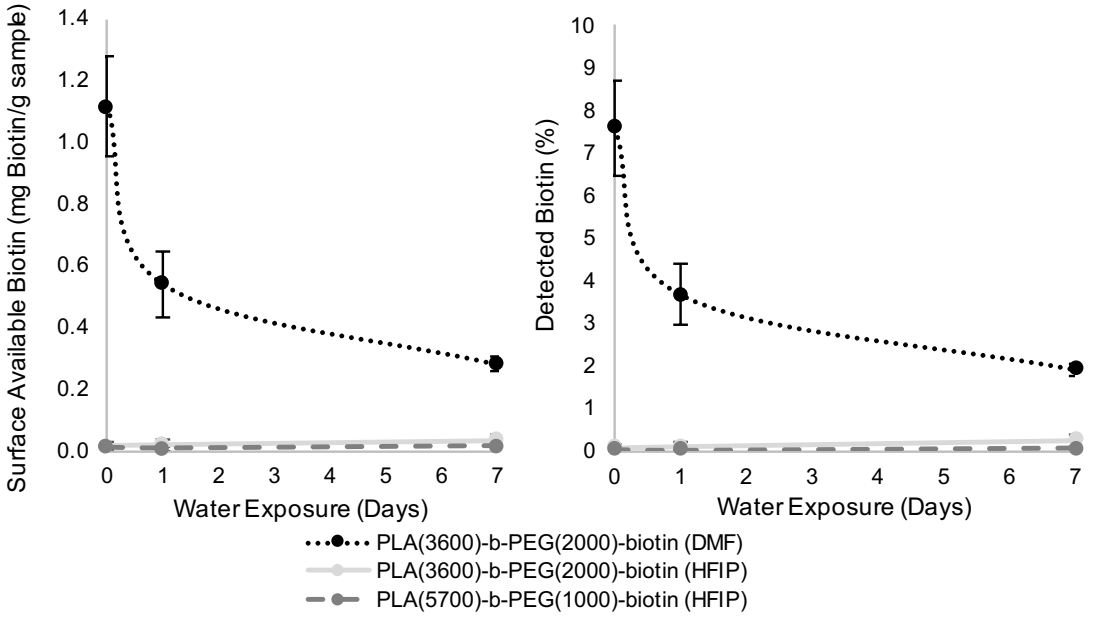

Figure 5.8 (Left) Surface available biotin and (Right) Percent biotin detected in relation to days exposed to water. Error bars represent standard error.

At this concentration of surface available biotin, the fibers made by Li et al. were sufficient for reliable detection[9], however, they were not studied for stability in aqueous solution. With similar amounts of initial biotin available, we expect the fibers produced in this study to also be viable for adequate detection. Our fibers spun from DMF with PLA(3600)-*b*-PEG(2000)-Biotin saw less biotin loss than that observed by Gonzalez et al., whose biotin when incorporated freely with PLA-PEG copolymers, after only one day of water exposure show no presence of biotin at the fiber's surface. With exposure to water over seven days, our fibers spun from DMF have 2 % biotin remaining at the fiber surface available for use in chemical detection.

5.4 Conclusions

In this study we have shown tailoring the block lengths of PLA-*b*-PEG copolymers can lead to increased stability of electrospun fibers of PLA/PLA-*b*-PEG and PLA/PLA-*b*-PEG-Biotin in water. While HFIP dopes provided electrospun samples that were more water stable than DMF dopes, the HFIP spun samples had no biotin present at the surface of fibers for detection. Electrspun samples of PLA(3600)-*b*-PEG(2000)-Biotin spun from DMF allowed for 1.1 mg of biotin per gram of fiber to be detected at the surface of fibers, with the incorporation of 85 % less biotin than previous studies.

With low hydrophilicity and no biotin detected from HFIP electrospun samples, it is necessary to continue future research with DMF as the solvent. It will be necessary to overcome the heat and organic solvent denaturing of proteins we seek to incorporate. Therefore, instead of attaching our proteins directly to PEG and electrospinning them,

we will create sensors by utilizing the biotin functionalized fibers spun from DMF. From this study, we have shown Avidin protein binding to biotin is achievable after the fiber mats are formed; this would allow sandwich type sensor assays to be developed for detection of specific contaminants.

5.5 Supplementary Materials

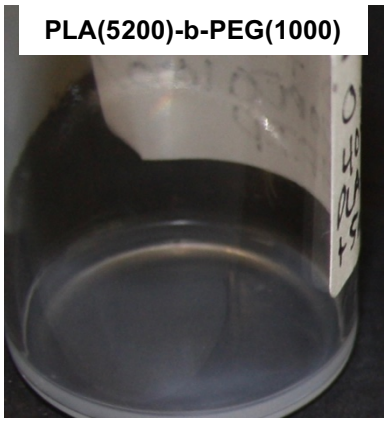

Figure 5.S1 Suspension of HFIP used to make 12 wt% PEG in the final fiber from PLA/PLA(5200)-*b*-PEG(1000). Figure shows settling of copolymer at the bottom of the vial.

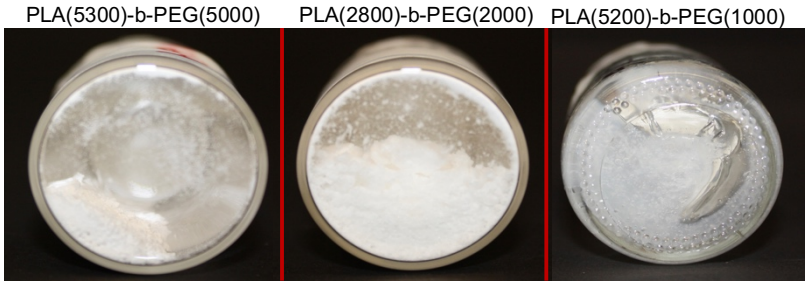

Figure 5.S2 The textural appearance of synthesized PLA-*b*-PEG block copolymers.

5.6 Acknowledgements

This work was supported by the USDA National Institute of Food and Agriculture, Hatch NC1194 project #3297816. Any opinions, findings, conclusions, or recommendations expressed in this publication are those of the author(s) and do not

necessarily reflect the view of the National Institute of Food and Agriculture (NIFA) or the United States Department of Agriculture(USDA). This work was also in part funded by a grant from the Department of Fiber Science & Apparel Design Graduate Student Research Awards Fund. Heating element apparatus used in electrospinning was provided by Dr. Daehwan Cho. This research made use of the Cornell Center for Materials Research Shared Facilities which are supported through the NSF MRSEC program (DMR-1120296). NSF-MRI (CHE-1531632 - PI: Aye) is acknowledged for NMR instrumentation support at Cornell University

REFERNCES

1. Steyaert, I.; Rahier, H.; De Clerck, K., Nanofibre-Based Sensors for Visual and Optical Monitoring. In *Electrospinning for High Performance Sensors*, Springer International Publishing: 2015; pp 157-177.
2. Tsou, P. H.; Chou, C. K.; Saldana, S. M.; Hung, M. C.; Kameoka, J., The Fabrication and Testing of Electrospun Silica Nanofiber Membranes for the Detection of Proteins. *Nanotechnology* **2008,** *19* (44), 445714 (6 pp).
3. Luo, Y.; Nartker, S.; Miller, H.; Hochhalter, D.; Wiederoder, M.; Wiederoder, S.; Setterington, E.; Drzal, L. T.; Alocilja, E. C., Surface Functionalization of Electrospun Nanofibers for Detecting E. coli O157:H7 and BVDV Cells in a Direct-Charge Transfer Biosensor. *Biosens. Bioelectron.* **2010,** *26* (4), 1612-1617.
4. Li, D. P.; Frey, M. W.; Baeumner, A. J., Electrospun Polylactic Acid Nanofiber Membranes as Substrates for Biosensor Assemblies. *J. Membr. Sci.* **2006,** *279* (1-2), 354-363.
5. Hendrick, E.; Frey, M., Increasing Surface Hydrophilicity in Poly(Lactic Acid) Electrospun Fibers by Addition of Pla-b-Peg Co-Polymers. *J. Eng. Fibers Fabr.* **2014,** *9* (2), 153-164.
6. Zhao, Y. H.; Zhu, B. K.; Kong, L.; Xu, Y. Y., Improving Hydrophilicity and Protein Resistance of Poly(vinylidene fluoride) Membranes by Blending with Amphiphilic Hyperbranched-Star Polymer. *Langmuir* **2007,** *23* (10), 5779-5786.
7. Luong, N. D.; Moon, I. S.; Lee, D. S.; Lee, Y. K.; Nam, J. D., Surface Modification of Poly(L-lactide) Electrospun Fibers with Nanocrystal Hydroxyapatite for Engineered Scaffold Applications. *Mate. Sci. Eng., C: Biomimetic Supramol. Syst.* **2008,** *28* (8), 1242-1249.
8. Buttaro, L. M.; Drufva, E.; Frey, M. W., Phase Separation to Create Hydrophilic Yet Non-Water Soluble PLA/PLA-b-PEG Fibers via Electrospinning. *J. Appl. Polym. Sci.* **2014,** *131* (19), 41030 (7 pp).

9. Li, D.; Frey, M. W.; Vynias, D.; Baeumner, A. J., Availability of Biotin Incorporated in Electrospun PLA Fibers for Streptavidin Binding. *Polymer* **2007,** *48* (21), 6340-6347.
10. Zhu, M.; Gong, X.; Hu, Y.; Ou, W.; Wan, Y., Streptavidin-Biotin-Based Directional Double Nanobody Sandwich ELISA for Clinical Rapid and Sensitive Detection of Influenza H5N1. *J. Transl. Med.* **2014,** *12*, 352 (10 pp).
11. Li, H.; Yan, J.; Ou, W.; Liu, H.; Liu, S.; Wan, Y., Construction of a Biotinylated Cameloid-Like Antibody for Lable-Free Detection of Apolipoprotein B-100. *Biosens. Bioelectron.* **2015,** *64*, 111-118.
12. González, E.; Shepherd, L. M.; Saunders, L.; Frey, M. W., Surface Functional Poly (lactic Acid) Electrospun Nanofibers for Biosensor Applications. *Materials* **2016,** *9* (1), 47.
13. Nuansing, W.; Frauchiger, D.; Huth, F.; Rebollo, A.; Hillenbrand, R.; Bittner, A. M., Electrospinning of Peptide and Protein Fibres: Approaching the Molecular Scale. *Faraday Discuss.* **2013,** *166*, 209-221.
14. Salem, A. K.; Cannizzaro, S. M.; Davies, M. C.; Tendler, S. J. B.; Roberts, C. J.; Williams, P. M.; Shakesheff, K. M., Synthesis and Characterisation of a Degradable Poly(lactic acid)-Poly(ethylene glycol) Copolymer with Biotinylated End Groups. *Biomacromolecules* **2001,** *2* (2), 575-580.
15. Molina, I.; Li, S. M.; Martinez, M. B.; Vert, M., Protein Release from Physically Crosslinked Hydrogels of the PLA/PEO/PLA Triblock Copolymer-Type. *Biomaterials* **2001,** *22* (4), 363-369.
16. Li, S. M.; Vert, M., Synthesis, Characterization, and Stereocomplex-Induced Gelation of Block Copolymers Prepared by Ring-Opening Polymerization of L(D)-lactide in the Presence of Poly(ethylene glycol). *Macromolecules* **2003,** *36* (21), 8008-8014.
17. Venkatraman, S. S.; Jie, P.; Min, F.; Freddy, B. Y. C.; Leong-Huat, G., Micelle-Like Nanoparticles of PLA-PEG-PLA Triblock Copolymer as Chemotherapeutic Carrier. *Int. J. Pharm.* **2005,** *298* (1), 219-232.

CHAPTER 6

THE DEGRADATION OF CELLULOSE BY RADIO FREQUENCY OXYGEN PLASMA[5]

6.1 Introduction

The textile industry must consider many things when producing and distributing goods, one of which is the inevitable disposal of their product at its lifecycle end. In 2012, the output of the textile industry exceeded 14 million tons with a component of that being cotton [1]. The cotton materials that end up in the waste stream contains valuable cellulosic material that could have potential use as alternative fuels.[2] Degradation methods of cellulose materials, however, generally use caustic agents for acid hydrolysis of the cellulose [3, 4]. It is therefore important to develop non-hazardous techniques to address the necessary degradation of cellulose, which has the potential to include textiles at the end of their lifecycle, decomposing them into useful products, such as fuel.

Plasmas show promise as safe, chemical free, high energy [5] sources that could be applied to the safe and clean processing of cotton. Research on treating textiles with various sources of plasmas has shown the potential to both process textiles via de-sizing [6, 7], as well as induce degradation in low molecular weight amorphous cellulose to produce biomass for fuels [8]. Additionally, plasmas have been used for surface functionalization of cotton [9].

[5] Shepherd, L.M.; Frey, M.W.: to be submitted.

Due to the electron and ion bombardment, like that provided by plasma exposed samples, backbone and side chain scissions may occur.[7] In the research described here, the objective was to explore the conditions that enable use of oxygen (O_2) plasma as a non-hazardous, and solvent free method to *significantly* degrade greige and scoured cellulose yarns. While argon and O_2 plasmas at short exposure times (less than 15 min.) have been researched on cotton by Hua et al., we chose to implement O_2 plasma, as Hu et al. found cotton to experience more pyranosidic bond cleavages with O_2 plasma than with an argon plasma [10].

In this work, we explored both long (30, 60, and 90 min.) and short (15 min.) plasma exposure times at a high power density of 0.46 W/cm^2 on cotton yarn samples. Other researchers have observed slight degradation of cotton fabrics using atmospheric pressure plasma treatments with exposure times less than or equal to 30 minutes [11-13]; we found, however, longer plasma exposure times greater than 30 min. with a power density of 0.46W/cm^2 to cause significant degradation of the both greige and scoured cellulose yarn. Mechanical testing of greige and scoured yarn had a reduction in load at break by 81.4 % and 92.5 %, respectively; gel permeation chromatography (GPC) revealed a significant decrease in degree of polymerization (DP) and weight average molecular weight (M_w). We also found differences in the surface chemistry of cotton with plasma exposure, as verified by X-ray Photoelectron Spectroscopy, showing the greater amount of oxygenated species as a result of the O_2 plasma treatment, at the yarn surfaces.

6.2 Experimental Section

6.2.1 Materials

For comparisons, skeins of greige and scoured (boiled off) cotton yarns (2 ply) were purchased from Test Fabrics, Inc. (West Pittston PA). Cotton is composed of cellulose, however a variety of other components such as waxes, proteins, sugars, organic acids, etc. are also present on fibers. [14, 15] Due to the scouring process of boiling off, scoured yarns should be free of these substances, however, while lower, they are still present. [16]

6.2.2 Plasma Treatment

Several plasmas could be used to purposely cause fiber degradation, including but not limited to helium, nitrogen, argon, and O_2. For this research, however, we chose to degrade cellulose with O_2 plasma. Skeins of yarn were exposed to O_2 plasma at various conditions in three different sized plasma units provided by Plasma Etch, Inc.; BT-1, PE50, and PE200RIE. All tests conducted in the various units are shown in the supplementary Table S6.1. All samples were tensile tested (Instron), however further experimental testing was limited to samples listed in Table 6.1 as these samples showed significant visual and tensile degradation at longer exposure times. During plasma treatment, the temperature of the sample platform was set at 40 ˚C for the BT-1 and PE200RIE units; the smaller PE50 units did not possess temperature control capabilities.

Table 6.1 Oxygen plasma conditions tested in PE200RIE machine on greige and scoured yarns.

Exposure Time (min)	RF Power (W)	Power Density (W/cm^2)	O_2 Flowrate (cc/min)
15	500	0.46	75
15	500	0.46	200
30	500	0.46	200
60	500	0.46	200
90	500	0.46	200

6.2.3 Field Emission Scanning Electron Microscopy (FESEM)

We used FESEM imaging to qualitatively investigate the morphology and surface characteristics of greige and scoured yarns before and after O_2 plasma treatments. The low accelerating voltage (1kV) used with the LEO 1550 FESEM allows samples to be imaged without sample coating.

6.2.4 Tensile Testing for Load at Break

Yarn samples were left at 21 °C and 65 % relative humidity for at least twenty-four hours prior to mechanical testing. Gauge length was set to 50 mm with a crosshead speed of 25mm min^{-1} using a 10N load cell. We performed five tests per sample, when possible, the exceptions being plasma treated yarns that were too weak to withstand testing. Tensile testing was used to examine the relationship between load at break, plasma exposure time, and plasma power density.

6.2.5 X-ray Photoelectron Spectroscopy (XPS)

Samples were analyzed approximately 1-2 months after plasma treatment by XPS, using Surface Science Instruments SSX-100 with operating pressure ~$2x10^{-9}$ Torr.

Monochromatic AlK-alpha x rays (1486.6eV) were used with a beam diameter of 1mm. Photoelectrons were collected at a 55-degree emission angle. A hemispherical analyzer determined electron kinetic energy, using the pass energy of 150V for wide/survey scans, and 50V for high resolution scans. A flood gun was used for charge neutralization of non-conductive samples. Wide scans provide evidence of elements on the cellulose samples such as nitrogen, calcium and potassium. By running XPS high resolution spectra we were able to investigate changes in elemental composition for C1s (C-C//C-H (C_1), C− O (C_2), C = O/O−C−O (C_3), and O − C= O (C_4)) that chemical changes occurring at the surface of samples. We are also able to compare the atomic ratios of O1s and C1s spectra. Sample spectra were analyzed using CASA XPS. A Shirley background was taken and the Gaussian-Lorentzian curve fitting was performed at 30% Gaussian and 70% Lorentzian. We shifted the spectra so that adventitious carbon was located at 285.0 eV. For C1s spectra, C_1 was constrained to a full width half max (fwhm) between 1 and 2.3, while C_2-C_4 were constrained to have the same fwhm value as C_1.

6.2.6 Gel Permeation Chromatography (GPC)

A Viscotek TDA 302 Triple Detection GPC with a 0.5 % LiCl in dimethylacetamide (DMAc) mobile phase was used to determine the polydispersity index (PDI) and average molecular weights (M_w, M_n) of the cellulosic yarns. Yarn samples were prepared in two steps: first the cellulose was activated for dissolution, after which, the yarns were dissolved in 8% LiCl dissolved in in DMAc. GPC samples were then prepared by diluting 100-200 μL of sample stock in 3.5-4.5 mL of mobile phase (0.5 % LiCl/DMAc) and stirred for 3hours at ambient temperature. Finally, the sample was

filtered and analyzed. Three replicates were done for each sample, except for greige yarn treated at 15 min at 200 cc/min O_2 flow rate and scoured yarn treated at 15 min at 75 cc/min O_2 flow rate; these samples were analyzed twice.

6.3 Results & Discussion

6.3.1 Visual Yarn Degradation

After we treat yarns with plasma, we are immediately able to see if severe degradation of the yarns has occurred. Control yarns have no breakages and and do no break upon handling. Plasma treated yarns, however, begin exhibiting visual breakages when treated for 15 minutes with an O_2 flow rate of 200 cc/min (not 75cc/min) as well as a severe decrease in structural integrity that was further amplified at longer exposure times. (Figure 6.1)

Figure 6.1 Control cotton yarn with no plasma exposure and no visual yarn breakages (a) and the visual breakages observed after plasma degradation of yarns exposed to 90 min plasma exposure at 0.46 W/cm^2

With SEM image analysis we achieved a more comprehensive visualization of polymer

degradation, or lack thereof. Scoured yarns are seen to have clear physical degradation including pitting and splitting of the fibers with as little as 15min of plasma exposure (Figure 6.2 (Left)). By contrast, greige yarns show less severe damage at 15min plasma exposure, but with increased plasma treatment time pitting and breakages become apparent (Figure 2 (Right)). The initial lack of significant degradation of greige yarn is attributed to the greater amount of waxes and other components present at the yarn surfaces as compared to scoured yarns. The degradation we observe is much more severe than that observed previously by other researchers who implemented varying plasmas (i.e. air, O_2) at shorter exposure times and/or lower power densities. [7, 17]

Plasma is known to etch cellulose [7, 15, 18], and based on the visual etching/degradation presented in this work, although we did not measure weight loss, we can infer that it has occurred. A decrease in cellulose sample weight has been associated with splitting off of hydroxyl groups, and free radical formation.[19]

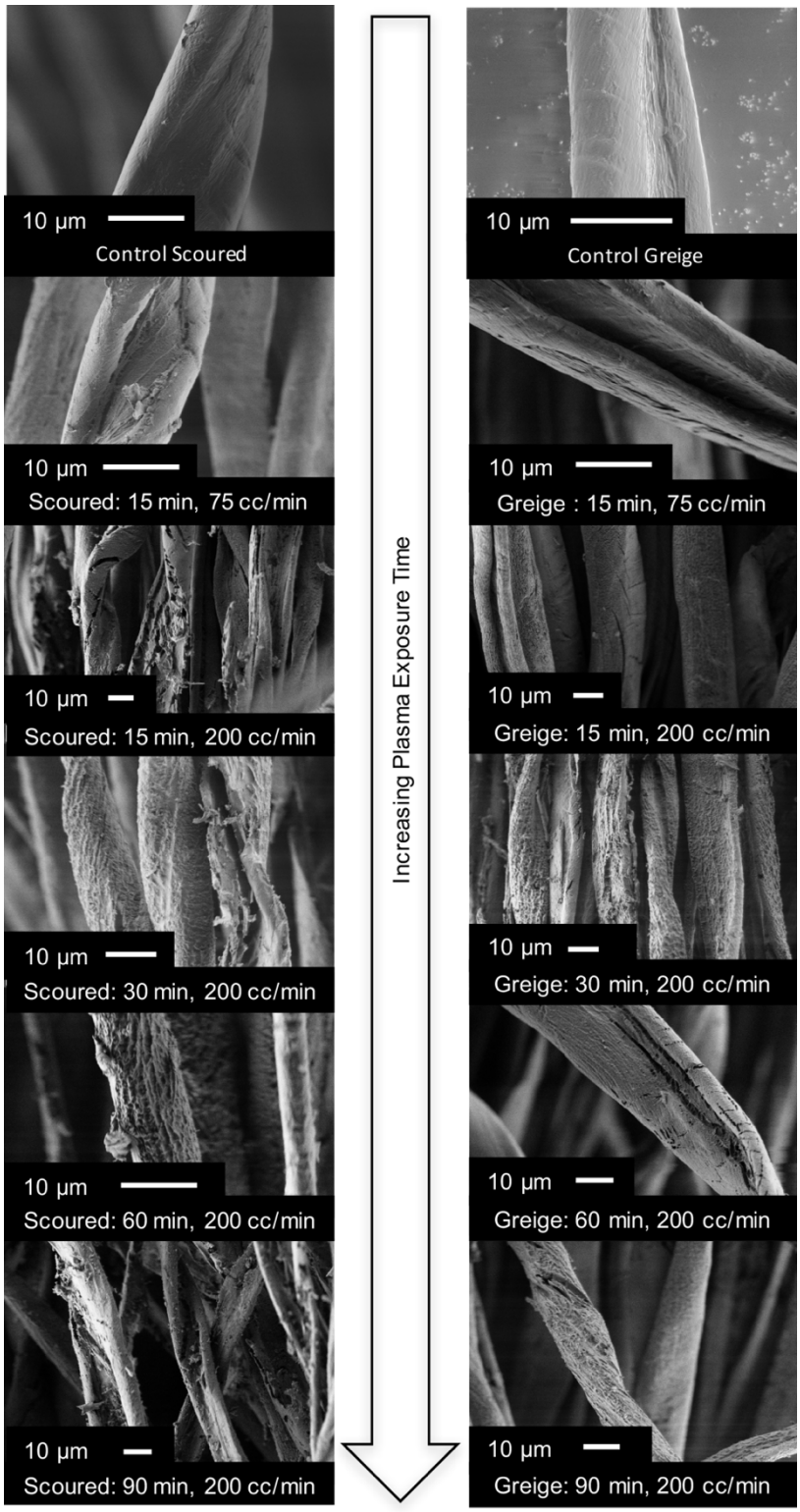

Figure 6.2 FESEM images of scoured yarn treated with 75 and 200 cc/min oxygen flow rate and 0.46W/cm^2 power density, with increasing exposure time (left) FESEM images of greige yarn treated with 75 and 200 cc/min oxygen flow rate and 0.46W/cm^2 power density with increasing exposure time (right)

6.3.2 Load at Break for Yarns

Power density, exposure time, and O_2 flowrate all impacted changes in load at break for cotton fibers. Power density is the power of radio frequency (RF) plasma over the area of the electrode. At first, under low power density, time, and O_2 flow rate breaking strength increases greater than the control greige and scoured yarns (Figure 6.3 a-b), which is likely due to crosslinking at the fiber's surface. After a sufficient duration of plasma exposure at high enough power densities (0.46 W/cm^2) and flow rates (200cc/min), the breaking strength begins to decrease; we attribute this effect to hydroxyl groups splitting off and glycosidic bond scissions in the backbone.

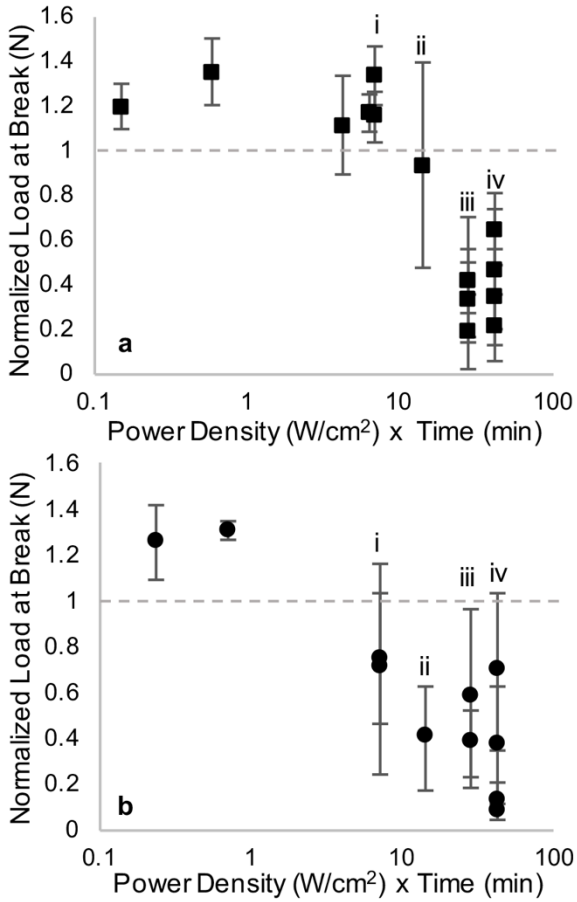

Figure 6.3 Load at break for yarns treated with O_2 plasma normalized by breaking strength of control yarns: greige yarn (a) and scoured yarn (b) Plasma exposures using 0.46 W/cm^2 at 15 min, (i) 30 min, (ii) 60 min (iii), and 90 min (iv) Bars = standard deviations

The lower amount of waxes, and other components on surfaces of scoured yarns yields an initially more severe decrease in load at break for scoured yarns than greige. It is also worth mentioning that skeins of the yarn were laid in the plasma chamber and not spread out, so the yarn properties may have been slightly different for yarns that were at the bottom versus yarns at the top; this may be why there was such large variation. Again, for power densities of 0.46 W/cm^2 and exposure times of 15, 30, 60, and 90 min, both the greige and scoured are physically damaged and visibly weaker. The samples with

severe physical breakages would represent zero strength, which is unaccounted for in these measurements.

6.3.3 Molecular Weight

Considering the number average molecular (M_n) values gathered by GPC, the DP was calculated using equation 1. The DP decreases by approximately half for both greige and scoured yarns (Figure 6.4a). We attribute the decrease of DP to main chain scissions. [19] In addition, the weight average molecular weight (M_w) decreases significantly for plasma treated samples, compared to control greige and scoured yarns (Figure 6.4b).

$$DP = \frac{M_n}{M_o} \text{ , where } M_o = 162\ g/mol \qquad \text{Equation 1}$$

As an indicator of the amount of variability in the types of polymers (i.e., heterogeneity index) comprising the fiber, the polydispersity index (PDI) stays around 1.8-2, with the exception of 15min where it increases (Figure 6.4c). This increase in PDI is explained by the onset of cellulosic degradation. Again, breakage is first observed visually at 15min of O_2 plasma treatment at 200cc/min for greige and scoured yarns. With an exposure time of 15 min and a flow rate of 75 cc/min scoured yarn differs from the griege yarn by having a lower load at break compared to its control, and although there were no visual breakages observed for the scoured yarn at these conditions, polymer degradation had occurred as evidenced by SEM, mechanical testing, and GPC. Further increase of plasma exposure time past the onset of degradation narrows the PDI.

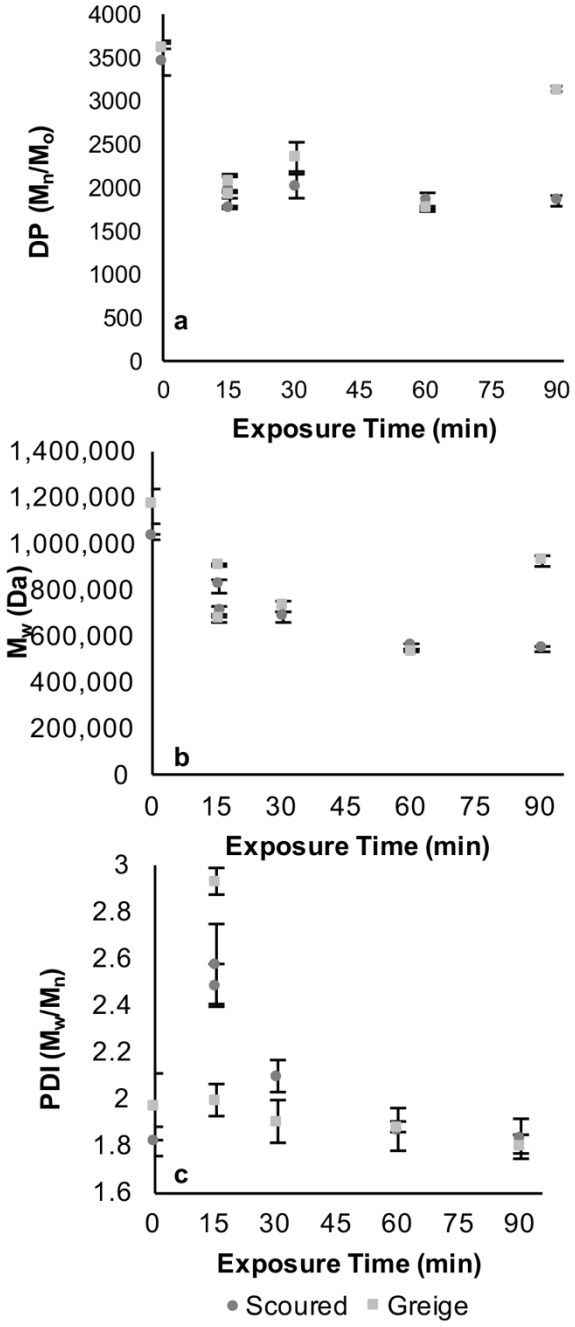

Figure 6.4 At 0.46 W/cm^2 power density, the effect of plasma exposure duration on the degree of polymerization (a), weight average molecular weight (b), and polydispersity (c), as determined by GPC Bars = standard deviations

6.3.4 Evaluation of C1s Deconvoluted Peaks

We implement XPS to investigate the low resolution survey scans for the non-cellulosic

components present on yarns (calcium, potassium, and nitrogen). Calcium and potassium are two of the most abundant metals naturally found in cotton. [20] Interestingly, however, potassium is present only for greige yarns, and only after they are treated with plasma exposure; this is evident in the low resolution survey scans as well as high resolution C1s scans. Due to the scouring process, that is used to remove contaminants, the potassium's presence in only griege yarns is reasonable. Example high resolution scans and deconvoluted peaks are shown in Supplementary Figure S6.3. With the low quantity of calcium, nitrogen, and potassium components we do not consider their contribution when determining the O:C atomic ratio in high resolution scans. For cellulose, the theoretical O:C atomic ratio is 0.83. For our control greige and scoured yarns, the O:C atomic ratio is 0.136 and 0.258, respectively (Table 6.2). These low atomic ratios are the result of waxes and other contaminants present at the surface of fibers. The scoured yarns have a slightly higher atomic ratio than greige yarns due to their scouring process that again removes, but does not eliminate waxes and contaminants. Aside from our high power density, our shortest plasma exposure time of 15 min is relatively long compared to other studies, therefore, we see a large increase in the O:C atomic ratio immediately. This value for greige yarns eventually increases above the the theoretical value of 0.83, which is due to the O_2 plasma that introduces more oxygenated species at the yarn surfaces.

Table 6.2 XPS C1s deconvoluted peak percent areas (C_1, C_2, C_3, and C_4) and the O1s and C1s atomic % ratio for greige and scoured yarns treated at 0.46W/cm^2 power density.

Yarn Type	Exposure Time (min)	C-C/C-H (C_1) (%)	C-O (C_2) (%)	C=O/O-C-O (C_3) (%)	O-C=O ($C_{4)}$ (%)	O:C Atomic Ratio
Greige	0	84.6	10.0	5.47	0	0.136
	15[a]	40.2	36.8	12.1	10.9	0.748
	15	47.4	27.3	14.5	10.8	0.733
	30	44.1	32.6	11.7	11.5	0.782
	60	32.2	38.9	4.61	14.3	0.852
	90	32.9	40.8	18.7	7.63	0.929
Scoured	0	72.1	18.8	6.38	2.75	0.258
	15[a]	43.0	33.8	10.5	12.7	0.582
	15	38.2	37.9	11.4	12.5	0.754
	30	45.8	32.9	11.1	10.2	0.620
	60	29.8	44.2	14.2	11.8	0.800
	90	30.9	42.9	13.3	12.9	0.765

C_1-C_4 are rounded to three significant figures and [a] represents yarns treated at 75cc/min oxygen flowrate

In addition to the O:C atomic ratio, the high resolution C1s peak of cellulose provides further information about the chemical nature at the yarn surfaces; we evaluate the % areas of deconvoluted peaks C_1-C_4 (Table 2). We assign C_1 (C-C/C-H bonds) at 285.0 eV, C_2(C-O bonds) at 286.6 ± 0.1 eV, C_3 (C=O/O-C-O) at 288.0± 0.1 eV, and C_4 (O-C=O) at 289.0 ± 0.1 eV. [15] Through the evaluation of the C1s peak, the the chemical changes occurring at surface of fibers can be determined in relation to plasma exposure. The C_1 peak decreases with plasma exposure as the C-C and C-H contaminants are being removed by the plasma process. For the most part, we find C_2-C_4 to increase compared to control yarns as more polar groups are forming as the result of the plasma treatment.[15, 18] Other researchers have attributed the increase of oxygen moieties present at cellulose surfaces to the increase in hydrophilicity often observed by cotton after plasma exposure [14, 15]. While we do not observe the expected decrease in C-O bonds that is attributed to main chain scissions [19], we are using O_2 plasma at significantly longer exposure times in comparison to other studies; this is our reasoning

for why we see such high percentages of C-O compared to our controls.

6.4 Conclusions

Using O_2 plasma with high power density and extended treatment times of 15 to 90 minutes, we are able to link the physical degradation observed in yarns to the degradation of cellulose structure. Based on the evidence here we can say that treatment times of 60-90 min for greige yarns, and 30-90 min for scoured yarns yield a significant amount of physical and chemical degradation of cellulose. We found decrease in the load at break for greige and scoured cotton yarns by approximately 80 and 90%, respectively. We start with high M_w and DP of cellulose and are able to reduce both by roughly 50 %. Although the DP is still quite high, plasma may be used as a "greener" pre-treatment to degrade high molecular weight cellulose for its potential use in biofuels, and ultimately lead to less cotton waste reaching landfills.

6.5 Supplementary Materials

Table S6.1 All experimental conditions performed on greige and scoured yarns.

Machine	*Exposure Time (min)*	*RF Power (W)*	*Plasma Power Density (W/cm^2)*	*Yarn Samples Tested*	*O_2 Flowrate (cc/min)*
PE200RIE	15	500	0.46	Greige & Scoured	75
PE200RIE	15	500	0.46	Greige & Scoured	200
PE200RIE	30	500	0.46	Greige & Scoured	200
PE200RIE	60	500	0.46	Greige & Scoured	200
PE200RIE	90	500	0.46	Greige & Scoured	200
PE50	15	100	0.28	Greige	10
PE50	15	150	0.42	Greige	10
BT-1	15	500	0.039	Greige & Scoured	75
BT-1	15	100	0.010	Greige & Scoured	75

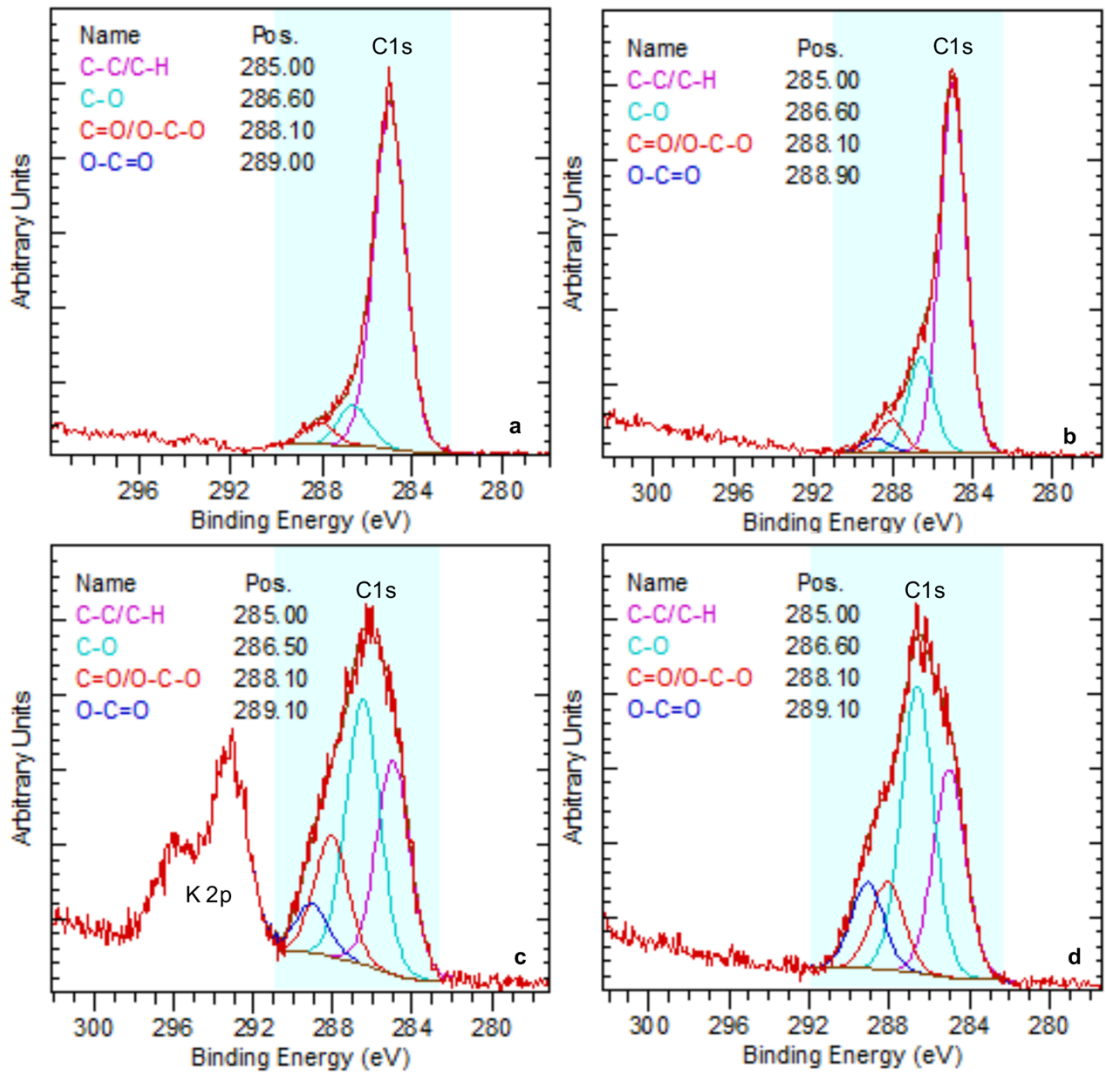

Figure S6.1 XPS data of C1s with four deconvoluted peak fittings for control greige yarn (a), control scoured yarn (b), greige yarn treated at 0.46 W/cm^2 for 60 min (c), and scoured yarn treated at 0.46 W/cm^2 for 60 min (d)

6.6 Acknowledgements

Monsanto Company and the College of Human Ecology at Cornell University provided funding for this research. We thank Plasma Etch, Inc. for onsite assistance with sample processing. This work made use of the Cornell Center for Materials Research Facilities supported by the National Science Foundation under Award Number DMR-1120296. We acknowledge PolyAnalytik, Inc. for performing GPC

experiments and providing experimental values. We recognize Dr. Jon Shu for running XPS analysis on cotton yarns and Dr. Darren Dale for aiding in the analysis. We also appreciate contributions from Dr. Alan Taylor and Dr. Catharine Catranis.

REFERENCES

1. Textiles. Last updated : 2014 http://www.epa.gov/epawaste/conserve/materials/textiles.htm.
2. Mu, B. N.; Xu, H. L.; Yang, Y. Q., Accelerated hydrolysis of substituted cellulose for potential biofuel production: Kinetic study and modeling. *Bioresour. Technol.* **2015,** *196*, 332-338.
3. Mukherjee, S. M.; Woods, H. J., X-ray and electron microscope studies of the degradation of cellulose by sulphuric acid. *Biochim. Biophys. Acta* **1953,** *10*, 499-511.
4. Lin, J.-H.; Chang, Y.-H.; Hsu, Y.-H., Degradation of cotton cellulose treated with hydrochloric acid either in water or in ethanol. *Food Hydrocolloids* **2009,** *23* (6), 1548-1553.
5. Morent, R.; De Geyter, N.; Vershuren, J.; De Clerck, K.; Kiekens, P.; Leys, C., Non-thermal plasma treatment of textiles. *Surf. Coat. Technol.* **2008,** *202* (14), 3427-3449.
6. Peng, S.; Gao, Z.; Sun, J.; Yao, L.; Qui, Y., Influence of argon/oxygen atmospheric dielectric barrier discharge treatment on desizing and scouring of poly(vinyl alcohol) on cotton fabrics. *Appl. Surf. Sci.* **2009,** *255* (23), 9458-9462.
7. Bhat, N. V.; Netravali, A. N.; Gore, A. V.; Sathianarayanan, M. P.; Arolkar, G. A.; Deshmukh, R. R., Surface modification of cotton fabrics using plasma technology. *Text. Res. J.* **2011,** *81* (10), 1014-1026.
8. Benoit, M.; Rodrigues, A.; Vigier, K. D. O.; Fourre, E.; Barrault, J.; Tatibouet, J.-M.; Jerome, F., Combination of ball-milling and non-thermal atmospheric plasma as physical treatments for the saccharification of microcrystalline cellulose. *Green Chem.* **2012,** *14* (8), 2212-2215.
9. Mihailovic, D.; Saponjic, Z.; Radoicic, M.; Lazovic, S.; Baily, C. J.; Jovancic, P.; Nedeljkovic, J.; Radetic, M., Functionalization of cotton fabrics with corona/air RF plasa and colloidal TiO2 nanoparticles. *Cellulose* **2011,** *18* (3), 811-825.
10. Hua, Z. Q.; Sitaru, R.; Denes, F.; Young, R. A., Mechanisms of oxygen- and argon-RF-plasma-induced surface chemistry of cellulose. *Plasmas Polym.* **1997,** *2* (3), 199-224.
11. Jinka, S.; Turaga, U.; Singh, V.; Behrens, R. L.; Gumeci, C.; Korzeniewski, C.; Anderson, T.; Wolf, R.; Ramkumar, S., Atmospheric Plasma Effect on Cotton Nonwovens. *Ind. Eng. Chem. Res.* **2014,** *53* (32), 12587-12593.
12. Karahan, H. A.; Ozdogan, E.; Demir, A.; Ayhan, H.; Seventekin, N., Effects of Atmospheric Pressure Plasma Treatments on Certain Properties of Cotton Fabrics. *Fibres Text. East. Eur.* **2009,** *17* (2), 19-22.

13. Sun, D.; Stylios, G. K., Investigating the plasma modification of natural fiber fabrics-the effect on fabric surface and mechanical properties. *Text. Res. J.* **2005,** *75* (9), 639-644.
14. Karahan, H. A.; Ozdogan, E., Improvements of surface functionality of cotton fibers by atmospheric plasma treatment. *Fibers and Polymers* **2008,** *9* (1), 21-26.
15. Inbakumar, S.; Morent, R.; De Geyter, N.; Desmet, T.; Anukaliani, A.; Dubruel, P.; Leys, C., Chemical and physical analysis of cotton fabrics plasma-treated with a low pressure DC glow discharge. *Cellulose* **2010,** *17* (2), 417-426.
16. Topalovic, T.; Nierstrasz, V. A.; Bautista, L.; Jocic, D.; Navarro, A.; Warmoeskerken, M., XPS and contact angle study of cotton surface oxidation by catalytic bleaching. *Colloids and Surfaces a-Physicochemical and Engineering Aspects* **2007,** *296* (1-3), 76-85.
17. Sun, D.; Stylios, G. K., Fabric surface properties affected by low temperature plasma treatment. *J. Mater. Process. Technol.* **2006,** *173* (2), 172-177.
18. Vasiljevic, J.; Gorjanc, M.; Jerman, I.; Tomsic, B.; Modic, M.; Mozetic, M.; Orel, B.; Simoncic, B., Influence of Oxygen Plasma Pre-treatment on the Water Repellency of Cotton Fibers Coated with Perfluoroalkyl-Functionalized Polysilsesquioxane. *Fibers and Polymers* **2016,** *17* (5), 695-704.
19. *Plasma Processing of Polymers*. Springer Science & Business Media 1997; p 532.
20. Brushwood, D. E.; Perkins, H. H., DETERMINING THE METAL CONTENT OF COTTON. *Textile Chemist and Colorist* **1994,** *26* (3), 32-35.

CHAPTER 7
CONCLUSIONS AND FUTURE WORK

7.1 Conclusions

The bulk of this work involves the process of electrospinning, however, due to the instabilities in traditional electrospinning controlling of the fiber's precise placement and patterning is limited. Therefore, a new method, Immersion Electrospinning has been developed. The objective of this work was to decrease the instabilities presently encountered in electrospinning to allow for greater control of the polymer fiber. This was achieved by spinning directly through a viscous medium. A brief study on the effect of the electric field strength/electric field parameter was performed to determine a proper field to apply so that fibers could be directed. Immersion Spun fibers formed with low enough momentum as dictated by the applied electric field allowed for them to be guided to spatially distributed and actively controlled electrodes. The deposition of a continuous PAN fiber was directed into a square path.

In Chapters 3-5, PLA/PLA-*b*-PEG (Poly (lactic acid)/Poly (lactic acid)-*b*-Poly(ethylene glycol)) electrospun fibers are the focus for their potential in biosensor applications. First, PLA/PLA-*b*-PEG fibers spun from Dimethylformamide (DMF) were aged for approximately 48 weeks in humid conditions. The main objective of this study was to see how the water wicking properties of the samples changed with time. Approximately every 8 weeks, water wicking and differential scanning calorimetry measurements were performed. PLA(1000)-*b*-PEG(5000) initially had a high water wicking ability but equilibrated quickly with little change being observed after 8 weeks of aging, wicking

approximately 5 g water/ g sample. PLA(1000)-*b*-PEG(10000), however, didn't follow a definite trend in wicking but did start to level out at about 7 to 8 g water/ g sample. While PLA/PLA-*b*-PEG fiber samples do decrease in water wicking ability, they both still remain higher than PLA spun samples. This study, therefore shows that the storage of PLA/PLA-*b*-PEG samples is an important parameter that must be considered if such samples are to be used for an in-field application.

Next, varying concentrations of biotin were incorporated freely into PLA/DMF, and PLA/PLA(730)-*b*-PEG(5000)/DMF spinning dopes (0 to 18 wt % biotin in the final fiber). With the incorporation of PLA-*b*-PEG copolymers, the surface available biotin dramatically increased compared to PLA fibers, resulting in fibers with up to 60% of their total amount of biotin available at the surface of fibers. Water stability tests, however, show that after immersing the fibers in water for long durations of time, both biotin and PLA-*b*-PEG block copolymers tended to migrate to the aqueous phase. The fibers formed in this study, therefore, have the potential for use in point-of-care diagnostics where short aqueous contact times are required.

By tailoring the block lengths of PLA-*b*-PEG copolymers, an increase in the stability of electrospun fibers of PLA/PLA-*b*-PEG and PLA/PLA-*b*-PEG-Biotin fibers was achieved. A comparison of two spinning solvents, 1,1,1,3,3,3- Hexafluoro-2-propanol (HFIP) and DMF, showed fibers spun from solvent HFIP provided samples that were more water stable than those spun from DMF dopes, but HFIP spun samples had no biotin present at the surface of fibers for detection. Electrspun samples of PLA(3600)-

b-PEG(2000)-Biotin spun from DMF, however, allowed for ~1.1 mg of biotin per gram of fiber to be detected at the surface of fibers, with the incorporation of 85 % less biotin than previous studies. These fibers therefore have the potential to be used in point-of-care diagnostics where slightly longer contact times are required due to the increased stability of these fibers by tailoring PLA-b-PEG block lengths and attaching biotin directly to the PLA-*b*-PEG.

In Chapter 6, again we moved away from electrospun samples to investigate the use of plasma on cotton yarn samples. Using Oxygen (O_2) plasma the modification of cotton yarns is achieved. With high power density and extended treatment times, we are able to link the physical degradation observed in yarns to the degradation of cellulose structure. Based on the evidence here we can say that treatment times of 60-90 min for greige yarns, and 30-90 min for scoured yarns yield a significant amount of physical and chemical degradation of cellulose. Plasma, therefore, may be used as a "greener" pre-treatment to degrade high molecular weight cellulose for its potential use in biofuels.

7.2 Future Work

The work presented here provides many opportunities to be expanded upon. Immersion Electrospinning, for example, in Chapter 2 is in the more preliminary stages of development. While I have shown that fibers can be directed by selectively applying voltage there is much to be developed further.

For Immersion Electrospinning, a thorough investigation into the coagulation bath components, and the diffusion rate is necessary for ideal fiber formation. In addition, experimentation with other polymers, besides PAN is necessary if Immersion Electrospinning is to be useful. With further understanding of this system, and slight system modification, as suggested in Figure 7.1, Immersion Electrospinning could provide a method for developing precise architectures with no mechanical motion necessary. If one were to create a multi-nozzle apparatus, with large electrode arrays (ie., Figure 7.1), individual layers within an architecture could be tailored for specific needs. Changing parameters such as the coagulation bath components and/or ratios, flowrate, needle size, etc. is another important study that should be done in order to determine the necessary conditions to have fibers adhere to the collector and achieve smaller fiber diameters.

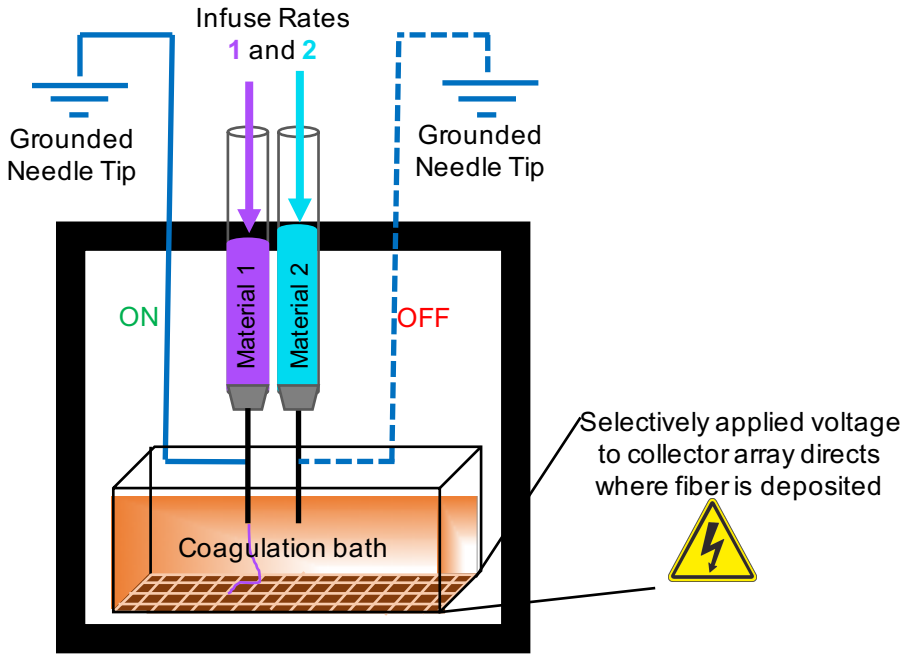

Figure 7.1 Suggested modifications to apparatus for Immersion Electrospinning: larger electrode arrays, multiple polymer solutions/suspensions, and vertically positioned syringes.

The work in this dissertation on functionalizing the surface of nanofibers could further be expanded as well. In Chapter 4, adding Biotin and PLA-*b*-PEG to PLA fibers, the amount of Biotin reaching the surface of fibers is increased over pure PLA fibers. While attaching the Biotin directly to PLA-*b*-PEG in Chapter 5 resulted in less overall Biotin at the fiber surface than when Biotin was added freely, the amount of Biotin leaching from the fiber mats was reduced.

A proof of concept should be worked on for attaching antibodies to the PLA fiber surfaces to target a specific antigen. This could potentially be done using several different methods and it would be of interest to compare the various methods of attachment in the ability of the PLA nanofiber mats to detect specific antigens. First,

PLA/PLA-*b*-PEG-Biotin fibers discussed in Chapter 5 could be used, where Avidin is attached post spinning followed by a biotinylated antibody that would be able capture the target antigen (Figure 7.2A). Li et al. was able to show avidin binding to PLA fibers containing biotin was a viable method for detecting.[1] Another option, is through the application of plasma to electrospun PLA and PLA/PLA-*b*-PEG fiber mats. As shown in chapter 6, the application of Oxygen (O_2) plasma resulted in more oxygen moieties at the yarn surfaces. Therefore, here I propose to use O_2 plasma treatments on the PLA and PLA/PLA-*b*-PEG electrospun fibers to form –COOH groups, which then could be used with 1-ethyl-3-(3-dimethylaminopropyl) carbodiimide (EDC)/N-hydroxysuccinimide ester (NHS) chemistry to attach the amine group of primary antibodies to the fiber surfaces (Figure 7.2 B and C). This proposed method should be feasible as other researchers have used plasma to introduce –COOH groups onto electrospun fibers as a way to attach biomolecules to the fiber surfaces. [2, 3] The suggested method of detection of a specific contaminant would utilize a fluorescently tagged antibody (Figure 7.2). One specific way to do this would be to use a dye encapsulated liposome tagged antibodies. Because liposomes can contain different types of signals (i.e. fluorescent dye, electrochemical, enzyme, etc.) [4], any mode should be viable.

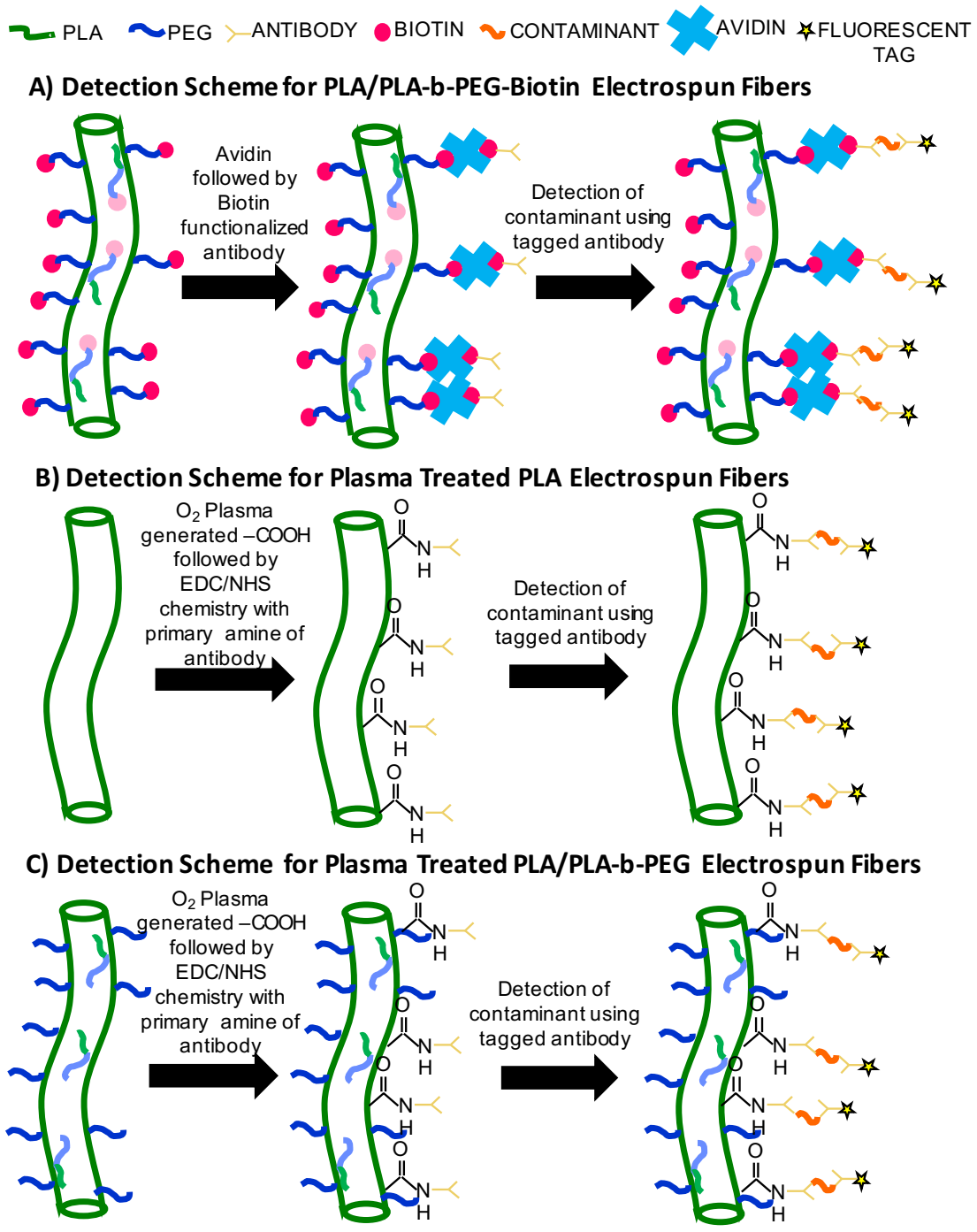

Figure 7.2 Proposed detection schemes.

REFERENCES

1. Li, D.; Frey, M. W.; Vynias, D.; Baeumner, A. J., Availability of Biotin Incorporated in Electrospun PLA Fibers for Streptavidin Binding. *Polymer* **2007,** *48* (21), 6340-6347.
2. Chen, J. P.; Su, C. H., Surface modification of electrospun PLLA nanofibers by plasma treatment and cationized gelatin immobilization for cartilage tissue engineering. *Acta Biomaterialia* **2011,** *7* (1), 234-243.
3. Mondal, K.; Ali, M. A.; Singh, C.; Sumana, G.; Malhotra, B. D.; Sharma, A., Highly sensitive porous carbon and metal/carbon conducting nanofiber based enzymatic biosensors for triglyceride detection. *Sensors and Actuators B: Chemical* **2017,** *246*, 202-214.
4. Liu, Q. T.; Boyd, B. J., Liposomes in biosensors. *Analyst* **2013,** *138* (2), 391-409.